Earth Surface Processes and Landforms

The active layer in gravel-bed rivers: an empirical appraisal

Journal:	*Earth Surface Processes and Landforms*
Manuscript ID	ESP-20-0073.R2
Wiley - Manuscript type:	Research Article
Date Submitted by the Author:	n/a
Complete List of Authors:	Vázquez Tarrío, Daniel; Centre Europeen de Recherche et d'Enseignement des Geosciences de l'Environnement, Terre et Planète Piqué, Gemma; Pontificia Universidad Católica de Valparaíso, Facultad de Ciencias Agronómicas y de los Alimentos Vericat, Damià; Univeristy of Lleida, Department of Environment and Soil Sciences Batalla, Ramon; University of Lleida, Department of Environment and Soil Sciences
Keywords:	active layer, active depth, bedload, particle entrainment, bed scour, flow strength, grain-size, river morphology
Abstract:	The vertical position of the streambed-water boundary fluctuates during the course of sediment transport episodes, due to particle entrainment/deposition and bedform migration, amongst other hydraulic and bedload mechanisms. These vertical oscillations define a topmost stratum of the streambed i.e. the 'active layer or active depth', which usually represents the main source of particles entrained during long and high-magnitude bedload transport episodes. The vertical extent of this layer is hence a capital parameter for the quantification of bedload volumes and a major driver of stream ecology in gravel-bed rivers. However, knowledge on how the active depth scales to flow strength and the nature of the different controls on the relation between the flow strength and the active depth is still scarce. In this paper we present a meta-analysis over active depth data coming from ~130 transport episodes extracted from a series of published field studies. We also incorporate our own field data for the rivers Ebro and Muga (unpublished), both in the Iberian Peninsula. We explore the database searching for the influence of flow strength, grain-size, streambed mobility, and channel morphology on the vertical extent of the active layer. A multivariate statistical analysis (stepwise multiple regression) confirms that the set of selected variables explains a significant amount of variance in the compiled variables. The analysis shows a positive scaling between active depth and flow strength. We have also identified some links between the active depth and particle travel distances. However, these relations are also largely modulated by other fluvial drivers, such as the grain-size of the bed surface and the dominant channel macro-bedforms, with remarkable differences between plane-bed, step-pool and riffle-pool channels.

THE ACTIVE LAYER IN GRAVEL-BED RIVERS: AN EMPIRICAL APPRAISAL

Vázquez-Tarrío D.[1, 2, 3]; Piqué G.[4]; Vericat D.[5,6] and Batalla, R.J.[5, 7, 8]

[1]University of Lyon, CNRS UMR 5600 EVS, Site ENS, F-69362, Lyon, France

[2]Department of Geology, University of Oviedo, c\Jesús Arias de Velasco, s/n 33005 Oviedo, Spain

[3]INDUROT, University of Oviedo, Campus de Mieres, s/n 33600 Mieres, Spain

[4] Escuela de Agronomía, Facultad de Ciencias Agronómicas y de los Alimentos, Pontificia Universidad Católica de Valparaíso, Quillota, Chile

[5]Fluvial Dynamics Research Group (RIUS), University of Lleida, 25003 Lleida, Catalonia, Spain

[6]Forest Science and Technology Centre of Catalonia (CTFC), Solsona, 25280 Solsona, Catalonia, Spain

[7]Catalan Institute for Water Research (ICRA), 17241 Girona, Catalonia, Spain

[8]Facultad de Ciencias Forestales y Recursos Naturales, Universidad Austral de Chile, 14101 Valdivia, Chile

Abstract

The vertical position of the streambed-water boundary fluctuates during the course of sediment transport episodes, due to particle entrainment/deposition and bedform migration, amongst other hydraulic and bedload mechanisms. These vertical oscillations define a topmost stratum of the streambed i.e. the 'active layer or active depth', which usually represents the main source of particles entrained during long and high-magnitude bedload transport episodes. The vertical extent of this layer is hence a capital parameter for the quantification of bedload volumes and a major driver of stream ecology in gravel-bed rivers. However, knowledge on how the active depth scales to flow strength and the nature of the different controls on the relation between the flow strength and the active depth is still scarce. In this paper we present a meta-analysis over active depth data coming from ~130 transport episodes extracted from a series of published field studies. We also incorporate our own field data for the rivers Ebro and Muga (unpublished), both in the Iberian Peninsula. We explore the database searching for the influence of flow strength, grain-size, streambed mobility, and channel morphology on the vertical extent of the active layer. A multivariate statistical analysis (stepwise multiple regression) confirms that the set of selected variables explains a significant amount of variance in the compiled variables. The analysis shows a positive scaling between active depth and flow strength. We have also identified some links between the active depth and particle travel distances. However, these relations are also largely modulated by other fluvial drivers, such as the grain-size of the bed surface and the dominant channel macro-bedforms, with remarkable differences between plane-bed, step-pool and riffle-pool channels.

43 *Keywords*: active layer, active depth, bedload, particle entrainment, bed scour,
44 flow strength, grain-size, river morphology.

1. Introduction

Bedload transport is a major physical process in gravel-bed rivers, insofar as bedload is behind the mechanisms governing river geometry and channel morphodynamics (Parker, 2004; Church, 2006). Bedload also influences the distribution and dynamics of the physical habitat for aquatic organisms and biotic communities (e.g. Gibbins et al., 2007; Rice et al., 2012). Therefore, bedload studies had been unavoidable for a list of scientific and applied questions, which include river engineering (e.g. Kondolf and Wilcock, 1996; Batalla and Vericat, 2009; Kondolf et al., 2014; Liedermann et al., 2018), river restoration (e.g. Dépret et al., 2019; Staentzel et al., 2020), fluvial ecology (e.g. Kondolf and Wolman, 1993; Gibbins et al., 2007; Tena et al., 2013; Haschenburger, 2017; Béjar et al., 2020), and channel evolution (e.g. Liébault and Piégay, 2002; Comiti et al., 2011; Liébault et al., 2013; Vázquez-Tarrío et al., 2019), amongst others.

Bedload is governed by the direct entrainment and deposition of sediment particles from and into the riverbed (Shields, 1936; Parker, 2008; Pähtz and Durán, 2016). Both mechanisms participate in the stochastic exchange of particles between the streambed surface and the flow that defines bedload. Consequently, the boundary between the riverbed and the flow vertically fluctuates over time and space, as long as entrainment and deposition of sediment particles produce an increase and a decrease in the elevation of the alluvial streambed (Haschenburger, 1999; Pierce and Hassan, 2020). Vertical fluctuations in the water-streambed boundary hence define the upper and lower edges for the topmost part of the bed material that is more actively involved in sediment transport, which constitutes the source from where mobile particles are entrained. This topmost layer of the streambed has been often referred to as

70 'active layer or disturbance depth' (e.g. Haschenburger, 1999; DeVries, 2002;
71 Church and Haschenburger, 2017; Hassan and Bradley, 2017; Ashmore and
72 Leduc, 2018).
73 Sediment transport literature offers two main ways of understanding the
74 significance and dynamics of the active layer (Church and Haschenburger, 2017;
75 Ashmore and Leduc, 2018). The first approach defines the active layer as an
76 interface (or boundary) of continual particle exchange between the bed material
77 and the bedload (Hirano, 1972; Parker and Sutherland, 1990). This dynamic
78 concept is that commonly employed in sediment transport and morphodynamical
79 modelling and, very often, it is labelled as the 'Hirano's exchange layer' (e.g.
80 Parker, 2004). The second approach offers a more geomorphological
81 conceptualization, and refers to the topmost stratum of streambed sediment that
82 is strongly disturbed (by scour and fill) during a bedload transport event, or during
83 the migration of bedforms such as dunes or gravel sheets (Ashmore and Leduc,
84 2018). Both approximations are somewhat equivalent, but they differ in the spatial
85 and time scale they address. Hereinafter, we will refer to the concept of 'event-
86 based' active thickness as active layer, i.e. the topmost layer of streambed
87 material that is actively implicated during a bedload transport episode, and from
88 which clasts are entrained and deposited (Church and Haschenburger, 2017).
89 The thickness or the depth of the active layer is one major dimension of the
90 bedload volumes, together with particle travel distances, active channel width and
91 the fraction of mobile particles (Wilcock and McArdell, 1997; Haschenburger and
92 Church, 1998; Liébault and Laronne, 2008). Thus, it is important in order to
93 understand and quantify how bedload volumes evolve with flow strength. Even
94 so, there are some contradictory field observations i.e. those that report that

active depth evolves with flow strength (Carling, 1998; Wilcock et al., 1996; Haschenburger, 1999), whereas there are others that suggest that its thickness is mostly controlled by the size of the bed grains (DeVries, 2002; Bigelow, 2005). In this regard, the role of surface grain-size appears to be crucial, so that coarser streambeds may be associated with thicker active layers at high flows through scaling the depth caused by particle entrainment (e.g. DeVries et al., 2002). However, gravel-bed rivers are often armoured, which means that the surface layer is coarser than the underlying substrate (Gomez, 1983; Parker and Sutherland, 1990; Richards et al., 1991; Vericat et al., 2006; Hassan et al., 2006; Venditti et al., 2017; Vázquez-Tarrío et al., 2020). At this stage, larger grains prevent entrainment, increasing the chances of sediment by-pass and decreasing the amount of vertical mixing during bedload (e.g. Gomez, 1983). In the same vein, flume experiments by Wilcock and McArdell (1997) documented how active depth increases with flow strength until approaching an upper limit of twice the thickness of the surface coarser layer at full mobility conditions. This somewhat supports the idea that active depth scales eminently with flow strength at low flow conditions, and with surface grain-size at high flow conditions. Hence, the relative mobility of the armour layer may potentially explain differences between different sites in whether the active depth scales to flow strength or (and) to grain-size.

Moreover, sharp contrasts in cross-sectional shear stress distributions, diverse paths of flow and sediment conveyances, and different patterns in grain-size sorting feature distinct channel morphologies (e.g. Beechie, 1991; Ferguson, 2003; Pyrce and Ashmore, 2005; Francalanci et al., 2012; Recking et al., 2016; Vázquez-Tarrío et al., 2019, Vázquez-Tarrío and Batalla, 2019). Consequently, macro-bedforms can influence the spatial distribution of particle entrainment and

the cross-sectional extent of mobile/non-mobile sediment patches (Laronne et al., 2001; García et al. 2007; Nelson et al., 2009). Thus, a given dominant channel morphology may also exert a significant and non-negligible control on the way active layer evolve with flow strength, by modulating the functional links between both physical parameters. This is particularly relevant when the study is one-dimensional and solely based on section averaged values of flow metrics and active thickness, a common approach in bedload computation (e.g. Ferguson, 2003; Recking, 2013).

Nonetheless, uncertainties on how active depth scales to flow strength remain. To the best of our knowledge, the work done by Haschenburger (1999) represents the only attempt to develop a quantitative general model of scour and fill depths and, apart from Bigelow (2005), no systematic validation has been tried since then. Within this context, in this paper we seek to explore the links between the depth or thickness of the active layer and flow discharge in relation to flow stages (i.e. bankfull) in gravel-bed rivers. To that end, we compiled a database of previous studies focused on the study of active depths in the field obtained by scour chains and tagged stones in coarse-bed rivers. This large amount of data helps to empirically explore the links between section-averaged flow parameters and event-averaged active layer depths, hence accomplishing a systematic analysis of the different sources of variance in the compiled field data. The main goal is thus to shed light on the controls on active depth in gravel-bed rivers. Accordingly, the three specific objectives of this work are: i. to outline how flow strength and armour mobility control active thickness or depth in gravel-bed rivers; ii. to identify potential morphological signatures in the functional links

144 between flow strength and active depth; and iii. to quantify the weight of those
145 variables, if significant, in controlling the active depth.
146
147 **2. Material and methods**
148 **2.1. Data compilation**
149 This research is based on a compilation of datasets on the thickness of the active
150 layer obtained from published field studies. The dataset is made up of results
151 extracted from 10 tracer studies in 31 streams and comprises information from
152 129 transport events (Table 1). In many of the study cases, data on the depth of
153 the active layer were obtained from scour chains. In other cases, active depth
154 information was obtained from the mean burial depth of tagged stones deployed
155 on the streambed. In one of the studies (Brousse et al., 2018), active depths were
156 obtained from active-RFID columns, used as an alternative to classical scour
157 chains. In one last study (Schneider et al., 2014), authors made an indirect
158 estimation of event-averaged active depths based on the bed material volumes
159 retained in a sediment trap and the travel distances of tagged stones.
160 Additionally, we incorporated into the analysis our own unpublished dataset from
161 33 transport episodes monitored in the Rivers Muga and Ebro. A detailed
162 description of the Rivers Ebro and Muga can be found in the supplementary files
163 (Document 1) included in the present manuscript, but some general information
164 of these two study cases is also presented here below:
165 i) The Muga is a 758 km^2 catchment located in the NE of the Iberian Peninsula.
166 Riverbed mobility was monitored in an unregulated gravel-bedded reach with a
167 mean slope of 0.008 located in the upper part of the catchment from October
168 2013 to April 2015. Surface Grain Size Distributions (GSD) were obtained in

exposed bars using the pebble count method (Wolman, 1954). A total of 842 particles were measured in two sampling campaigns. Subsurface material was sampled once following the volume-by-weight method (Church et al., 1987), in three different bar locations. Particle travel length was measured from two painted areas located at the head of an exposed river bar, and from 50 RFID-tagged particles placed in the mainstem river. The depth of the active layer was measured by means of four scour chains also installed at the head of the bar. Overall, six flood episodes were monitored, and riverbed mobility was observed in five of them. For more information on sediment transport studies in the Muga see Piqué et al. (2017).

ii) The River Ebro drains an area of ca. 85,000 km^2 in the NE of the Iberian Peninsula. Riverbed dynamics were studied from October 2002 to September 2004 at ten study sites in the lowermost part of the river, below two large dams. The mean slope of the study reach is 0.00085. Riverbed materials were characterised on three occasions. Surface GSD was measured in open gravel bars by means of the pebble count method (Wolman, 1954) and the area-by-weight method (Kellerhals and Bray, 1971). Subsurface materials were measured in each study site by the volume-by-weight method (Church et al., 1987). When an armour layer was not present, surface and subsurface material were sampled together, as a bulk sample, using the volumetric method. Particle size varied greatly between sites and over time. Particle travel length was measured by means of painted areas and painted pebble lines at the ten study sites and, additionally, with magnetic tracers in two of the sites. The thickness of the active layer was measured using two different methods: differences in the exposed length of installed scour chains and metallic rods, and the burial of magnetic-

194 tagged particles. Riverbed mobility was observed on four occasions during the
195 study period (i.e. high flows between floods often hampered fieldwork in bars).
196 For more information on bed-material and entrainment in the Ebro see Vericat et
197 al., 2006 and Vericat et al., 2008, respectively.
198 The final database is made up of active depth data for a total number of 171
199 transport episodes in 33 rivers from eight countries (Belgium, Canada, France,
200 Great Britain, Italy, Spain, Switzerland, and USA) with a wide range of slopes
201 (ranging over 0.0009 to 0.15) and channel widths (spanning from 2 to 250 m).
202 Data also cover several hydrological regimes (rainfall-dominated, snowmelt
203 dominated, and glacial-fed). With regard to channel morphology, 78% of data
204 correspond to riffle-pool channels (7 studies, 26 rivers), 24% to step-pool (2
205 studies, 3 streams), 9% to plane-bed streams (2 studies, 2 streams) and 3% to
206 multi-thread rivers (1 study, 2 rivers). In terms of the methods used to measure
207 the active depth in the field, 44% of points correspond to scour chains/scour
208 monitors (6 studies, 22 rivers), 42% to average tracer burial (6 studies, 9 rivers),
209 11% points come from an indirect estimation of active depth (1 study, 2 streams),
210 and 3% of points were obtained from using (buried) active RFID columns (1 study,
211 2 streams). Thus, the database comprises a wide diversity of channel
212 morphologies and experimental conditions, incorporating all the field data that we
213 could identify in the scientific literature concerning active depths in gravel-bed
214 rivers.

215 **2.2. Data analysis**

216 *2.2.1. Data preparation*

217 Information on GSD, event-averaged (tracer) travel length and (tracer) burial
218 depth, event averaged scour-and-fill thicknesses from scour chains and peak

discharge (*Q*) for each study case were compiled and grouped according to the main channel morphology i.e. step-pool (SP), riffle-pool (RP), plane-bed (PB) and multi-thread (MT), following Montgomery and Buffington (1997) classification. The ratio between peak *Q* for the transport episode and the bankfull *Q* (hereinafter called dimensionless flow intensity) was designated as the dimensionless flow parameter used to characterize and quantify flow strength. Due to the difficulty to define the bankfull discharge in the two braided/wandering study cases (Rivers Drac and Vénéon), we took the ~1-year return-period flood as reference discharge in these two cases. There are three advantages of using the dimensionless flow intensity as flow parameter: i. *Q* is the flow descriptor most widely reported in the compiled papers, so this ratio is easy to compute; ii. the bankfull *Q* is commonly considered as the dominant channel-forming discharge and it has been traditionally associated to 1.5-2 year return period flood (Leopold et al., 1964), although the exact recurrence of the bankfull flow differs with the hydroclimatic setting and the use of partial vs full duration series (Van Campehout et al., 2020); and iii. the bankfull *Q* has been consistently related to a near-threshold discharge for bed sediment movement in gravel-bed rivers (e.g. Phillips and Jerolmack, 2019). Hence this ratio provides at the same time an idea of flow magnitude, frequency and strength.

Additionally, bedload transport in gravel bed rivers is largely controlled by the relative mobility of the streambed surface, which is often armoured (Vázquez-Tarrío et al., 2020). Thus, we could expect some covariation between the relative mobility of the streambed surface and the depth of the active layer. In principle, we can imagine that bed surface mobility is driven by the entrainment of the coarser particles in the streambed (MacKenzie and Eaton, 2017; MacKenzie et

al., 2018), so the ratio between the peak shear stress (τ) and the critical threshold stress (τ_c) (transport stage ratio) for incipient motion of coarse bed particles may provide an idea of bed surface mobility. We considered a value of the computed transport stage equal to 1 as an approximation to a situation when the coarse clasts in the riverbed start to be entrained and the bed surface becomes to destabilize; values <1 may represent *stable* riverbeds with intact or quasi-intact armour layers, whereas values >1 approximate transport events capable of incorporating the coarser particles within the riverbed, thus breaking the surface layer.

Due to limitations in the data available within the compiled papers (usually only *Q* and an average bankfull width), it was not possible to know the true τ for each study case, so we were obliged to approach it through hydraulic computations based on the available information. We used the peak *Q* information and the Rickenmann and Recking (2011) friction equation to estimate peak τ. To estimate the value of the critical Shields parameter (τ^*) for the 84th percentile (D_{84}) and the median size (D_{50}) of the surface grain-size distribution we used the slope-dependant relation proposed by Recking (2009). More details on how we estimated these ratios from a range of *Q* can be found in the appendix of the manuscript. Limitations inherent to this approach should be kept in mind. Shear stress show a large variability within the same channel, both in time and space (Ferguson, 2003; Recking, 2013; Francalanci et al., 2012; Recking et al., 2016). Thus, rather than the actual absolute transport stages, our estimations should be considered as relative transport stages for comparing between streams.

In the analysis, we have also normalized the active depths by the D_{50} of the surface grain-size distribution with the aim of establishing the active depth scaling

caused by particle entrainment. On this point, it is true that the active layer, in general, has historically been described in terms of the D_{90}. For instance, it is a common assumption that the active depth is ~ 2 D_{90} in gravel-bed rivers (e.g. Andrews and Erdman, 1986; Wilcock et al., 1996; Haschenburger and Church, 1998). However, the value of the D_{90} was not available for all the selected study cases, but the D_{50} was. This is the main reason why we finally decided to use the D_{50} as scaling parameter. Nevertheless, in order to have an idea on how the active depth scales to the coarser particles of the streambed, we have also normalized the active depth by the D_{84} (value available for almost all the selected study cases) and added this analysis as supplementary materials (Document 2).

2.2.2. Statistical analysis

As pointed out above, the main aim was to analyse the dataset to seek empirical relations between active depths, flow strength/intensity and channel morphology. To do this, we searched for the best power regression fit between event-averaged active depths and several flow metrics. We also used quantile regression analysis in order to define the upper and lower envelopes of the data as well as the probability of a given active depth occurring under a certain flow *Q*.

Simple regressions allowed to discriminate and discuss which parameters played a role driving active depths in gravel-bed rivers. However, we were also interested in quantifying the influence of the different parameters relative to the others. Consequently, a statistical test combining all the different variables together was performed. Our main aim was identifying which physical parameter (or subset of parameters) is the dominant one in explaining the variability in active-depth in the

compiled database. To do so, we used stepwise multiple linear regression on the selected variables. We started by testing the following model:

$$\log H = A + a \cdot log\left(\frac{\tau^*}{\tau_c^*}\right) + b \cdot log D_{50} + c \cdot log\left(\frac{Q}{Q_{bf}}\right) + d \cdot dRP + e \cdot dSP + e \cdot dBR + f \cdot dTR + g \cdot dSCR \quad \text{Eq. 1}$$

where H is the active depth, Q_{bf} is the bankfull discharge, τ^* is the estimated peak Shields stress, τ_c^* is the critical Shields stress for incipient sediment motion, A is the model intercept and a, b, c, d, e, f and g are empirical coefficients. To incorporate channel morphology into the regression analysis, we defined a set of three dummy variables (*dRP*, *dSP* and *dBR*) that take the value 1 in case of RP, SP and BR rivers, respectively, and 0 in the other cases, i.e. the three are 0 in case of flatbed channels with no macroforms (PB streams). Similarly, we defined two other dummy variables (*dTR* and *dSCR*) taking a value of 1 in case of tracer data and scour-chain (and active RFID columns), respectively, and 0 in case of other conditions. We decided to take logarithms for some of these variables, accounting for the large range of variability spanned by these variables within the raw data. The Variance Inflation Factor (VIF) was computed to assess how much the variance of R^2 in the model is inflated due to collinearity between the predictor variables, using as a rule of thumb that a value of VIF is acceptable if it is less than 10 (James et al. 2014). Lastly, with the aim of assessing the relative size of each one of the independent variables, we used the method proposed by Lindeman et al. (1980) (LMG metrics), which assigns shares of the relative weight of predictors to R^2, while also accounting for the sequence of how predictors appears in the regression model.

3. Results and discussion

3.1. Active layer and flow strength

Results show a statistically significant (p-value < 0.001) positive correlation between flow strength and event averaged active depth (Figure 1). Other authors also found positive trends between the depth of the active layer and flow metrics. For instance, Gottesfeld et al. (2004) observed that burial depth of tagged stones increased with *Q*; Houbrechts et al. (2012) showed that the depth of the active layer was positively correlated to the specific (peak) stream power (ω) of the flow event; Mao et al. (2016) found a positive relation between the dimensionless τ and the thickness of the active layer, though data showed considerable scatter (up to one order of magnitude at certain shear stress values); and Brousse et al. (2018) also documented some kind of increase in the active depth with increasing *Q*. However, other authors did not find a clear trend between active layer depth and increasing Shields stress (De Vries, 2002). Papangelakis (2015) and Papangelakis and Hassan (2016) observed no relation between flow and burial in East Creek and indicated grain-size as the main control on burial. In this regard, according to the quantile regression analysis, the performance of the regression model is better when using active depths normalized by surface grain-size: roughly 90% of data spans over a range of one order of magnitude around the mean regression line, while ~70% of data does so in the case of non-normalized active depths. This suggests that data scatter reduces when normalizing active depth by surface D_{50} and highlights the role of surface particle size on the vertical extent of the active layer. Moreover, Wilcock et al. (1996) and Haschenburger and Church (1998) reported how the thickness of the active layer increases asymptotically with *Q* until approaching a limiting value of ~1.7-2 D_{90}, which is coherent with results obtained by Wilcock and McArdell (1997) in the flume. Our results do not show such limiting value, but quantile regression analysis indicates

that the different quantile curves tend to converge at high flow intensities (Figure 1A). In addition, when active depths are normalized by D_{50}, the 95th-quantile curve and the mean regression curve tend to concentrate in a short range of 2-4 times the D_{50} at very high flows (Figure 1B). In summary, our results point to the importance that both the flow strength and the surface grain-size have on controlling the depth of the active layer. Results also show that active depth (normalized by surface grain-size) increases with flow strength, despite the important scatter displayed by the compiled data. In the following sections, we explore the potential sources for such variance.

3.2. Active layer and sampling method

Some of the observed scatter in Figure 1 can be related to methodological aspects. Differences between methods used to measure the thickness of the active layer may introduce scatter and may bias the observed trends. In this study we treat data from scour chains and tracer burial information together. We are aware, however, that tracers need to experience some flows of a certain magnitude before they are representatively mixed throughout the entire potentially movable bed layer, and this normally requires 5 to 7 years after they are deployed (Ferguson et al., 2002). Tracer data compiled for the purpose of this work come, in general, from studies with shorter times of deployment (Table 1), and this is likely to introduce a degree of bias, i.e. tracer depths are expected to be smaller than in well-mixed conditions. In addition, scour chains (and similar scour indicators) provide net scour and fill depth observations at a fixed location, thus delineating the maximum extent of the active layer (Laronne et al., 1994; Haschenburger and Church, 1998). Nonetheless, burial depths associated with deposited tracers indicate the net fill since the time of deployment

(Haschenburger and Church, 1998). Therefore, these methods may provide different estimates and all of them are considered isolated observations, i.e. do not represent a cross-section average value. The detection range of tracking devices (e.g. iron detectors, RFID-antenna) is in many cases of 0.5 to 1 m, which may establish an upper boundary of the fill depths that can be recorded from tracer burial. Nonetheless, it is true that the insertion depth of scour chains is often ~1 m (Table 1), hence both methods show a comparable limit of the maximum scour depth they can provide. Additionally, it should be noticed that the use of tracers and scour chains to approach the active thickness is limited by the tracer size (usually larger than ~20 mm) and the length of the scour chain links. This may underestimate the importance of finer particles such as the sand and small gravel on river's load.

In order to explore the potential influence of the sampling strategy in the active depth measurements, we compared the data grouped in relation to the method employed to estimate the active layer (Figures 1 and 2). Figure 1 shows comparable trends in the relationship between flow strength and active depth. Even so, it is worth mentioning that the number of observations per method is not the same, which may affect the observed trends. Even though flow intensity is very variable, no large differences between methods are observed (i.e. differences between median values are minimum in Figure 2A). Conversely, some differences are observed in terms of the active depth between the different methods, i.e. data from indirect estimations and active RFID columns report overall larger active depths with equivalent (or even lower) flow intensities (Figure 2B). The differences are statistically significant at a 95% confidence level (Welch's t-test, p-value <0.05) between the RFID columns and the rest of

393 methods, but not amongst the scour chain, tracer burial and indirect estimations.
394 In principle, this may suggest some effect of the sampling methods on the active
395 depth observations. However, the different groups of data are not well balanced
396 in terms of dominant channel morphology (Table 1). Active depth data from tracer
397 burial and scour chains correspond mainly to riffle-pool rivers while data from
398 indirect estimations come from step-pool streams (Erlenbach, Rio Cordon;
399 Schneider et al., 2014), and data from active RFID column come from a single
400 study in two highly dynamic braided alpine rivers (Drac and Vénéon, French Alps;
401 Brousse et al., 2018). Consequently, thicker active depths observed in active
402 RFID data may reflect higher active depths in braiding morphologies rather than
403 a methodological bias. Similarly, the different slope in data trends observed
404 between active depth and flow strength from indirect estimations (Figure 1) could
405 also point to different behaviour in step-pools compared to other morphologies,
406 rather than a methodological issue.

407 In addition to the uncertainties given by the method used to measure the active
408 layer, the way in which flow metrics are estimated may also be relevant. For
409 example, we have linked active depth to flow metrics estimated based on the
410 peak *Q*; however, active depth might better relate to time-integrated flow metrics,
411 as happens with travel lengths of tagged stones (Haschenburger, 2013; Phillips
412 and Jerolmack, 2014; Schneider et al., 2014; Papangelakis and Hassan, 2016).

413 Unfortunately, the general lack of data on cumulated streamflow in the compiled
414 papers do not allow us to explore in depth this question for the complete dataset.
415 Nevertheless, some of the selected studies do provide time-integrated flow
416 metrics, which allowed us to estimate the cumulated streamflow over the critical
417 discharge for a few case studies (Figure 3A).

We observe a large scatter between the different streams when using the time-integrated flow metrics (R^2 is 0.36 when using the peak discharge, while in case of cumulated discharge R^2 is 0.12), which contrasts with the tendency of the data to converge into a common trend when using the peak flow intensity (compare figure 3A to 3B). Even though a good positive covariation could be observed between cumulated competent flow and active depth at the scale of each single study case, the peak Q appears as a more adequate metric when describing the overall trends in active depths in the compiled data as a whole. In truth, we could expect active depths to be related to competent sizes, through the scaling between active thickness and particle entrainment. That said, a clast of a given size would not move until the value of its entrainment τ is reached, independently of the flow duration. In this regard, Hassan et al. (1992) also reported how the virtual velocity of travel was better correlated to the first peak of the flow event rather than to the total time for which the flow is larger than that needed to initiate clast movement. Hence, the larger competent particle-size during floods should be more driven by the attained peaks of discharge, rather than by the total competent flow duration; the latter being more influent on other aspects such as bulk bedload volumes or particle transport distances.

3.3. Active layer and channel morphology

Data were grouped according to channel morphology (PB: plane-bed, RP: riffle-pool, SP: step-pool and MT: multi-thread) in order to then re-analyse how the active depth correlates with flow strength. We applied an ANCOVA test and we observed some statistically significant effects (p-value<0.05) of channel morphology on the regression between active depth and flow intensity. In this regard, several trends according to dominant channel morphology were identified

443 (Figure 4A, 4B and Table 2). PB and RP show comparable scaling between active
444 depth and flow metrics, whereas SP values tend to plot above the other
445 morphologies, altogether suggesting that active layer tends to be thicker in SP
446 than in RP and PB streams for equivalent flow strengths, especially in floods
447 larger than bankfull discharge. Furthermore, SP streams scale steeper with flow
448 strength, indicating a larger difference between low flow and high flow episodes
449 in terms of active depth compared to RP and PB. The differences between MT,
450 RP/PB and SP are statistically significant at 95% confidence level, but not the
451 differences between PB and RP (Student's-Newman-Keuls posthoc test).
452 Despite scarce data from MT streams, they tend to plot closer to the upper
453 envelope of data and above RP and PB. It is also worth noting that at relatively
454 low flow intensities, observations from the different channel morphologies tend to
455 converge, while at higher flow intensities SP and RP display clearly separated
456 trends.
457 Different geomorphological processes controlling active layer depth in gravel-bed
458 rivers have been described (e.g. Bigelow, 2005), which include uniform
459 entrainment of the armour layer during bedload transport (Wilcock et al., 1996;
460 DeVries, 2002), localized scour and fill caused by secondary flows around
461 boulders and obstructions (Lisle, 1986; Rennie and Millar, 2000), stage-
462 dependent variations of τ in pools and riffles (Keller, 1971; Lisle, 1979), bedform
463 and gravel sheet migration that cause net aggradation or degradation over one
464 or a few events (DeVries et al., 2002), and large-scale channel aggradation and
465 or degradation (Grifits, 1979; Madej and Ozaki, 1996). The relative influence of
466 these factors can vary between sites and settings (Bigelow, 2005) and this may
467 help to explain the different trends reported here. The SP configuration is defined

by an accumulation of jammed cobbles and boulders that are transverse or oblique to the channel (Zimmerman and Church, 2001), alternating with pools containing finer materials. During low flow conditions, active layer depth should be mainly controlled by the exportation and recharge of the relatively fine bed-material (Piton et al., 2016; Piton and Recking, 2017) stocked in pools and around large immobile boulders; then, a relatively thin active layer could be expected. With high flow conditions, a breakup and rearranging of the SP structure could otherwise be expected (Church and Zimmerman, 2007; Zimmerman et al., 2010), thus a sudden increase in the depth of the active layer. This may explain larger differences in active depth between low-flow and high-flow conditions in SP streams and consequently, the steeper scaling between active depth and flow intensity reported here. Additionally, this also explains the convergence of the trends for low intensities. Conversely, in RP and PB streams, the thickness of the active layer is hypothetically controlled mostly by the disorganization of the streambed surface i.e. this may involve a more progressive increase in active depth with flow strength, which may account for the gentler scaling observed with flow strength. Also, grain-size tends to be coarser in SP than in RP and PB channels, so this may explain why SP channels show an overall coarser active layer than RP and PB streams. Finally, in the case of MT channels, the migration of large gravel-sheet bodies might control active depths rather than grain entrainment; this could be the reason for the relatively larger active depths observed in MT channels in comparison to RP and PB channels. When the active depth is normalized by median grain-size (Figure 4B), SP, PB and MT data plot in the same area as RP observations. This again indicates some influence of grain-size on the scaling of the active depth to flow strength, and shows that in

493 SP rivers the D_{50} entrains with Q close to the bankfull, while larger flow intensities
494 are required for the PB and RP. Apart from this, the slope in SP is steeper (as
495 shown in Figure 4A), involving larger differences between low- and high-
496 magnitude flows in SP compared to RP/PB streams and illustrating again the
497 importance of channel configuration in the thickness of the active layer.

498 In this regard, the differences observed in the goodness-of-fit between the
499 different group of data could be also partially related to a different behaviour of
500 active layer according to channel morphology, although the differences in the
501 number of studies available for each group of data should not be disregarded:
502 available data is particularly low in case of MT and PB (5 and 9 points,
503 respectively). When active depths are normalized by D_{50}, the strength of the
504 correlation decreases in case of RP and PB channels, whereas we observe a
505 slight increase in SP streams; in case of PB, the correlation is even not
506 statistically significant when normalizing by D_{50}. Perhaps in PB streams the cross-
507 sectional component of the bedload and the increase in the bed surface particles
508 recruited into the bedload is more important in controlling the extent of the active
509 layer, rather than the size of the bed particles in itself. On the other hand, in SP
510 channels, it could happen that the larger scale of protruding keystones and
511 boulders involve a more important control of grain-size on active depth compared
512 to RP and PB. Additionally, results from the simple regression analysis (Table 2)
513 show some moderate and significant positive power correlation between active
514 depth and flow intensity in case of RP, SP and PB channels, but not in case of
515 MT. In laterally unstable MT rivers, surface-exchange of particles could not be
516 the most important mechanism in driving active depth, but the changes in channel
517 form, as suggested by Ashmore and Leduc (2018). In this case, flow intensity

would not be a relevant control of active depth in MT rivers, bust mostly flow duration; this may help explain the poorer goodness-of-fit observed in this group of data.

3.4. Active layer and bed surface (in)stability

Here we compared active depth to grain-size, accounting for differences in streambed mobility and bed surface stability (Figure 5).

To characterize streambed mobility conditions, we used the ratio between the computed τ at the peak Q and τ_c for inception of motion of the surface D_{84} (i.e. transport stage ratio), assuming that entrainment of the coarser particles in the streambed drives bed surface destabilization. According to Wilcock and McArdell (1993), bed surface mobility evolves from entrainment to full-mobility conditions with the progressive increase in τ from 1 to 2 times τ_c, with the transition from one stage to the other being governed by the progressive increment in the fraction of mobile particles (partial mobility). Then, we considered that a transport stage equal to 1 defines a bed-averaged threshold between stability and entrainment, whereas a transport stage equal to 2 defines an average threshold between partial- and full-mobility conditions within the compiled data, following Wilcock and McArdell (1993) and MacKenzie et al. (2018). The comparison shows a conspicuous difference between those transport events with more ability to destabilize the bed surface layer ($\tau^*/\tau_c^*>1$) and the episodes where the coarse grains would, in principle, remain static ($\tau^*/\tau_c^*<1$), i.e. the thickness of the active layer tends to be greater than the D_{50} in the former, whereas it tends to be less in the latter. Indeed, the active layer tends to approach 1 to 5 times the D_{50} when transport stages are between 1 and 2, and tends to be finer than the D_{50} when transport stages are below 1 (no bed surface destabilization). Differences are

543 statistically significant at a 95% confidence level (one-way ANOVA, p-value <
544 0.05). This finding highlights the importance of coarser-grain entrainment and the
545 armour break-up in defining the depth of vertical exchanges during bedload. In
546 this regard, Houbrechts et al. (2012) reported relatively low thicknesses for the
547 active layer in comparison to other published values (e.g. DeVries, 2002; Lenzi
548 et al., 2006; Rovira and Kondolf, 2008). They attributed this to the flatness of the
549 schist pebbles present in their research, and to the consequent imbricated and
550 armoured bed surface. Similarly, Reid and Frostick (1984) and Church and
551 Hassan (2002) previously reported how particle arrangements could increase the
552 thresholds for incipient motion. More recently, Perret et al. (2020) have observed
553 similar trends in a flume. These previous field and flume observations are in the
554 same vein as the results reported here and outline the importance that bed
555 surface destabilization may have on the active layer depth, i.e. coarser
556 streambed surfaces prevents bed scouring and limits the depth of the active layer
557 for low flow intensities.

558 River morphologies also show differences when plotting the relation between
559 active depth and D_{50} and accounting for streambed mobility conditions. RP rivers
560 display along the whole range of D_{50} particle sizes, and also registered a wide
561 range of active depths. In fact, this morphology is the only one for which active
562 layer depth data is available for streams with relatively small D_{50}, i.e. all river
563 reaches with $D_{50} \leq 40$ mm display in the upper left part of the graph (Figure 5).
564 PB observations with transport stage ratios <1 show small values of active layer
565 thickness (< 80 mm) and also large D_{50} (> 60 mm). Conversely, PB observations
566 with transport stage ratios between 1 and 2 show very similar values of active
567 layer thickness and D_{50}. Data for SP rivers correspond in all cases to rivers with

568 D_{50} > 50 mm. When SP observations correspond to transport stage ratios where
569 the bed surface layer was destabilised (larger than 1), active depth is again
570 coarser than the D_{50}. However, when transport stages are lower than 1, the depth
571 of the active layer is close to the D_{50} and thicker compared to PB and RP
572 observations. MT data have D_{50} between 35 and 80 mm and no clear trends are
573 observed between bed surface destabilization, active depth and grain-size. Data
574 for MT morphologies are scarce and they do not allow to further explore this
575 issue, but the dynamic and complex morphological patterns of MT channels
576 introduce a large cross-section variability, not adequately grasped with a section
577 averaged transport stage ratio.

578 Haschenburguer (1999) already related the average scour and fill depth of a
579 gravel bed reach to the streambed mobility quantified through the transport stage
580 ratio. This author proposed the following expression:

581 $$h = \alpha \cdot e^{\beta \cdot \frac{\tau^*_{50}}{\tau^*_{ref}}}$$ Eq. 2

582 where h is the average scour and fill depth (in mm), τ^* is the Shields' stress
583 (estimated for the D_{50}), τ_{ref}^* is a reference threshold stress for incipient motion.
584 Haschenburger (1999) followed the common practice of using 0.045 as τ_{ref}^*.
585 Concerning α and β, these are the empirical intercept and exponent, for which
586 this author proposed the values of 3 and 1.52, respectively. We compared the
587 compiled data with Haschenburger's (1999) model (Figure 6). In general, RP and
588 PB data plot close to the curve defined by Eq. 2 (Figure 6A). Conversely, data
589 from SP fall well below the model estimation. Since Haschenburger (1999),
590 several authors have shown how the threshold stresses for the D_{50} in gravel-bed
591 rivers may vary with bed slope (example, Mueller et al., 2005; Lamb et al., 2008;

592 Recking, 2009); with data tending to get closer and collapse around the curve
593 defined by Eq. 2 when using a slope-dependent threshold stress (Figure 6B)
594 (based on Recking, 2009). However, there are again differences between the
595 different channel morphologies (Table 3). Specifically, SP and MT data tend to
596 plot over RP. Differences are statistically significant at a 95% confidence level
597 between MT and SP/RP/PB, but not between SP, RP and PB (ANCOVA
598 Student's-Newman-Keuls posthoc tests, p-value<0.05). In addition, comparison
599 between different shapes for the regression equations suggest that a power-law
600 provides a similar or slightly better description of active depths (Table 4).

601 The degree of correlation between the active depth and the transport stage
602 increases when active depth is normalized by surface D_{50} (Figure 6C). Again, this
603 fact highlights the influence of bed sediment size on the thickness of the active
604 layer. Differences between different morphologies persist: at low transport
605 stages, step-pool streams tend to show lower active depths than RP. However,
606 once the bed surface layer starts to destabilize ($\tau^* / \tau_{ref}^* > 1$), SP data tend to plot
607 in the upper envelope of RP values. Similarly, MT tend to show larger active
608 depths than the other channel configurations for equivalent transport stages. PB
609 data again display in the same zone as RP.

610 Moreover, it should not be neglected that some of the observed differences
611 between the different channel morphologies could be related to the way we
612 computed the transport stage ratios. First, we assumed a rectangular uniform
613 channel. We proceed like this because this was the only possible way to treat
614 homogeneously all the compiled data with the available information contained
615 within the original papers. However, as the irregularity of channel cross-sectional
616 geometries adds significant variation to hydraulic radius compared to rectangular

cross-sections, this inevitably introduces bias (particularly in case of MT and RP rivers with well-developed channel morphologies). Also, our estimations represent section-averaged computations of transport stages. Therefore, it is probable that 1D averaged τ have different meaning in MT and RP streams compared to SP and PB channels in terms of cross-sectional variability in τ_c distributions (Recking et al., 2016). Despite this, the previous findings still represent a good empirical confirmation on how the increase in mobility of the bed sediment and the progressive recruitment of increasingly larger grains controls the vertical extent of the active layer, despite the dominant channel morphology largely nuancing the links between bed remobilization and active depths.

3.5. Active depth and particle transport distances

The event-based bedload volume equals the dimensions of the active layer (active width times depth) times the mean distance of transport of individual particles (e.g. Haschenburger and Church, 1998; Liébault and Laronne, 2008). Consequently, bedload accommodates increasing volumes with increasing discharges through deeper active depths, wider active widths, longer particle transport distances and also with a higher fraction of mobilized particles (F_i) and so a relation can be expected between these four distinct bedload dimensions. Figure 7A shows the relation between two of these dimensions: active depth and mean travel distance i.e. an overall linear correlation between mean transport distances and active depths exists (p-value <0.05), which suggests that both the active depth and the transport distances increase linearly with the rise in flow intensity. In this regard, DeVries (2002) suggested that bedload transport rate in coarse streambeds increases primarily with the mobile fraction of bed surface

642 and the grain velocity, rather than with the active layer thickness. However,
643 Schneider et al. (2014) documented the opposite trend in the Erlenbach and
644 Cordon rivers, where they observed that bedload volumes scale steeper with ω
645 than transport distances. This led them to suggest that larger bedload volumes
646 arise primarily from deeper bed scouring and only secondarily from longer
647 transport distances. Some of these differences may result from geomorphic
648 controls on bedload transport processes. Indeed, in our database, we can
649 observe a different behaviour between the different channel morphologies in the
650 way the active depth and travel lengths scale together (Figure 7B; Table 5), with
651 SP plotting in the upper envelope of data and showing a gentler slope than RP
652 and PB data. These differences between SP, RP and PB data are statistically
653 significant (ANCOVA and Student's-Newman-Keuls posthoc tests, p-
654 value<0.05).

655 Distinct channel morphologies and dominant macro-bedforms involve differences
656 in 3D water flow patterns and the cross-sectional τ distribution (Ferguson, 2003;
657 Francalanci et al., 2012; Recking et al., 2016), which in turn influences bedload
658 fluxes, sediment sorting and particle trajectories (Recking et al., 2016; Vázquez-
659 Tarrío et al., 2018; Vázquez-Tarrío and Batalla, 2019). In this regard, macro-
660 bedforms influence travel distances in two contrasting ways. On the one hand,
661 gravel bars, transverse ribs and keystones can entrap sediment at low flow
662 intensities and slow down downstream particle transfer. On the other hand,
663 macro-bedforms concentrate flow and sediment particles into preferential paths,
664 which promote a faster sediment conveyance when particles 'fall' into them.
665 Similarly, causes for active depth fluctuations may differ according to channel
666 morphology. For instance, bed surface disorganization may be a major driver of

667 active depth oscillations in PB and RP channels, while gravel sheet migration
668 could more likely control active depth in MT (and RP rivers well supplied in
669 sediment). In the case of SP streams, the removal/recharge of fine sediments
670 from pools would also influence the vertical extent of the active layer.
671 Furthermore, our PB data show how mean travel distances have a steeper power
672 scaling to flow intensity than active depths (~1.62 *vs* ~0.40 power exponents:
673 Figure 8A). This implies that increasing bedload volumes are accommodated
674 primarily by further travel distances in such streams, which may relate to the lack
675 of macro-bedforms entrapping travelling particles. In RP channels travel
676 distances still show a steeper scaling than active depth (Figure 8C). In addition,
677 active depths scale steeper to flow strength in RP than in PB rivers, and at the
678 same time mean travel distances show a gentler scaling than in PB data. Thus,
679 the rise in bedload volumes with *Q* is still primarily accommodated by larger
680 transport distances in RP rivers, but the vertical component of the bedload gains
681 in importance compared to PB, altogether outlining the influence of particle
682 trapping in gravel-bars and pool-riffle units. Conversely, in the case of SP
683 channels we observe the opposite trend (Figure 8B). Active depths show a
684 steeper scaling with flow intensity than transport distances; thus, the increase in
685 active depths has a relative greater importance when accommodating increasing
686 bedload volumes in this type of channels when compared to RP and PB streams.
687 The lower importance of mean travel distances for bedload volumes may be
688 related to the trapping of traveling particles in pools or behind boulders and
689 keystones, which temporally cease their movement until step-pool configuration
690 is disorganized by a major flood, notably extreme and rare floods (Lenzi, 2004;
691 Lenzi et al., 2006).

692 In summary, our analysis confirms that a linear correlation exists between
693 transport distances and active depths, considering that the event averaged
694 bedload volumes constitute some kind of irregular polyhedron defined by three
695 dimensions in space, represented by the active thickness, the active channel
696 width and the downstream distance encompassed by the travelling particles.
697 Apparently, the exact shape of this polyhedron is largely controlled by the
698 dominant channel morphology, which influences how sediment particles are
699 conveyed (Vázquez-Tarrío et al., 2019; Vázquez-Tarrío and Batalla, 2019), the
700 kind of mechanism involved in active depth fluctuations (Haschenburger, 1999;
701 Bigelow, 1999) and the amount of sediment that is mobilized during floods
702 (Recking et al., 2016). This explains the observed 'morphological imprint' that
703 blurs and introduces scatter over the general linear scaling between transport
704 distances and active depths (Figure 7).

705 **3.6. Active depth and the fraction of mobile tracers**

706 In all the previous analysis we are not considering the changes in active width
707 (as a major component of channel geometry) and the fraction of mobile tracers
708 with flow strength, two another major dimensions of the active layer. Fluctuations
709 in active width and particle mobility can be a key control on bedload volumes and
710 fluxes (Wilcock and McArdell, 1997), particularly at low flow intensities, i.e., those
711 conditions close to thresholds for entrainment, where slight changes in flow
712 strength may involve a large variability in the amount of bed surface involved in
713 bedload motion, and in particular to MT channels.

714 Unfortunately, data on active width are in general lacking in the compiled papers,
715 so as of yet it has not been possible to explore in depth this issue. Nevertheless,
716 there was available information on the fraction of mobile tracers for some of the

compiled studies, so we decided to explore these data. On this point, we should highlight how tracer data are limited by the tracer size, i.e. in general only multi-centimetre pebbles can be tagged, as already stated above. This means that the finer portions of the bedload, such as the sand and small gravel, are unfortunately disregarded from our analysis.

We documented a very weak (but still statistically significant at a 95% confidence level, p-value < 0.05) exponential correlation between active depth and the fraction of mobile tracers (Figure 9). Hence, although there is a very slight increase in active depth with the mobility of bed particles, apparently, both parameters evolve one relatively independent to each other, i.e. they may represent two different 'degrees of freedom' through which gravel-bed rivers could accommodate increasing bedload volumes.

On the other hand, the fraction of mobile tracers represents somewhat a proxy for the 'pickup' or entrainment probability of bed particles. Bearing this in mind, the product of the fraction of mobile particles times the active depth and bankfull channel width provides an approximation to the cross-sectional active layer surface. Then, we based on this product to explore how active surface evolves with flow intensity in the compiled data. In general, we observe a moderate positive power correlation between flow intensity and active surface (Figure 10A). The observed trends are comparable between the different channel morphologies, although SP data shows a larger scatter and a slightly gentler slope (PB data as well). Nevertheless, differences are only statistically significant between PB and SP/RP, but not between SP and RP (ANCOVA and Student's-Newman-Keuls posthoc tests, p-value<0.05).

Moreover, when the data are segregated according to the dominant channel morphology, the mean tracer travel distances also show a moderate positive correlation with cross-sectional active surface in SP and PB, but not in case of RP (Figure 10B). The differences are statistically significant (at a 95% confidence level) between the SP/RP and PB groups of data (ANCOVA and Student's-Newman-Keuls posthoc tests, p-value<0.05). SP data plot in the upper envelope of the point cloud, which involves larger travel distances in SP streams for equivalent cross-sectional active surfaces. We also observe differences in the slope-coefficient. In PB data, mean travel distance increases with the ~1.4 power of active surface, a scaling considerably steeper than that observed in SP channels, i.e. mean travel distances increase faster as progressively more particles are liberated from the streambed in PB channels than in SP channels. Conversely, in RP group of data, there is large scatter in data and no clear correlation between the mean travel distances and the areal extent of the active layer (R^2=0.05; p-value>0.05). Yet again, these differences point at the distinct control exerted by the different channel morphologies on bed load transport. For instance, the steeper increase in mean travel distances with the extent of the active layer, observed in PB compared to SP/PB streams, may outline the importance of the increase in the cross-sectional extent of the active layer, involving a larger amount of particles set into motion, promoting a steep increase in mean travel distances. Conversely, the gentler scaling observed in case of SP streams and the lack of a clear correlation in RP rivers indicates that channel macroforms blunt the links between mean travel distance and the extent of the active layer observed in flat riverbeds. In this regard, the different behaviour observed in SP compared to PB may relate to the concept of travelling bedload

766 in SP streams, as proposed by Piton and Recking (2017). Whereas in RP and
767 PB streams, the transported bedload is mainly fed by the bed itself, in SP streams
768 it is very common to observe how sediment supplied by external sources can be
769 efficiently transported during floods, with marginal morphological activity and
770 without the breaking up of coarse armoured surfaces. This situation is close to
771 that of a tracer experiment, so the behaviour in terms of bedload transport of SP
772 streams may explain the observed gentler co-variation of mean travel distances
773 with the surface of the active layer in these streams, i.e. an increase in the extent
774 of the active layer with rising flow strength does not reflect in an equivalent
775 increase in mean travel distances. Finally, the lack of a clear covariation between
776 mean travel distances and active surface in RP streams may likely relate to
777 sediment trapping in bars, with the increase in particle mobility with increasing
778 flow strengths being balanced by sediment trapping of travelling gravels in bars.

779 **3.7. Multiple regression model**

780 Simple regressions allowed to discuss how active depths in gravel-bed rivers co-
781 vary with each considered variable separately. Following this first exploratory
782 analysis of each factor separately, we accomplished a stepwise multiple
783 regression analysis to understand the relative importance of each variable
784 compared to the others.

785 After applying stepwise regression procedures, the obtained multiple regression
786 model was (Table 5):

787 $$\log H = 0.556 + 1.878 \cdot log\left(\frac{\tau^*}{\tau_c^*}\right) + 1.287 \cdot log D_{50} + 0.126 \cdot log\left(\frac{Q}{Q_{bf}}\right) + \cdot 1.367 \cdot dBR \quad \text{Eq. 3}$$

788 The multiple regression analysis shows a strong and statistically significant
789 relationship between the active depth and the predictor variables (adjusted-R^2 =

790 0.58, p-value < 0.05). The fitted model coefficients are shown in Table 5. All
791 values of VIF are well below 10, which indicate that multicollinearity can be
792 dismissed.

793 The analysis of the relative weight of each predictor in explaining data scatter
794 indicates that flow intensity and transport stage are the two variables explaining
795 the larger amount of data variance (23% and 48% of R^2, respectively), followed
796 by the D_{50} of the bed surface (19% of R^2) and channel morphology (10%). The
797 influence of sampling methods is not significant in explaining the variance in data.
798 Although the multiple regression model explains a significant amount of variability
799 in the compiled field data, it remains an important amount of unexplained
800 variance (~40%). We think this is likely related to three potential sources: i.
801 methodological bias inherent to field measures; ii. the use of section- and time-
802 averaged values for parameters (grain size, shear stress, active depths, flow
803 discharge) that are intrinsically unsteady and heterogeneous in natural gravel-
804 bed rivers; and iii. the configuration of the bed surface in terms of protrusion,
805 imbrication, packing, particle shapes, etc. that may be highly variable across the
806 different study sites.

807

808 **4. Concluding remarks**

809 This paper analyses the relation between the active depth, the flow intensity and
810 the bed grain size dynamics for a variety of channel morphologies. The depth of
811 the active layer is a major component of the bedload and constitutes a major
812 driver in stream ecology by the creation and maintenance of physical habitat for
813 aquatic biota. The work is accomplished through a meta-analysis of published
814 and unpublished field data.

There were some contradictory previous observations in the geomorphological literature, some suggested that active depth is mostly controlled by flow strength, while others reported how active depths scale mainly with particle size. We believe that the large database here compiled, and the subsequent analysis, put us in a position to comment on what the dominant controls on the active depth in gravel-bed rivers are. Our results outline a compelling control of flow strength on active depths, but they also indicate the large influence that surface grain-size and particle entrainment exert on the vertical extent of the active layer. Furthermore, we have shown how dominant channel morphologies modulate the links between the flow strength and the active depth, documenting the existence of an important 'morphological imprint' on such fundamental geomorphic relation. Additionally, dominant macro-bedforms seem to control the way flow intensity scales to active depths and particle transport distances.

Our study also highlights the scarcity of data from braided rivers, probably linked to the difficulties inherent to sampling in this type of highly dynamic and often inaccessible rivers. This is due to the fact that multithread channels tend to be wide, with a large active surface, and this poses problem linked to the complexities when surveying tagged stones, and difficulties when retrieving scour-chains after floods. New methods based on passive (Papangelakis et al., 2019; Cain and MacVicar, 2020) and active RFID tracking (Brousse et al., 2018) appear to be promising for monitoring active depth in such complex systems.

By comparing field data for such a wide amount of rivers in this paper, we believe that we are teasing out relevant lessons on how bedload transport behaves in natural gravel-bed rivers, which in turn provides a wonderful example of how field observation can provide very interesting information about sediment transport

processes in gravel-bed rivers. The strength of the 'field approach' increases when data from very different settings and streams can be ensembled and jointly analysed. However, this kind of analyses require the availability of good data, once more outlining the importance of field studies for the progress of fluvial geomorphology.

Appendix: computing hydraulic parameters from water discharge data

Discharge was the most widely available information used to characterize flow magnitude in the compiled papers. For this reason, we based our meta-analysis on discharge as reference flow metrics. Nevertheless, for some of the analysis it was necessary to estimate transport stages, hence shear stress was estimated from flow *Q*. We followed a workflow based on Rickenmann and Recking's fit (2011) to Ferguson (2007) flow resistance equation in order to compute flow depth from event discharge data:

$$U^{**} = 1.5471 \cdot q^{** 0.7062} \cdot \left[1 + \left(\frac{q^{**}}{10.31}\right)^{0.6317}\right]^{-0.4930} \quad \text{Eq. 4}$$

where:

$$U^{**} = \frac{U}{\sqrt{g \cdot S \cdot D_{84}}} \quad \text{Eq. 5}$$

$$q^{**} = \frac{Q}{w \cdot \sqrt{g \cdot S \cdot D_{84}^3}} \quad \text{Eq. 6}$$

where *g* is the gravity acceleration, *S* the bed slope, *w* the channel width, D_{84} is the 84th percentile of the surface grain-size distribution, *U* the average water velocity and *Q* the water discharge. This formulation was tested against a wide database of field data from gravel-bed rivers with satisfactory results (Rickenmann and Recking, 2011). Then, based on this set of equations and *Q*, we first estimated *U* and then derived section average flow depths (*d*) from:

$$d = \frac{Q}{U \cdot w} \quad \text{Eq. 7}$$

Later, and assuming a rectangular shape for channel cross-section, we computed the hydraulic radius (*R*):

$$R = \frac{w \cdot d}{2 \cdot d + w} \quad \text{Eq. 8}$$

Subsequently, we estimated section averaged bed shear stresses using the classical 'hydraulic radius-slope' product:

$$\tau = \rho \cdot g \cdot S \cdot R \quad \text{Eq. 9}$$

Once estimated the section averaged bed shear stresses, we also computed the dimensionless Shields stresses (τ^*):

$$\tau^* = \frac{\tau}{1650 * g \cdot D} \quad \text{Eq. 10}$$

where D is the grain-size. In this regard, we computed Shields stresses based on both the median size of surface sediment (D_{50}) and the D_{84}.

Finally, we estimated the critical Shields number for incipient motion, in order to compute the transport stage ratio, based on the slope-dependent critical Shields relation proposed by Recking (2009):

$$\tau^*_{c50} = 1.32 \cdot S + 0.037 \quad \text{Eq. 11}$$

$$\tau^*_{c84} = \tau^*_{c50} \cdot \left(\frac{D_{84}}{D_{50}}\right)^{-0.93} \quad \text{Eq. 12}$$

where τ_{c50}^* and τ_{c84}^* are the critical Shields for D_{50} and D_{84} entrainment, respectively.

Acknowledgements.

The present work has been possible thanks to the financial support provided by the grant ACB17-44, co-funded by the post-doctoral 'Clarín Program-FICYT' (Government of the Principality of Asturias) and the Marie Curie Co-Fund. This research was partly undertaken and benefited of the results and discussions provided in the background of the MorphPeak (CGL2016-78874-R) and MorphHab (PID2019-104979RB-I00) projects funded by the Spanish Ministry of Economy and Competiveness, Science and Innovation, and the European Regional Development Fund Scheme. Authors acknowledge the support of the Economy and Knowledge Department of the Catalan Government through the Consolidated Research Group 'Fluvial Dynamics Research Group' -RIUS (2017SGR-0459) and the CERCA Program. Damià Vericat is funded through the Serra Húnter Programme (Catalan Government). We would like to thank Daniel Grace for their review of the English version of the manuscript. We finally thank the Managing Editor, the Associate Editor and the two anonymous reviewers for their comments that substantially improved the final version of the manuscript.

Data availability statement

Data available in article supplementary material

REFERENCES

Andrews E.D. and Erman D.C. 1986: Persistence in the size distribution of surficial bed material during an extreme snowmelt flood, Sagehen Creek, northeastern California. Water Resources Research 22, 191-197.

Ashmore P, Peirce S and Leduc P. (2018) Expanding the “Active Layer”: Discussion of Church and Haschenburger (2017) What Is the “Active Layer”? Water Resources Research 53, 5–10, Doi:10.1002/2016WR019675. Water Resources Research 54: 1425– 1427.

Batalla RJ and Vericat D. (2009) Hydrological and sediment transport dynamics of flushing flows: implications for management in large Mediterranean rivers. River Research and Applications 25: 297-314.

Beechie TJ. (2001) Empirical predictors of annual bed load travel distance, and implications for salmonid habitat restoration and protection. Earth Surface Processes and Landforms 26 (9): 1025– 1034.

Béjar M, Gibbins C, Vericat D and Batalla RJ. (2020) Influence of habitat heterogeneity and bed surface complexity on benthic invertebrate diversity in a gravel-bed river. River Research and Applications: 1– 15.

Bigelow PE. (2005) Testing and improving predictions of scour and fill depths in a northern California coastal stream. River Research and Applications: 21, 909-923.

Brousse G, Liébault F, Arnaud-Fasseta G. and Vázquez-Tarrío D. (2018) Experimental bed active-layer survey with active RFID scour chains: Example of two braided rivers (the Drac and the Vénéon) in the French Alps. E3S Web of Conferences 40, 04016 (2018).

926 Cain A. and MacVicar B. (2020) Field tests of an improved sediment tracer
927 including non-intrusive measurement of burial depth. Earth Surface Processes
928 and Landforms.

929 Carling PA. (1987) Bed stability in gravel streams, with reference to stream
930 regulation and ecology. In: Richards, K. S. (ed). River Channels: Environment
931 and ProcessK, Instit. of Br. Geogr. Oxford, England; pp. 321-347.

932 Cassel M, Dépret T and Piegay H. (2017) Assessment of a new solution for
933 tracking pebbles in rivers based on active RFID. Earth Surface Processes and
934 Landforms 42 (13): 1938-1951.

935 Church M. (2006) Bed material transport and the morphology of alluvial river
936 channels. Annual Review of Earth and Planetary Sciences 34: 325– 354.

937 Church M and Haschenburger JK. (2017) What is the “active layer”? Water
938 Resources Research 53: 5– 10.

939 Church MA, McLean DG and Wolcott JF. (1987) River Bed Gravels: Sampling
940 and Analysis. In: Thorne, C. R., Bathurst, J. C. and Hey, R. D. (eds). Sediments
941 transport in Gravel Bed Rivers, John Wiley and Sons, New York; pp. 43-88.

942 Church M and Zimmermann A. (2007) Form and stability of step-pool channels:
943 research progress. Water Resources Research 43: W03415.

944 Comiti F, Da Canal M, Surian N, Mao L, Picco L and Lenzi MA. (2011) Channel
945 adjustments and vegetation cover dynamics in a large gravel bed river over the
946 last 200 years. Geomorphology 125 (1): 147– 159.

947 Dépret T, Piégay H, Dugué V, Vaudor L, Noirot B, Faure J-B, Cassel M, Le Coz
948 J and Camenen B. (2019) Estimating and restoring bedload transport through a

949 run-of-river reservoir. Science of the Total Environment (STOTEN) 654: 1146-
950 1157.

951 DeVries P. (2000) Scour in low gradient gravel bed streams: patterns, processes,
952 and implications for the survival of salmonid embryos. PhD dissertation,
953 University of Washington.

954 DeVries P. (2002) Bedload layer thickness and disturbance depth in gravel bed
955 streams. Journal of Hydraulic Engineering 128 (11): 983-991.

956 Ferguson RI. (2003) The missing dimension: Effects of lateral variation on 1-D
957 calculations of fluvial bedload transport. Geomorphology 56: 1–14.

958 Ferguson R, Bloomer D, Hoey T and Werritt A. (2002) Mobility of river tracer
959 pebbles over different timescales. Water Resources Research 38: 1045

960 Francalanci S, Solari L, Toffolon M and Parker G. (2012) Do alternate bars affect
961 sediment transport and flow resistance in gravel-bed rivers? Earth Surface
962 Processes and Landforms 37 (8): 866– 875.

963 Garcia C, Cohen H, Reid I, Rovira A, Úbeda X and Laronne JB. (2007) Processes
964 of initiation of motion leading to bedload transport in gravel-bed rivers.
965 Geophysical Research Letters 34: L06403.

966 Gibbins CN, Vericat D and Batalla RJ. (2007) When is stream invertebrate drift
967 catastrophic? The role of hydraulics and sediment transport in initiating drift
968 during flood events. Freshwater Biology 52: 2369-2384.

969 Gomez B. (1983) Temporal variations in bedload transport rates: the effect of
970 progressive bed armouring. Earth Surface Processes and Landforms 8 (1): 41–
971 54.

Gottesfeld AS, Hassan MA, Tunnicliffe JF and Poirier RW. (2004) Sediment dispersion in salmon spawning streams: The influence of floods and salmon redd construction. Journal of the American Water Resources Association 40: 1071–1086.

Griffiths GA. (1979) Recent sedimentation history of the Waimakariri River, New Zealand. Journal of Hydrology 18: 6–28.

Hales GM. (1999) Bed scour as a function of shields parameter: evaluation of a predictive model with implications for river management. MS thesis, Humboldt State University, Arcata, California.

Haschenburger JK. (1996) Scour and fill in a gravel-bed channel: observations and stochastic models. PhD thesis, University of British Columbia, 144 pp.

Haschenburger JK. (1999) A Probability model of scour and fill depths in gravel-bed channels. Water Resources Research 35 (9): 2857– 2869.

Haschenburger JK. (2013) Tracing river gravels: insights into dispersion from a long-term field experiment. Geomorphology 200: 121– 131.

Haschenburger JK. (2017) Streambed disturbance over a long flood series. River Research and Applications 33: 753– 765.

Haschenburger JK and Church M. (1998) Bed material transport estimated from the virtual velocity of sediment. Earth Surface Processes and Landforms 23: 791-808.

Hassan MA. Egozi R and Parker G. (2006) Experiments on the effect of hydrograph characteristics on vertical grain sorting in gravel bed rivers. Water Resources Research 42: W09408.

995 Hassan M and Bradley DN. (2017) Geomorphic controls on tracer particle
996 dispersion in gravel bed rivers. In: Tsutsumi, D. and Laronne, J. B. (eds).
997 Gravel-Bed Rivers, Processes and Disasters, Wiley-Blackwell, UK; pp. 439– 466.

998 Hirano M. (1972) Studies on variation and equilibrium state of a river bed
999 composed of nonuniform material. Transactions of the Japanese Society of Civil
1000 Engineers 4: 128–129.

1001 Houbrechts G, Van Campenhout J, Levecq Y, Hallot E, Peeters A and Petit F.
1002 (2012) Comparison of methods for quantifying active layer dynamics and bedload
1003 discharge in armoured gravel-bed rivers. Earth Surface Processes and
1004 Landforms 37: 1501-1517.

1005 James G, Witten D, Hastie T and Tibshirani, R. (2014) An Introduction to
1006 Statistical Learning: With Applications in R. Springer Publishing Company,
1007 Incorporated: Berlin/Heidelberg, Germany.

1008 Keller EA. (1971) Areal sorting of bed-load material: the hypothesis of velocity
1009 reversal. Geological Society of America Bulletin 82: 753–756.

1010 Kellerhals R and Bray DI. (1971) Sampling procedures for coarse fluvial
1011 sediments. *Journal of the Hydraulics Division ASCE* 97: 1165-1180.

1012 Kondolf GM, Gao Y, Annandale GW, Morris GL, Jiang E, Zhang J, Cao Y, Carling
1013 P, Fu K, Guo Q, Hotchkiss R, Peteuil C, Sumi T, Wang H, Wang Z, Wei Z, Wu B,
1014 Wu C and Yang C. (2014) Sustainable sediment management in reservoirs and
1015 regulated rivers: experiences from five continents. Earth's Future 2: 256-280.

1016 Kondolf GM and Wilcock PR. (1996) The Flushing Flow Problem: Defining and
1017 Evaluating Objectives. Water Resources Research 32 (8): 2589– 2599.

1018 Kondolf GM and Wolman MG. (1993) The sizes of salmonid spawning gravels.
1019 Water Resources Research 29 (7): 2275– 2285.

1020 Lamb MP, Dietrich WE and Venditti JG. (2008) Is the critical Shields stress for
1021 incipient sediment motion dependent on channel-bed slope? Journal of
1022 Geophysical Research 113: F02008

1023 Laronne J, Outhet DN, Carling P and McCabe PJ. (1994). Scour chain
1024 deployment in gravel-bed rivers. Catena 22 (4): 299-306.

1025 Laronne, J. B.; Garcia, C. and Reid, I. (2001). Mobility of patch sediment in gravel
1026 bed streams: patch character and its implications for bedload. In: Mosley, M. P.
1027 (ed). Gravel-Bed Rivers V, edited. N. Z. Hydrological Society, Wellington; pp.
1028 249–289.

1029 Lenzi MA. (2004). Displacement and transport of marked pebbles, cobbles and
1030 boulders during floods in a steep mountain stream. *Hydrological Processes*,18,
1031 1899–1914.

1032 Lenzi MA, Mao L and Comiti F. (2006) When does bedload transport begin in
1033 steep boulder-bed stream? Hydrological Processes 20: 3517–3533.

1034 Leopold LB, Wolman MG and Miller JP. (1964) Fluvial processes in
1035 geomorphology. W. H. Freeman and Company, San Francisco, California.

1036 Liébault F and Laronne JB. (2008) Factors affecting the evaluation of bedload
1037 transport in gravel-bed rivers using scour chains and painted tracers: the case of
1038 the Esconavette Torrent. Geodinamica Acta 21: 23– 34.

1039 Liébault F, Lallias-Tacon S, Cassel M and Talaska N. (2013) Long profile
1040 responses of Alpine braided rivers in SE France. River Research and
1041 Applications 29: 1253-1266.

1042 Liébault, F. and Piégay, H. (2002). Causes of 20th century channel narrowing in
1043 mountain and piedmont rivers of Southeastern France. Earth Surface Processes
1044 and Landforms, 27 (4), 425– 444.

1045 Liedermann M, Gmeiner P, Kreisler A, Tritthart M and Habersack H. (2018)
1046 Insights into bedload transport processes of a large regulated gravel-bed river.
1047 Earth Surface Processes and Landforms 43: 514– 523.

1048 Lindeman RH, Merenda PF and Gold RZ. (1980) Introduction to Bivariate and
1049 Multivariate Analysis; Scott Foresman & Co: Glenview, IL, USA.

1050 Lisle TE (1979). A sorting mechanism for a riffle-pool sequence. Geological
1051 Society of America Bulletin 91: 1142–1157.

1052 Lisle TE. (1986) Stabilization of a gravel channel by large streamside obstructions
1053 and bedrock bends, Jacoby Creek, northwestern California. Geological Society
1054 of America Bulletin 97: 999–1011.

1055 Madej MA and Ozaki V. (1996) Channel response to sediment wave propagation
1056 and movement, Redwood Creek, California, USA. Earth Surface Processes and
1057 Landforms 21: 911–927.

1058 Mao L, Picco L, Lenzi MA and Surian N. (2017) Bed material transport estimate
1059 in large gravel-bed rivers using the virtual velocity approach. Earth Surface
1060 Processes and Landforms 42: 595– 611.

1061 MacKenzie LG and Eaton BC. (2017) Large grains matter: contrasting bed
1062 stability and morphodynamics during two nearly identical experiments. Earth
1063 Surface Processes and Landforms 42: 1287– 1295.

1064 MacKenzie LG, Eaton BC and Church M. (2018) Breaking from the average: Why
1065 large grains matter in gravel-bed streams. Earth Surface Processes and
1066 Landforms, 43: 3190– 3196.

1067 Montgomery DR and Buffington JM. (1997) Channel-reach morphology in
1068 mountain drainage basins. Geological Society of America Bulletin 109: 596–611.

1069 Mueller ER, Pitlick J and Nelson JM. (2005) Variation in the reference Shields
1070 stress for bed load transport in gravel-bed streams and rivers. Water Resources
1071 Research 41: W04006

1072 Nelson PA, Venditti JG, Dietrich WE, Kirchner JW, Ikeda H, Iseya F and Sklar
1073 LS. (2009) Response of bed surface patchiness to reductions in sediment supply.
1074 Journal of Geophysical Research 114: F02005.

1075 Pähtz T. and Durán O. (2018) The cessation threshold of nonsuspended
1076 sediment transport across aeolian and fluvial environments. Journal of
1077 Geophysical Research: Earth Surface 123: 1638– 1666.

1078 Papangelakis E. (2015) The Effects of Channel Morphology on the Mobility and
1079 Dispersion of Sediment in a Small Gravel-bed Stream. MSc thesis, UBC
1080 (Vancouver, Canada), 84 pp.

1081 Papangelakis E. and Hassan MA. (2016) The role of channel morphology on the
1082 mobility and dispersion of bed sediment in a small gravel-bed stream. Earth
1083 Surface Processes and Landforms 41: 2191– 2206.

1084 Papangelakis E, Muirhead C, Schneider A and MacVicar B. (2019) Synthetic
1085 radio frequency identification tracer stones with weighted inner ball for burial
1086 depth estimation. Journal of Hydraulic Egineering 145: 12.

Parker G. (2004) 1D Sediment Transport Morphodynamics with Applications to Rivers and Turbidity Currents. Copyrighted ebook, available at:http://hydrolab.illinois.edu/people/parkerg//morphodynamics_e-book.htm.

Parker G. (2008) Transport of Gravel and Sediment Mixtures. In: García, M. (ed). Sedimentation Engineering: Processes, Measurements, Modeling, and Practice. Manual and Reports in Engineering Practice No. 110. American Society of Civil Engineers. Reston, USA; pp. 165-264.

Parker G and Sutherland AJ. (1990) Fluvial armor. Journal of Hydraulic Research 28 (5): 529–544.

Phillips CB and Jerolmack DJ. (2014) Dynamics and mechanics of bed-load tracer particles. Earth Surface Dynamics 2: 513– 530.

Phillips CB and Jerolmack DJ. (2019). Bankfull transport capacity and the threshold of motion in coarse-grained rivers. Water Resources Research 55: 11316– 11330.

Pierce JK and Hassan MA (2020). Joint stochastic bedload transport and bed elevation model: Variance regulation and power law rests. *Journal of Geophysical Research: Earth Surface*, 125, e2019JF005259.

Piqué G, Batalla RJ, Lopez R and Sabater S. (2017) The fluvial sediment budget of a dammed river (upper Muga, southern Pyrenees). Geomorphology 293 (A): 211-226.

Piton G and Recking A. (2017) The concept of travelling bedload and its consequences for bedload computation in mountain streams. Earth Surface Processes and Landforms 42 (10): 1505-1519.

1110 Piton G, Vázquez-Tarrío D and Recking A. (2016) Can bed-load help to validate
1111 hydrology studies in mountainous catchment? The case study of the Roize
1112 (Voreppe – FR). FloodRisk, Lyon, E3S Web of Conferences (Volume 7): 04020,
1113 12.

1114 Pyrce RS and Ashmore PE. (2005) Bedload path length and point bar
1115 development in gravel-bed river models. Sedimentology 52: 839– 857.

1116 Recking A. (2009) Theoretical development on the effects of changing flow
1117 hydraulics on incipient bed load motion. Water Resources Research 45: W04401.

1118 Recking A. (2013) An analysis of nonlineary effects on bedload transport
1119 prediction. Journal of Geophysical Research: Earth Surface 118 (3): 1264-1281.

1120 Recking A., Piton G., Vázquez-Tarrío D. and Parker G. (2016) Quantifying the
1121 morphological print of bedload transport. Earth Surface Processes and
1122 Landforms 41 (6): 809– 822.

1123 Rennie CD and Millar RG. (2000) Spatial variability of stream bed scour and fill:
1124 a comparison of scour depth in chum salmon (Oncorhynchus keta) redds and
1125 adjacent bed. Canadian Journal of Fisheries and Aquatic Sciences 57: 928–938.

1126 Rice SP, Johnson MF and Reid I. (2012) Animals and the Geomorphology of
1127 Gravel-Bed Rivers. In: Church, M.; Biron, P. M. and Roy, A. G. (eds).

1128 Rickenmann D and Recking A. (2011). Evaluation of flow resistance in gravel-bed
1129 rivers through a large field data set. Water Resources Research, 47, W07538.

1130 Richards K and Clifford N. (1991) Fluvial geomorphology: structured beds in
1131 gravelly rivers. Progress in Physical Geography 15 (4): 407-411.

1132 Roriva A.and Kondolf GM. (2008) Bed mobility on the Deschutes River, Oregon:
1133 tracer gravel results. Geodinamica Acta 21: 11–22.

1134 Schneider J, Turowski J, Rickenmann D, Hegglin R, Arrigo S, Mao L and Kirchner
1135 J. (2014) Scaling relationships between bed load volumes, transport distances,
1136 and stream power in steep mountain channels. Journal of Geophysical
1137 Research:. Earth Surface 119 (3): 533– 549.

1138 Shields A. (1936) Application of similarity principles and turbulence research to
1139 bedload movement. Originally published in german in 1936, english translation
1140 by W. P. Ott and J. C. van Uchelen, available in Hydrodynamics Laboratory
1141 Publication No. 167. Hydrodynamics Laboratory, California Institute of
1142 Technology, Pasadena, California.

1143 Staentzel C, Kondolf GM, Schmitt L, Combroux I, Barillier A and Beisel J-N.
1144 (2020) Restoring fluvial forms and processes by gravel augmentation or bank
1145 erosion below dams: A systematic review of ecological responses. Science of the
1146 Total Environment (STOTEN) 706: 135743.

1147 Tena A, Książek L, Vericat D and Batalla RJ. (2013) Assessing the geomorphic
1148 effects of a flushing flow in a large regulated river. River Research and
1149 Applications 29: 876-890.

1150 Van Campenhout J, Houbrechts G, Peeters A and Petit F. (2020) Return Period
1151 of Characteristic Discharges from the Comparison between Partial Duration and
1152 Annual Series, Application to the Walloon Rivers (Belgium). Water 12: 792.

1153 Vázquez-Tarrío D and Batalla RJ. (2019) Assessing controls on the displacement
1154 of tracers in gravel-bed Rivers. Water 11: 1598.

1155 Vázquez-Tarrío D and Menéndez-Duarte R. (2014). Bedload transport rates for
1156 coarse-bed streams in an Atlantic region (Narcea River, NW Iberian Peninsula).
1157 Geomorphology 217: 1– 14.

1158 Vázquez Tarrío D, Piégay H and Menéndez-Duarte R. (2020). Textural
1159 signatures of sediment supply in gravel-bed rivers: revisiting the armour ratio.
1160 Earth-Science Reviews.

1161 Vázquez-Tarrío D, Recking A Liébault F, Tal M and Menéndez-Duarte R. (2019)
1162 Particle transport in gravel-bed rivers: Revisiting passive tracer data. Earth
1163 Surface Processes and Landforms 44: 112–128.

1164 Vázquez-Tarrío D, Tal M, Camenen B and Piégay H. (2019) Effects of continuous
1165 embankments and successive run-of-the-river dams on bedload transport
1166 capacities along the Rhône River, France. Science of the Total Environment
1167 (STOTEN) 658: 1375-1389.

1168 Venditti JG, Nelson PA, Bradley RW, Haught D and Gitto AB. (2017) Bedforms,
1169 structures, patches, and sediment supply in gravel-bed rivers. In: Tsutsumi, D.
1170 and Laronne, J. B. (ed). Gravel-Bed Rivers: Processes and Disasters, chapter
1171 16. Wiley & Sons, Chichester, UK; pp. 439– 466.

1172 Vericat D, Batalla RJ and Garcia C. (2006) Breakup and reestablishment of the
1173 armour layer in a large gravel-bed river below dams: the lower Ebro.
1174 Geomorphology 76: 122–136.

1175 Vericat D, Batalla RJ and Garcia C. (2008) Bed-material mobility in a large river
1176 below dams. Geodinamica Acta 21(1-2): 3-10.

1177 Vericat D, Batalla RJ and Gibbins CN. (2008) Sediment entrainment and
1178 depletion from patches of fine material in a gravel-bed river. Water Resources
1179 Research: 44.

1180 Wilcock PR, Barta AF, Shea CC, Kondolf GM, Matthews WVG and Pitlick J.
1181 (1996) Observations of flow and sediment entrainment on a large gravel-bed
1182 river. Water Resources Research 32: 2897–2909.

1183 Wilcock PR and McArdell BW. (1997) Partial transport of a sand/gravel sediment,
1184 Water Resources Research 33: 235–245.

1185 Wolman M. (1954) A method for sampling coarse river-bed material. American
1186 Geophysical Union Transactions 35: 951–956, 1954.

1187 Zimmermann A and Church M. (2001) Channel morphology, gradient profiles and
1188 bed stresses during flood in a step-pool channel. Geomorphology 40: 311– 327.

1189 Zimmermann A, Church M and Hassan MA. (2010) Step-pool stability: testing the
1190 jammed state hypothesis. Journal of Geophysical Research. Earth Surface: 115,
1191 F2.

River	Source	S	W (m)	Q_{bf} (m^3/s)	D_{50s} (mm)	D_{50ss} (mm)	Morph	H (mm)	Method	L (m)	%	Q (m^3/s)	Observations	Duration tracer deployment
Great Eggleshop Beck	Carling (1987)	0.010	5.5	5.6	63	27	RP	15 - 45	Scour chains	No info	No info	0.8 – 7.4	Scour and fill were treated separately and averaged	
Lainbach	Gintz et al. (1996)	0.020	10.0	30.0	120	50-65	SP	50 - 910	Tracer burial	15.0 – 271.0	23 - 92	4.3 – 165.0	Tracer burial averaged over ~500 - 1000 initially seeded tracers	Up to 4 years, but after each survey, tracers were collected, carried and relocated at initial positions
Carnation Creek	Haschenburger and Church (1998)	0.006-0.012	11.7 – 18.3	~ 4.0	47	29	RP	44 - 240	Tracer burial / Scour chains (1 m depth)	25.8 – 125.9	9 - 70	17.7 – 36.3	Scoured and deposited tracers were treated separately, and averaged / Several scour indicators placed across the cross section	Up to 3 years
Forfar creek	Gottesfeld et al. (2004)	0.005-0.010	~ 12.0	No info	40-50	29	RP	0 – 180	Tracer burial	0.6 – 26.7	60 - 100	2.9 – 9.5	Tracer burial averaged over ~200 – 300 initially seeded tracers	Up to 5 years. Buried tracers were dug during recovery, which disturbs the bed
O'ne-ell Creek	Gottesfeld et al. (2004)	0.020	~12.0	No info	40-50	31	RP	0 – 80	Tracer burial	4.9 – 75.1	46 – 97	11.1 – 17.7	Tracer burial averaged over ~200 – 300 initially seeded tracers	Up to 5 years. Buried tracers were dug during recovery, which disturbs the bed
Freshwater Creek	Bigelow (2005)	0.007-0.011	12.0 – 13.0	14.2 – 21.6	39 – 46.5	-	RP	96 - 104	Scour chains	No info	90	17.1 – 25.9	Two reaches. Upper reach: 67 scour chains installed across 16 cross-sections. Lower reach: 98 scour chains installed across 15 cross-sections	
Ardenian rivers (17 streams)	Houbrechts et al. (2012)	0.002-0.010	2.0 – 24.0	1.3 - 300.0	30 - 95	-	RP / PB	9 – 80	Scour chains (1 m length)	4.9 – 297.0	No info	1.1 – 153.5	5-6 scour chains were placed transversally at each cross-section	
Erlenbach	Schneider et al. (2014)	0.150	3.5	2.0	64	~20	SP	4 – 570	Indirect estimation	6.9 -161	24 - 91	0.5 – 10.0	Active depth was back calculated from tracer travel distance and bedload data	Up to 2 years

River	Source	S	W (m)	Q_{bf} (m^3/s)	D_{50s} (mm)	D_{50ss} (mm)	Morph	H (mm)	Method	L (m)	%	Q (m^3/s)	Observations	Duration tracer deployment
Rio Cordon	Schneider et al. (2014)	0.130	5.7	3.0	90	~30	SP	7 – 550	Indirect estimation	1.0 – 142.0	52 - 100	0.9 – 10.4	Active depth was back calculated from tracer travel distance and bedload data	Up to 5 years
Pigüeña	Vázquez-Tarrío and Menéndez-Duarte (2014)	0.007	45.0	70.0	56	28	RP	100	Tracer burial	6.0	77	107.5	Tracer burial averaged over ~180 initially seeded tracers	~ 1 year
Coto	Vázquez-Tarrío and Menéndez-Duarte (2014)	0.010	30.0	17.0	88	70	RP	80	Tracer burial	15	30	25.6	Tracer burial averaged over ~130 initially seeded tracers	~1 year
East Creek	Papangelakis and Hassan (2016)	0.002/0.020	2.3 / 2.8	2.0	55/49	~20/30-40	PB / RP	27 – 79	Tracer burial	0.2 – 35.7	77-88	0.9 – 4.7	Tracer burial averaged over ~730 initially seeded tracers	Up to 8 years, 1 - 8 years. Buried tracers were dug during recovery, which disturbs the bed
Vénéon	Brousse et al. (2018)	0.016	141.5	80.0*	38	-	MT	55 - 1220	1-m active RFID columns	No info		53.0 – 113.5	Two 1-meter columns of active tags were deployed	
Drac	Brousse et al. (2018)	0.008-0.010	81.4 – 109.4	27.2*	61	-	MT	228-330	1-m active RFID columns	No info		85.1	Eight 1-meter columns of active tags were deployed	
Muga	University of Lleida, ICRA (unpublished)	0.008	19.2	8.9	53	37	RP	29 – 196	Scour chains (1 m length)	0.2 – 125.0	20 - 92	16.8 – 164	Four scour chains installed in a gravel bar. Painted and RFID tagged stones were used to track travel distance	1 year 7 months
Ebro	University of Lleida (unpublished)	0.00085	250.0	1100.0	12 - 68	12-32	RP	6 - 537	Scour chains (1 m length), metallic sticks and tracer burial	0.7 – 31.2		685.0 – 2498.0	Scour and fill were treated separately and averaged. Tracer burial was averaged over 69 initially seeded magnet-tagged stones	

Table 1. Sources of data and information about the field experiments compiled for the present study. *S*: Bed slope. *W*: Channel width. Q_{bf}: Bankfull discharge. D_{50s}: Median size of surface sediment. D_{50ss}: Median size of subsurface sediment. *Morph*: Channel morphology. *H*: Active depth. *L*: Mean tracer travel distance. *Q*: Discharge. %: Tracer recovery. PB: Plane-bed. SP: Step-pool. RP: Riffle-pool. MT: Multi-thread. *1-year discharge.

Morphology	Intercept[a]	Exponent[a]	R^2 [a]	*p-value*[a]	Intercept[b]	Exponent[b]	R^2 [b]	*p-value*[b]	*N*
Plane-bed	46.89	0.40	0.49	0.03	0.80	0.28	0.32	0.11	9
Step-pool	118.98	1.12	0.58	0.00	1.50	1.16	0.63	0.00	24
Riffle-pool	36.81	0.63	0.40	0.00	0.82	0.79	0.27	0.00	124
Multi-thread	131.98	0.98	0.26	0.38	3.34	0.57	0.10	0.60	5

Table 2. Results of the regression analysis shown in figure 4. Data were grouped according to channel morphology and fitted to a power law, after log transforming the dependent (active depth) and independent (flow intensity) variables. *N*: number of data. [a]Results obtained using the non-normalized active depths. [b]Results obtained using the active depth normalized by the median grain size of the surface sediment.

Morphology	α	β	R^2	*p-value*	N
Plane-bed	20.98	0.73	0.25	0.17	9
Step-pool	7.02	1.90	0.53	0.00	24
Riffle-pool	21.52	0.57	0.26	0.00	124
Multithread	46.45	1.13	0.11	0.58	5

Table 3. Results of the regression analysis fitting active depth to transport stage ratio (Eq. 1). Data were grouped according to channel morphology and fitted to an exponential law, after log transforming the dependent (active depth) variable. *N*: number of data.

Morphology	Power		Exponential	
	R^2	*p-value*	R^2	*p-value*
Plane-bed	0.25	0.17	0.25	0.17
Step-pool	0.56	0.00	0.53	0.00
Riffle-pool	0.32	0.00	0.26	0.00
Multi-thread	0.07	0.67	0.11	0.58

Table 4. Comparison between a power and an exponential regression fit between active depth and transport stage ratio. Data were grouped according to channel morphology. See main text for details and discussion

Variable	Coefficient	Standard error	t	*p-value*	VIF[1]	LMG[2]
Intercept	0.556	0.757	0.465	0.234	-	-
log D_{50}	1.287	0.157	8.184	0.000^{++}	2.012	0.195
log τ^*/τ_c^*	1.878	0.197	9.536	0.000^{++}	2.753	0.475
dBR	1.367	0.308	4.435	0.000^{++}	1.001	0.098
log Q/Q_{bf}	0.126	0.079	8.184	0.000^{++}	1.577	0.232

Residual standard error: 0.626 on 97 degrees of freedom. Multiple R^2: 0.621. Adjusted R^2: 0.601. F-statistic: 31.79 on 5 and 97 degrees of freedom. *p-value* = 2.2 × 10-6.

Tabla 5. Summary results of the stepwise multiple regression analysis. [1] Variance Inflation Factor. [2] Relative fraction of R^2 explained by each variable. [++] Variable statistically significant at a 95% confidence level.

Figure 1. A: Active depth plotted versus dimensionless flow intensity. B: Active depth (normalized by the surface D_{50}) plotted versus dimensionless flow intensity. In this figure, data have been grouped according to field methodology. Grey dashed lines represent (from up to down) the 99-th, 95-th, 75-th, 25-th, 5-th and 1-st quantile regression lines. Number of data: i) Average tracer burial: 69; ii) Scour chains/monitors: 71; iii) Indirect estimation: 17; iv) Active RFID: 5.

Figure 2. A: Differences in flow intensity according to field methodology in the compiled database. B: Differences in the active depth / D_{50} ratio. The boxes represent the range between the 25th and 75th percentiles, the dark lines the 50th percentile and the whiskers the upper and lower values corresponding to 1.5 times the interquartile range. Number of data: i) Average tracer burial: 69; ii) Scour chains/monitors: 71; iii) Indirect estimation: 17; iv) Active RFID: 5.

Figure 3. A: Active depth (normalized by the median size of bed surface) plotted versus the time-integrated dimensionless flow intensity, i.e. the cumulated flow discharge divided by the bankfull flow discharge. B: Active depth (normalized by the median size of bed surface) plotted versus the peak dimensionless flow intensity. For figure 3A, cumulated discharge was estimated based on our own data (for Coto, Pigüeña and Muga), and the information provided by the original papers. In case of East Creek (Papangelakis and Hassan, 2015), authors provided information on total excess energy expenditure. Schneider et al. (2014) provided information on excess specific stream power (Erlenbach data). Both excess energy expenditure and specific stream power were inverted to get the information on the cumulated stream power. For Lainbach data, Gintz et al. (1996) provided information on flow duration and peak discharge, so cumulated flow was approached as the product of peak discharge times flow duration.

Figure 4. A: Active depth plotted versus dimensionless flow intensity. B: Active depth Active depth (normalized by the surface D_{50}) plotted versus dimensionless flow intensity. Data have been grouped according to channel style.

Figure 5. Active depth plotted versus the median size of the surface sediment (D_{50}). Data were grouped according to streambed mobility conditions, quantified using the transport stage ratio (τ^* / τ_{c84}^*). τ^* is the peak Shields stress estimated based on the 84-th percentile of the surface sediment (D_{84}). τ_{c84}^* is the critical Shields stress for the surface D_{84}, computed based on Recking (2009).

Figure 6. Active depth plotted versus the transport stage ratio and compared to Haschenburger's (1999) active depth model. A: Transport stage estimated assuming a 0.045 value for the critical Shields stress. B: Transport stage estimated using a slope dependent critical Shields for the median size (D_{50}) of surface sediment (τ_{c50}^*), computed following Recking (2009). τ^* is the peak Shields stress estimated based on the D_{50} of the surface sediment. C: Active depth, normalized by the median size of the surface sediment (D_{50}), plotted versus the transport stage ratio.

Figure 7. Mean particle travel distance plotted versus the active depth. A: Plot for the ungrouped data. Upper and lower grey dash lines represent the 95-th and 5-th quantile regression lines. Dark line represents the mean regression line, which was accomplished only on the data plotting between the 95-th and 5-th quantile lines. B: Data grouped according to channel morphology. Multi-thread channel data are absent because there are no data available on particle travel distances for this group of data. Number of data: i) PB: 9; ii) SP: 22; iii) RP: 91.

Figure 8. Comparison between the mean particle travel distance and the active depth scaling to flow intensity. A: Plane-bed data. B: Step-pool data. C. Riffle-pool data. Data for multi-thread channels (MT) are absent, because there was no information on particle travel distances for MT rivers.

Figure 9. Active depth (normalized by the median size of bed surface), plotted versus the fraction of mobile tracers (Fi). Number of data: i) PB: 8; ii) SP: 17; iii) RP: 64.

Figure 10. A: Active surface plotted versus the dimensionless flow intensity. B: Mean tracer travel distance plotted versus active surface. Active surface was estimated as the product of the active depths, times the channel width times the fraction of mobile tracers. Number of data: i) PB: 8; ii) SP: 17; iii) RP: 55.

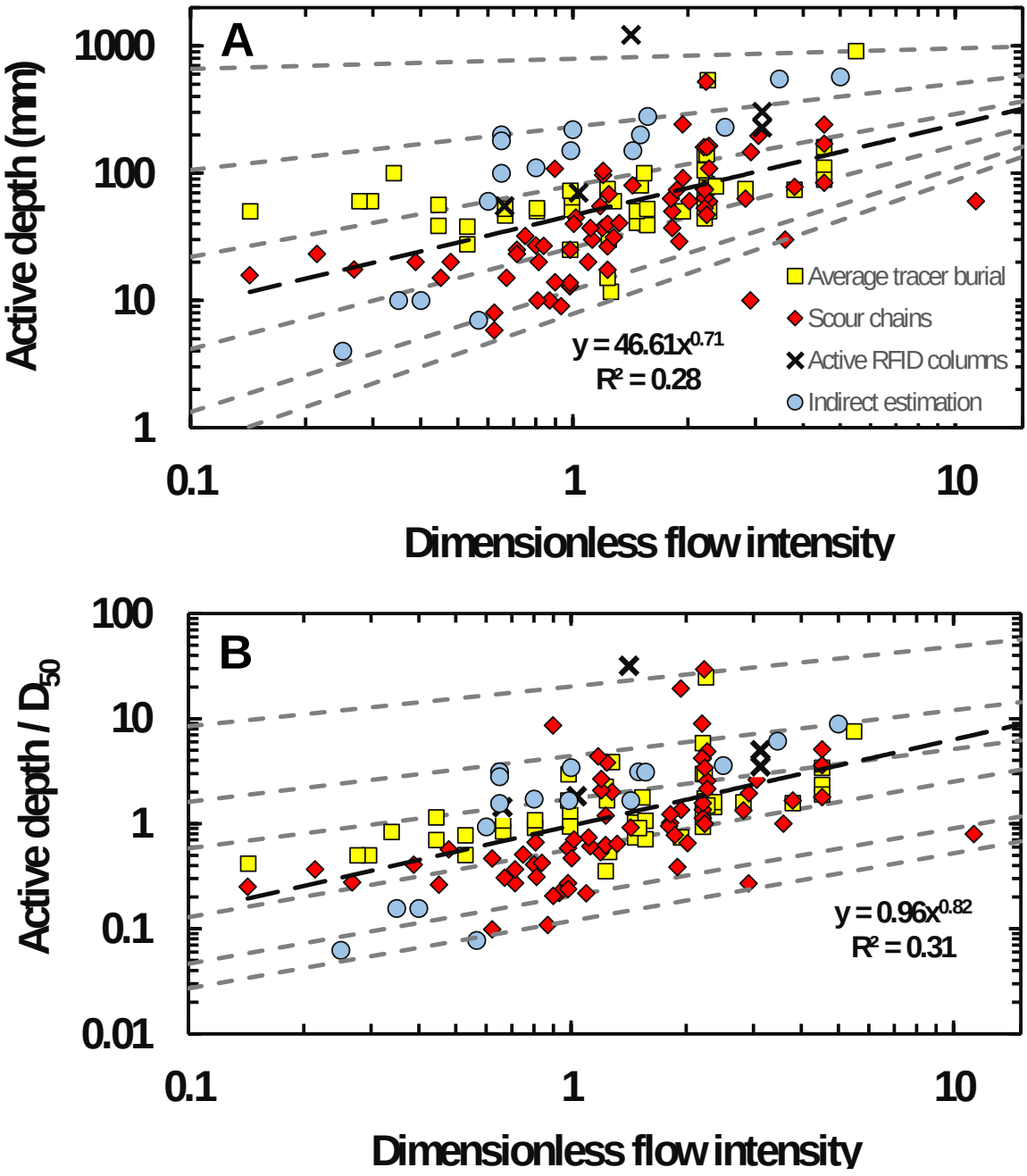
A
1000
100
10
1
0.1
1
10
Active depth (mm)
Dimensionless flow intensity
Average tracer burial
Scour chains
Active RFID columns
Indirect estimation
y = 46.61x^0.71
R² = 0.28
B
100
10
1
0.1
0.01
0.1
1
10
Active depth / D50
Dimensionless flow intensity
y = 0.96x^0.82
R² = 0.31

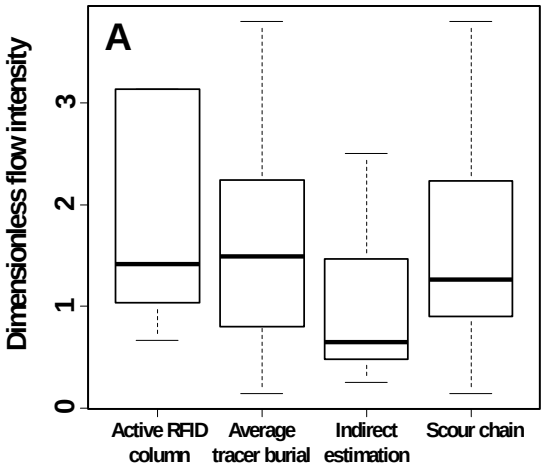

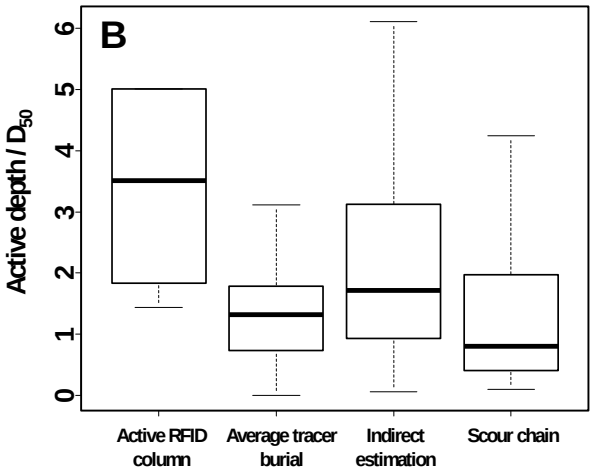

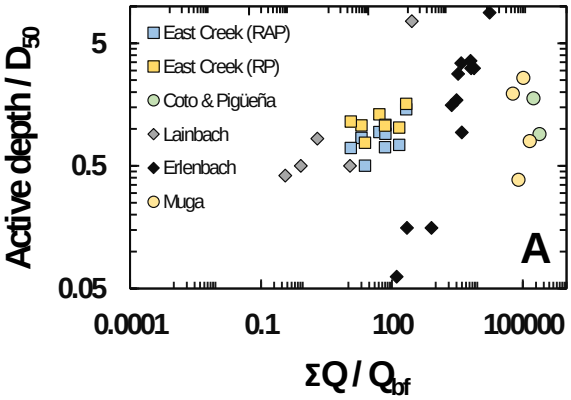

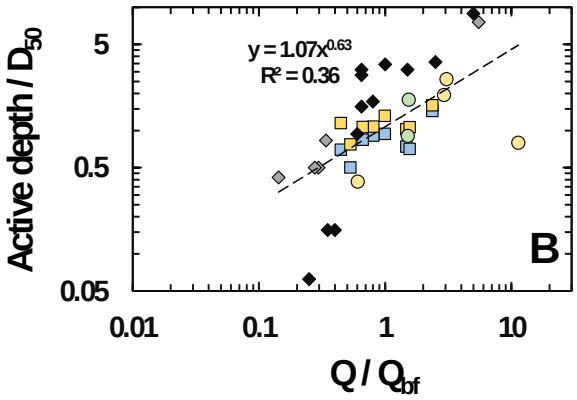

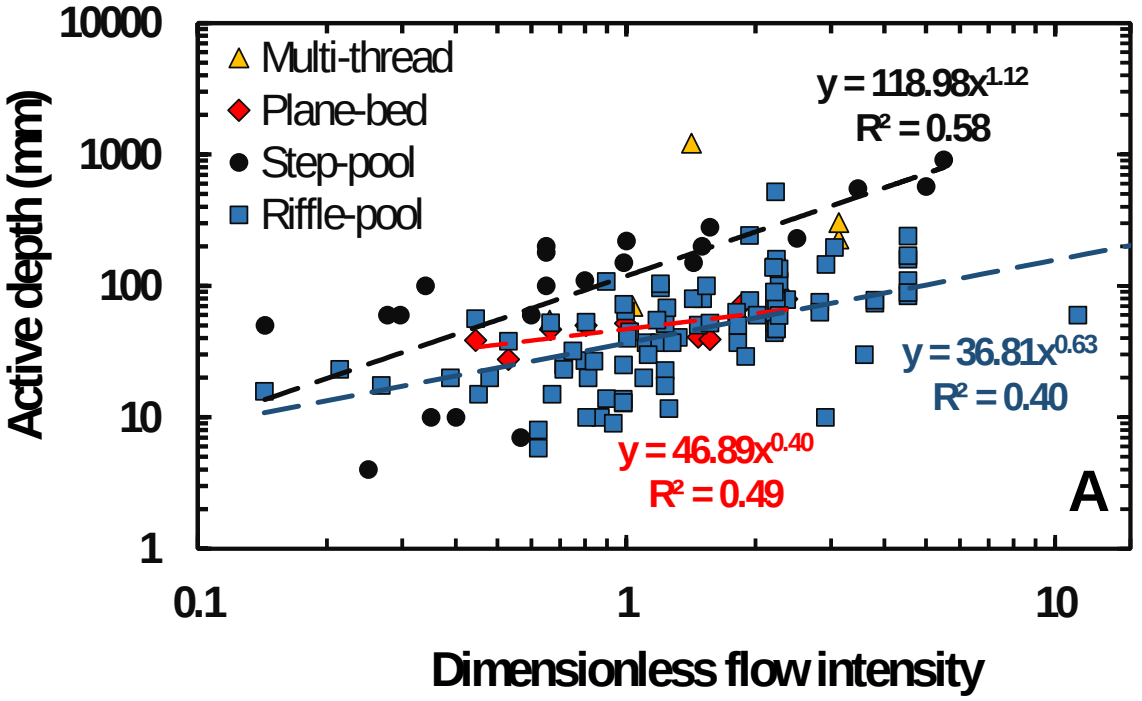
Active depth (mm)
10000
1000
100
10
1
0.1
1
10
Dimensionless flow intensity
Multi-thread
Plane-bed
Step-pool
Riffle-pool
y = 118.98x^1.12
R² = 0.58
y = 36.81x^0.63
R² = 0.40
y = 46.89x^0.40
R² = 0.49
A

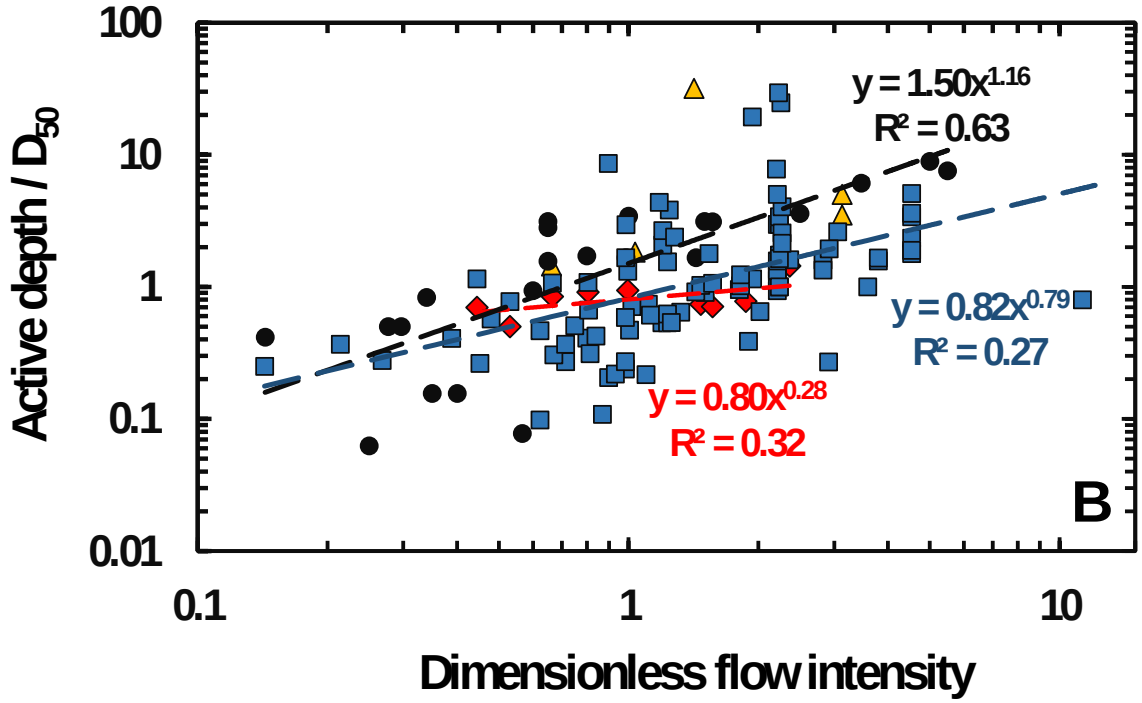
Active depth / D50
100
10
1
0.1
0.01
0.1
1
10
Dimensionless flow intensity
y = 1.50x^1.16
R² = 0.63
y = 0.82x^0.79
R² = 0.27
y = 0.80x^0.28
R² = 0.32
B

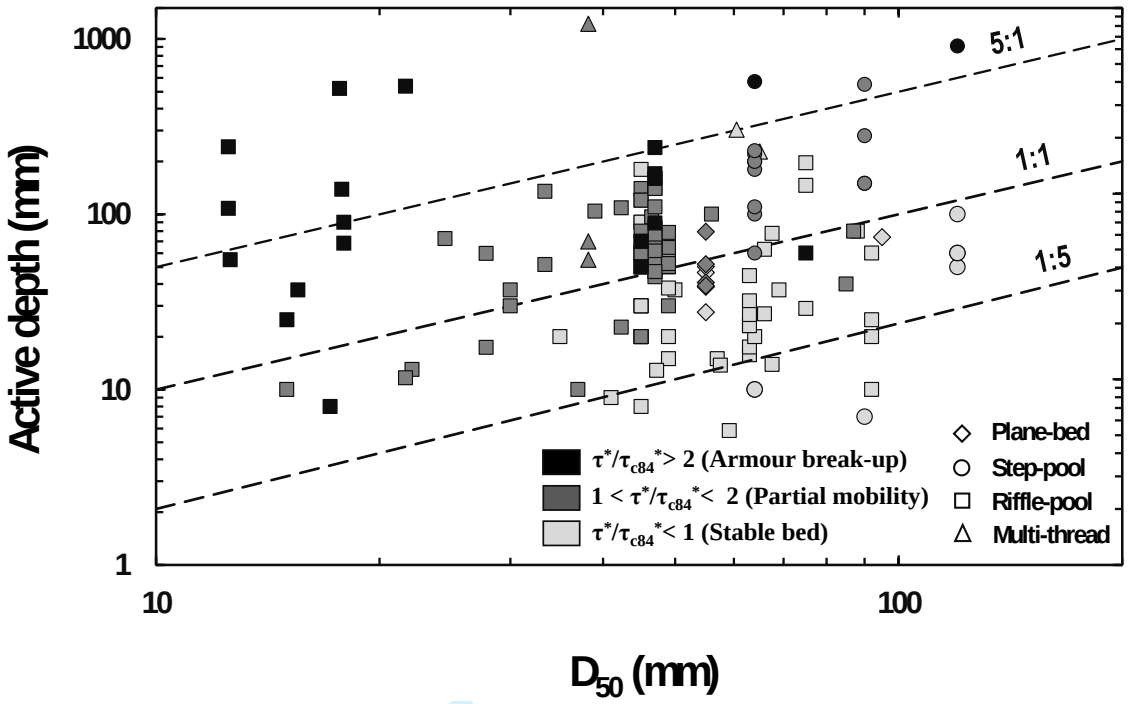
1000
100
10
1
10
100
Active depth (mm)
D50 (mm)
5:1
1:1
1:5
τ*/τc84*> 2 (Armour break-up)
1 < τ*/τc84*< 2 (Partial mobility)
τ*/τc84*< 1 (Stable bed)
Plane-bed
Step-pool
Riffle-pool
Multi-thread

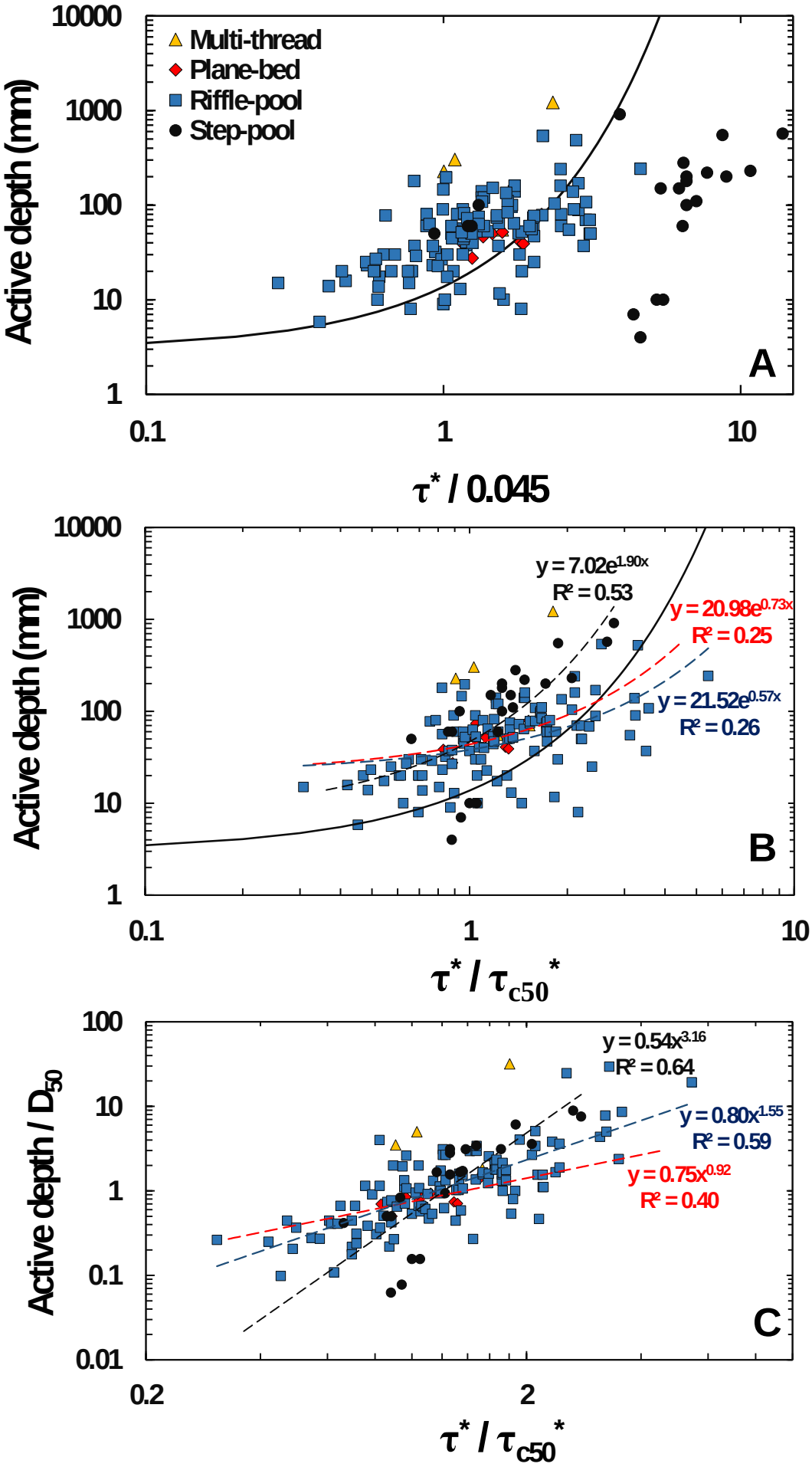
Multi-thread
Plane-bed
Riffle-pool
Step-pool
Active depth (mm)
10000
1000
100
10
1
0.1
1
10
τ* / 0.045
A
y = 7.02e1.90x
R² = 0.53
y = 20.98e0.73x
R² = 0.25
y = 21.52e0.57x
R² = 0.26
τ* / τc50*
B
Active depth / D50
100
10
1
0.1
0.01
0.2
2
y = 0.54x3.16
R² = 0.64
y = 0.80x1.55
R² = 0.59
y = 0.75x0.92
R² = 0.40
C

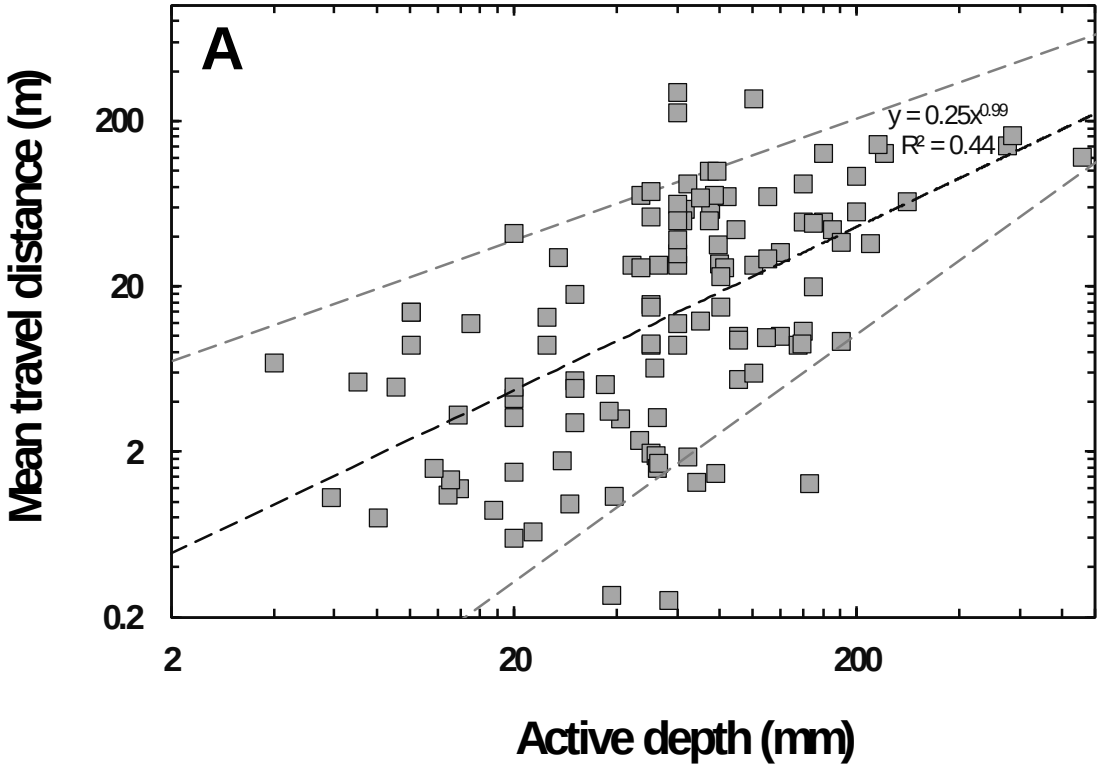
A
y = 0.25x^0.99
R² = 0.44
Mean travel distance (m)
200
20
2
0.2
2
20
200
Active depth (mm)

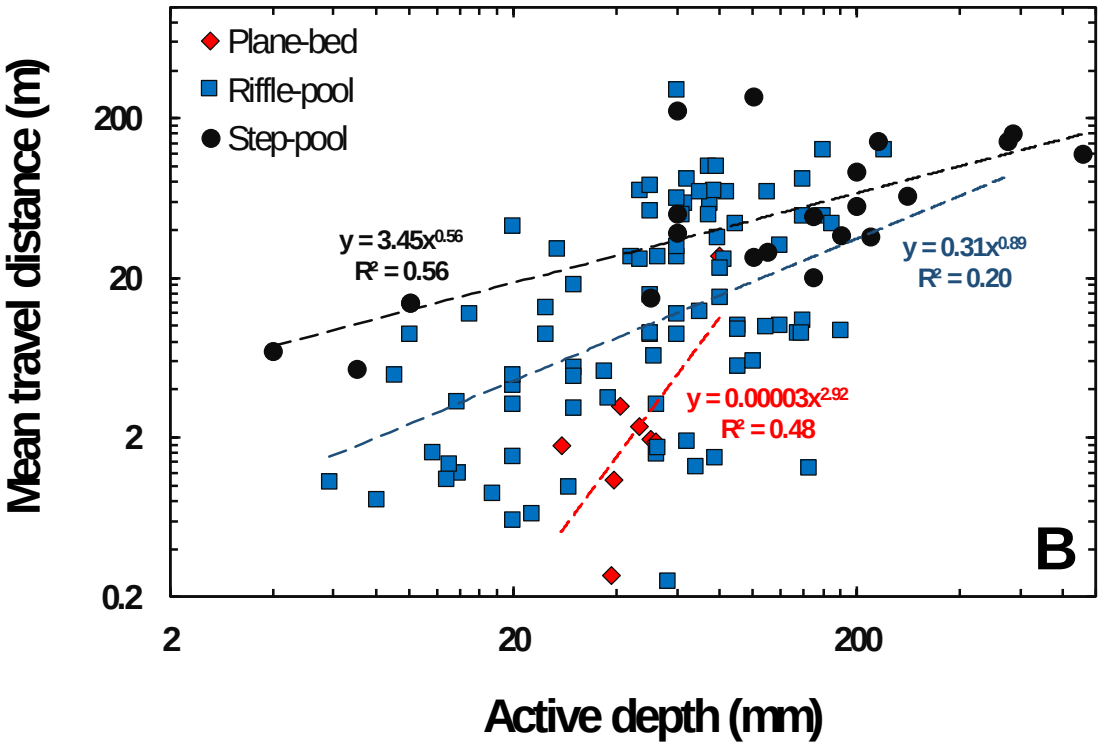
Plane-bed
Riffle-pool
Step-pool
y = 3.45x^0.56
R² = 0.56
y = 0.31x^0.89
R² = 0.20
y = 0.00003x^2.92
R² = 0.48
B
Mean travel distance (m)
200
20
2
0.2
2
20
200
Active depth (mm)

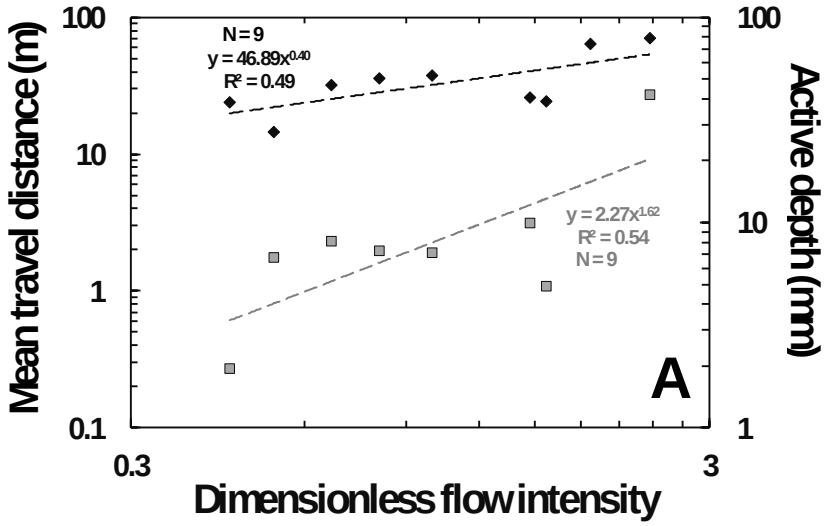
N = 9
y = 46.89x^0.40
R² = 0.49
y = 2.27x^1.62
R² = 0.54
N = 9
A
Mean travel distance (m)
Active depth (mm)
Dimensionless flow intensity
100
10
1
0.1
0.3
3

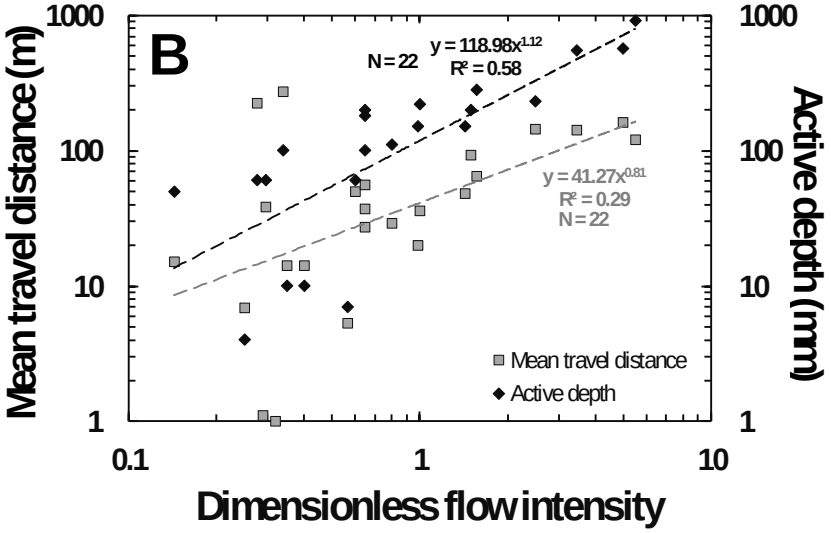
B
N = 22
y = 118.98x^1.12
R² = 0.58
y = 41.27x^0.81
R² = 0.29
N = 22
Mean travel distance
Active depth
Mean travel distance (m)
Active depth (mm)
Dimensionless flow intensity
1000
100
10
1
0.1
1
10

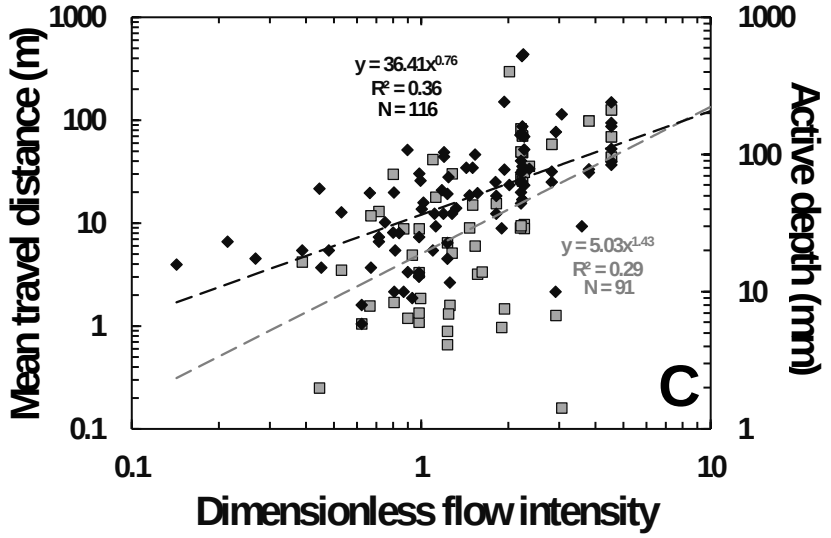
y = 36.41x^0.76
R² = 0.36
N = 116
y = 5.03x^1.43
R² = 0.29
N = 91
C
Mean travel distance (m)
Active depth (mm)
Dimensionless flow intensity
1000
100
10
1
0.1
1
10

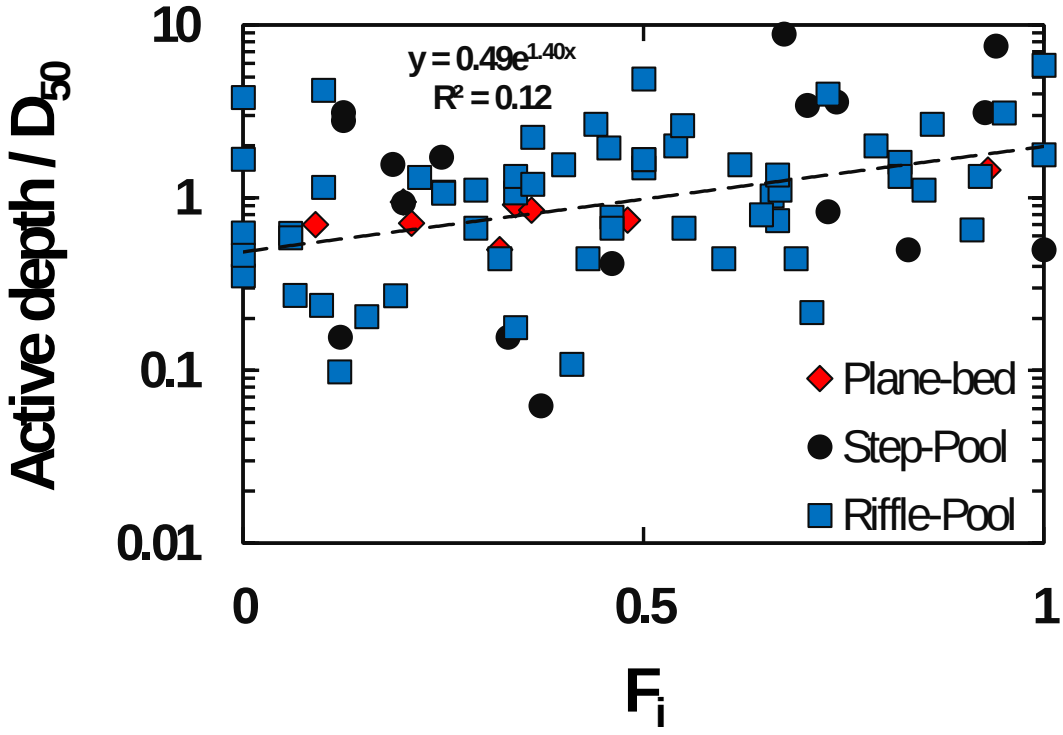
y = 0.49e1.40x
R² = 0.12
Active depth / D50
10
1
0.1
0.01
0
0.5
1
Fi
Plane-bed
Step-Pool
Riffle-Pool

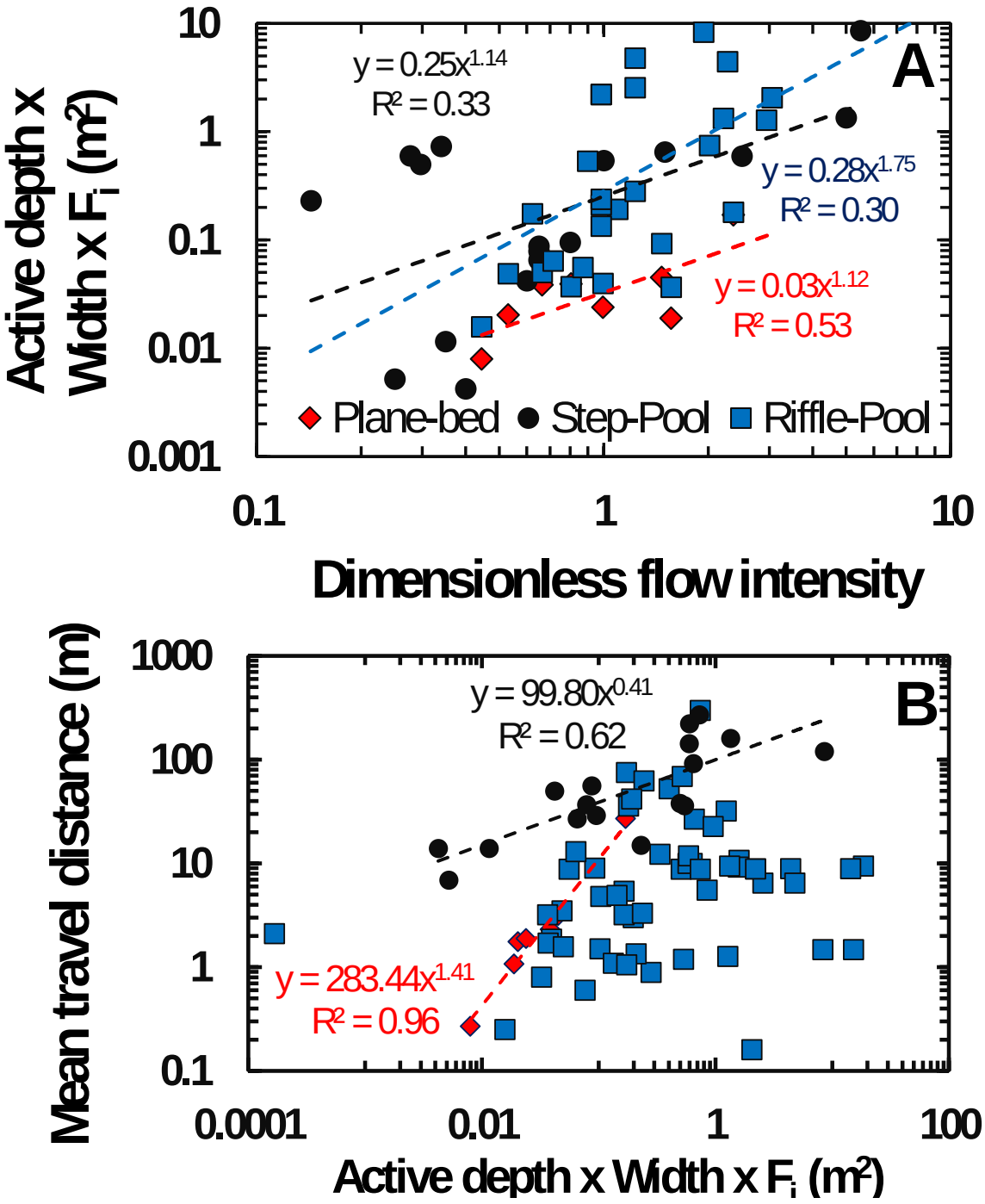
A
y = 0.25x^1.14
R² = 0.33
y = 0.28x^1.75
R² = 0.30
y = 0.03x^1.12
R² = 0.53
Plane-bed
Step-Pool
Riffle-Pool
Active depth x Width x Fi (m²)
Dimensionless flow intensity
10
1
0.1
0.01
0.001
0.1
1
10
B
y = 99.80x^0.41
R² = 0.62
y = 283.44x^1.41
R² = 0.96
Mean travel distance (m)
Active depth x Width x Fi (m²)
1000
100
10
1
0.1
0.0001
0.01
1
100

SUPPLEMENTARY MATERIAL TO "*THE ACTIVE LAYER IN GRAVEL-BED RIVERS: AN EMPIRICAL APPRAISAL*". DOCUMENT 1.

1. RIVER EBRO DATA

The River Ebro is located in the NE of the Iberian Peninsula, and drains an area of 85,530 km^2. It is regulated by almost 190 dams that impound >60% of the annual runoff of the basin (Batalla et al., 2004). Mean annual precipitation in the basin is around 600 mm, with high temporal and spatial variability. Rainfall ranges from 900-2000 mm at the headwaters, to 300 mm and 500 mm at the central depression and Mediterranean zone, respectively.

This study focuses on the lowermost reach of the River Ebro, from the Flix dam to the mouth in the Mediterranean Sea (Figure S1.1). This reach is located immediately downstream the dam chain composed by Mequinenza (1534 hm^3, built in 1966), Riba-roja (207 hm^3, 1969), and Flix (11 hm^3, 1948), which impound the 97% of the catchment. These dams have altered the magnitude and frequency of floods downstream, being reduced in 25% (Batalla et al., 2004). Sediment transport processes have been also altered due to the high trapping efficiency of the reservoir (90% for fine sediments and 100% for bedload), which translates in a reduced sediment supply to the study reach (Vericat and Batalla, 2005). Mean annual discharge at the lowermost gauging station (Tortosa) is 438 m^3/s, and the annual water yield is 13,810 hm^3 with a SD ±5474 hm^3 (Tena and Batalla, 2013).

Study Sites and Methods

Riverbed dynamics were studied in ten study sites (Figures S1.2 and S1.3) downstream the mentioned dam chain from October 2002 to September 2004.

- Grain size distribution (Figure S1.4): When an armour layer was present, surface and subsurface sediments were sampled separately. Surface grain size distribution was measured by the pebble count method (Wolman, 1954) and the area-by-weight method (Kellerhals and Bray, 1971). Subsurface material was sampled by the volumetric method (Church et al., 1987). Where there was no armour layer, surface and subsurface sediments were sampled together with the volumetric method.

- Particle travel length: Measured by painted areas and painted lines in the ten study sites, and by magnetic tracers in two of the sites (Tables S1.1 and S1.2).

- Active layer depth: Measured by the scour chain method, by the exposure of metallic rods, and by the burial of tracers (Tables S1.1 and S1.2).

Figure S1.3 and S1.4 present the cross sections and grain-size distribution, respectively, of the study sites in the lower River Ebro, while tables S1.1 and S1.2 summarise the papers where part of the data used in this manuscript has been published. It is worth to mention that most of the data on riverbed mobility (based on tracers) and active layer (based on scour-chains) were not published before.

Figure S1.1. a) Location map of the River Ebro and b) location of the study sites in the lower Ebro.

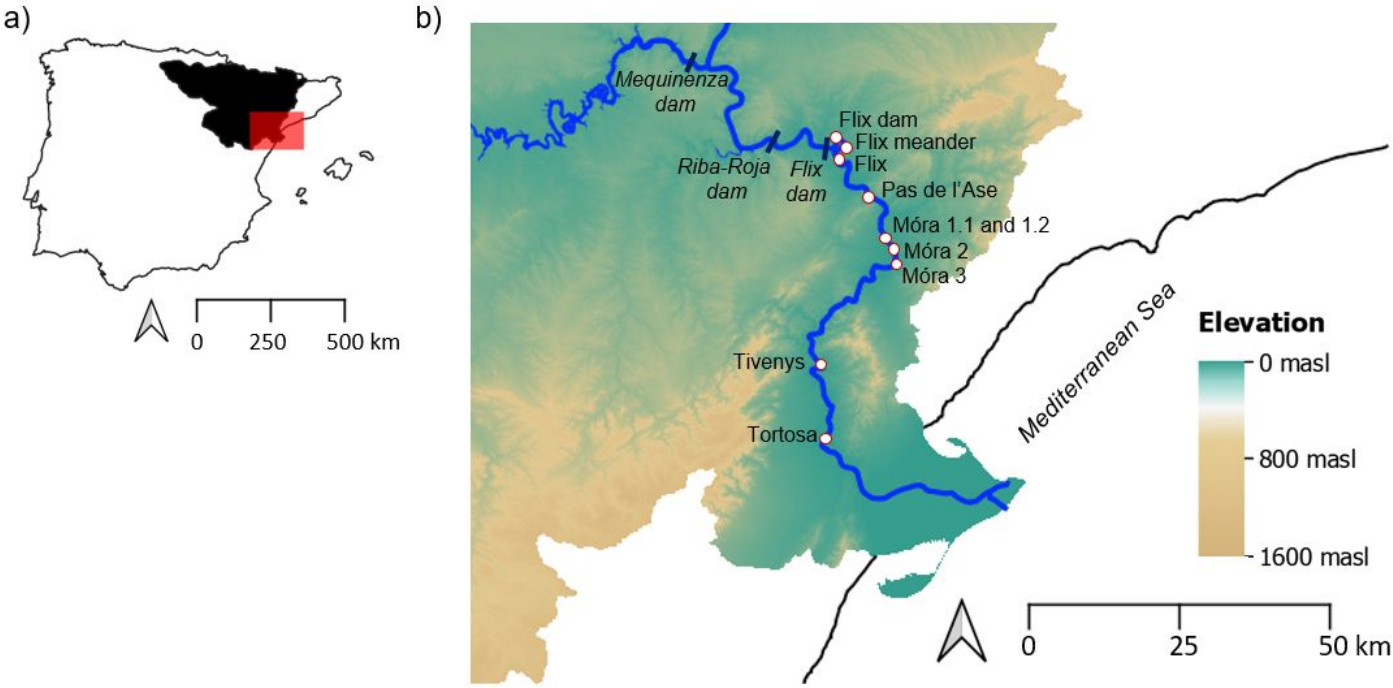

Figure S1.2. Photographs the study sites.

Flix dam – 27/07/2004

Flix meander – 27/07/2004

Flix – 18/07/2003

Pas de l'Ase – 18/07/2003

Móra 1.1 – 24/07/2003

Móra 1.2 – 24/07/2003

Móra 2 – 23/12/2002

Móra 3 – 25/07/2003

Tivenys – 28/07/2003

Tortosa – 28/07/2003

Figure S1.3. Cross-sections of the study sites.

Flix dam

Channel morphology: Riffle-pool / Slope: 0.00085 m/m / Width: 250 m / $Q_{bankfull}$: 1100 m^3/s

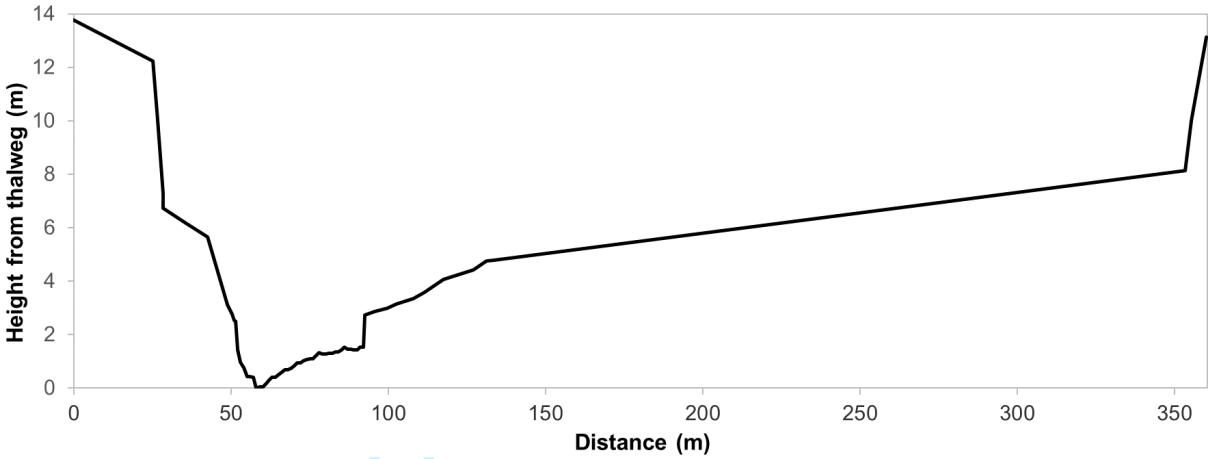

Flix meander

Channel morphology: Riffle-pool / Slope: 0.00085 m/m / Width: 108.5 m / $Q_{bankfull}$: 1100 m^3/s

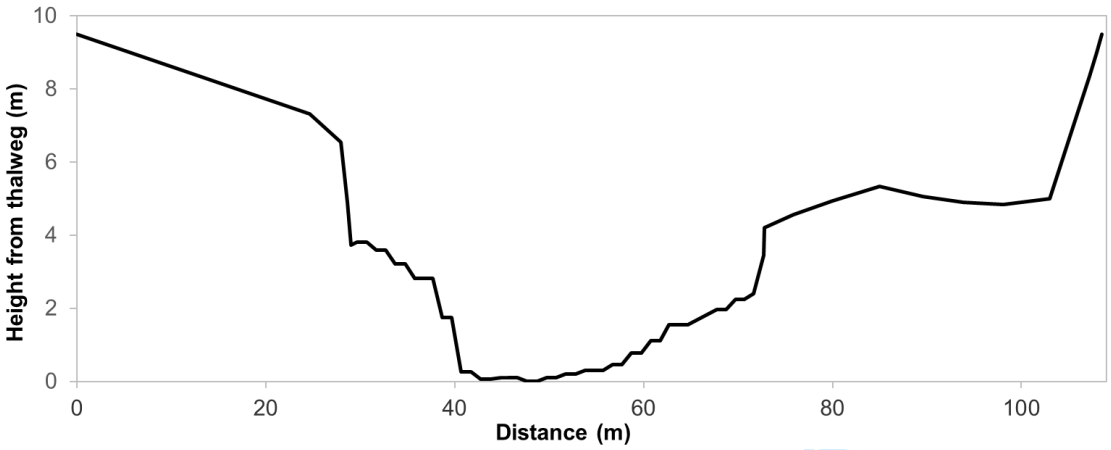

Flix

Channel morphology: Riffle-pool / Slope: 0.00085 m/m / Width: 205.5 m / $Q_{bankfull}$: 1100 m^3/s

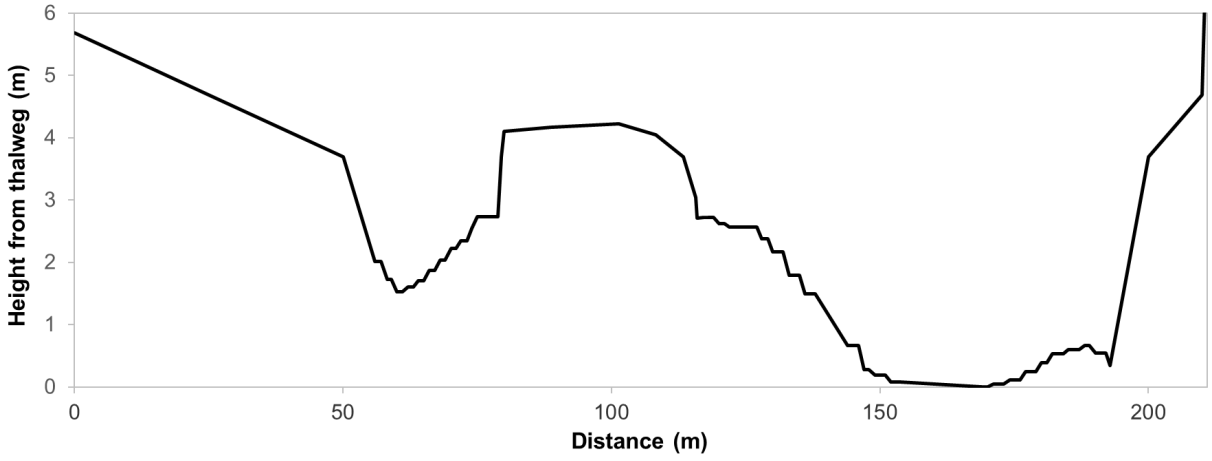

Móra 1.1

Channel morphology: Riffle-pool / Slope: 0.00085 m/m / Width: 161.6 m / $Q_{bankfull}$: 1100 m^3/s

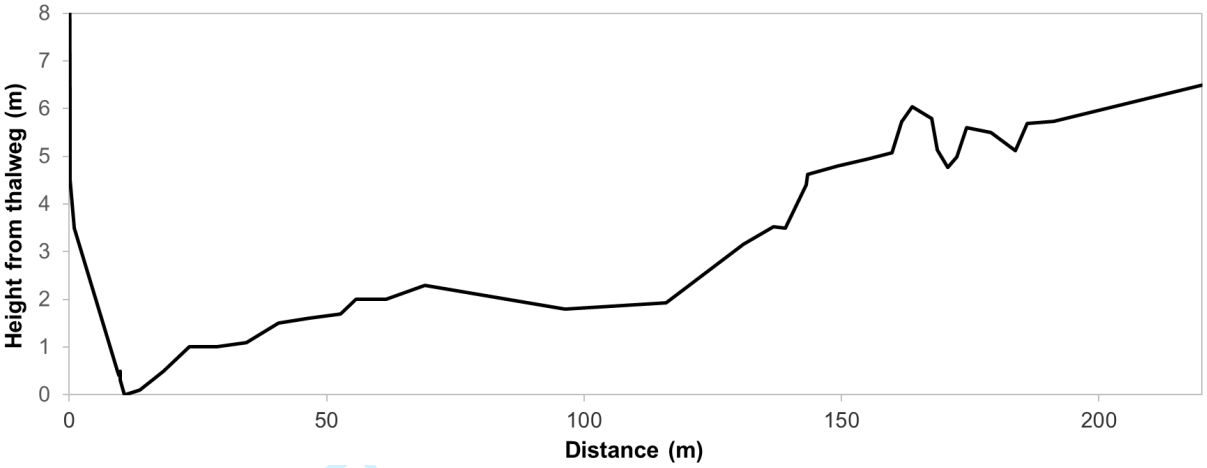

Móra 1.2

Channel morphology: Riffle-pool / Slope: 0.00085 m/m / Width: 275.4 m / $Q_{bankfull}$: 1100 m^3/s

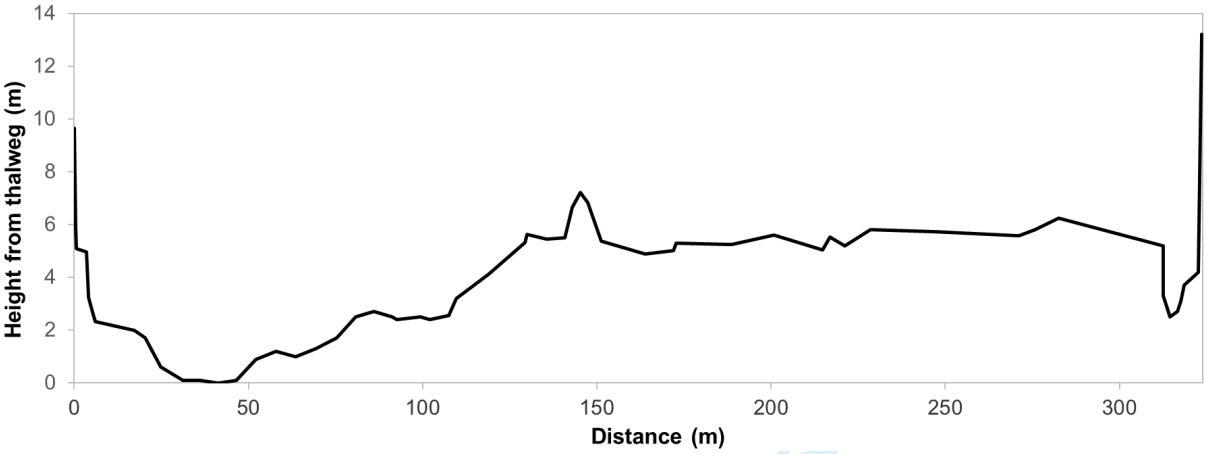

Móra 3

Channel morphology: Riffle-pool / Slope: 0.00085 m/m / Width: 177 m / $Q_{bankfull}$: 1100 m^3/s

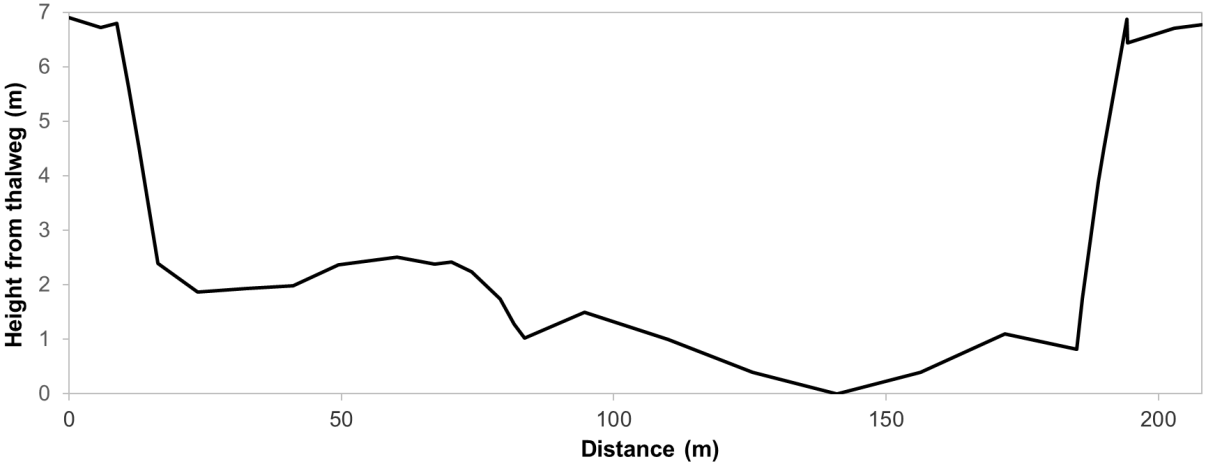

Figure S1.4. GSD of river bed material in the study sites. Measurements were done in July 2002, July 2003, and July 2004 (except for Tortosa in 2004, which were carried out in August).

Flix dam

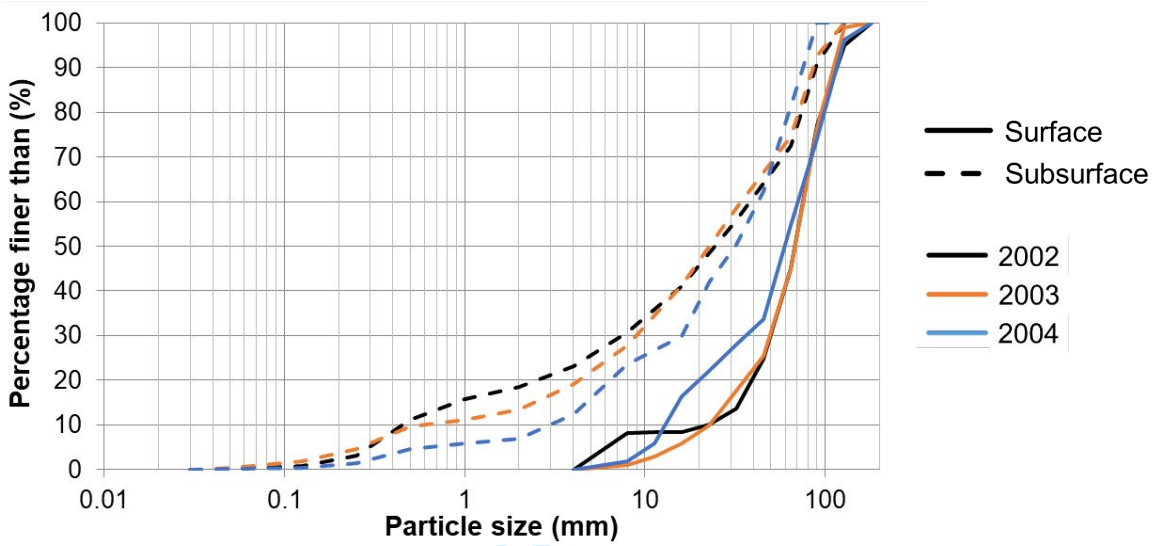

Flix meander – Combined surface and subsurface material

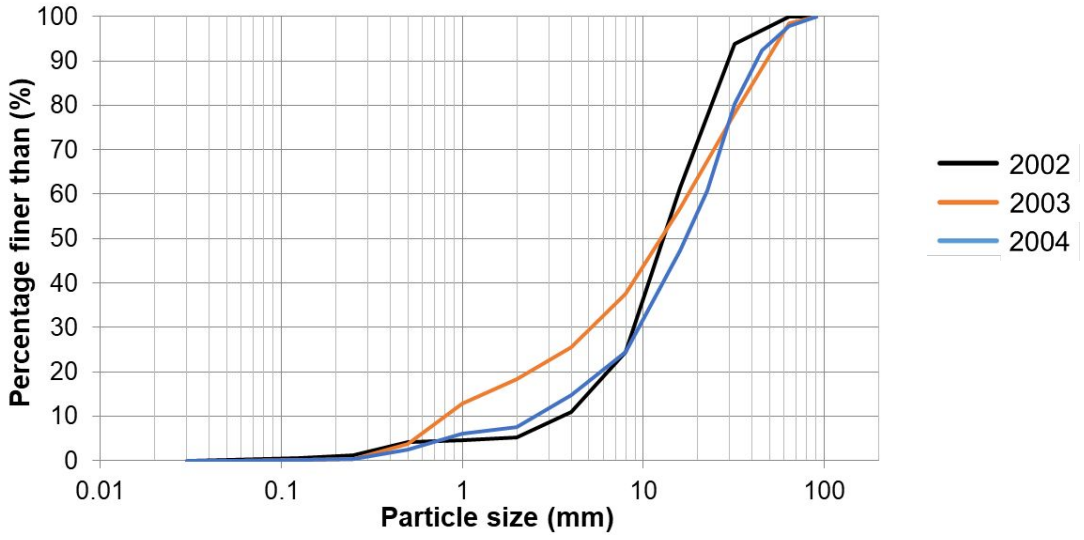

Flix

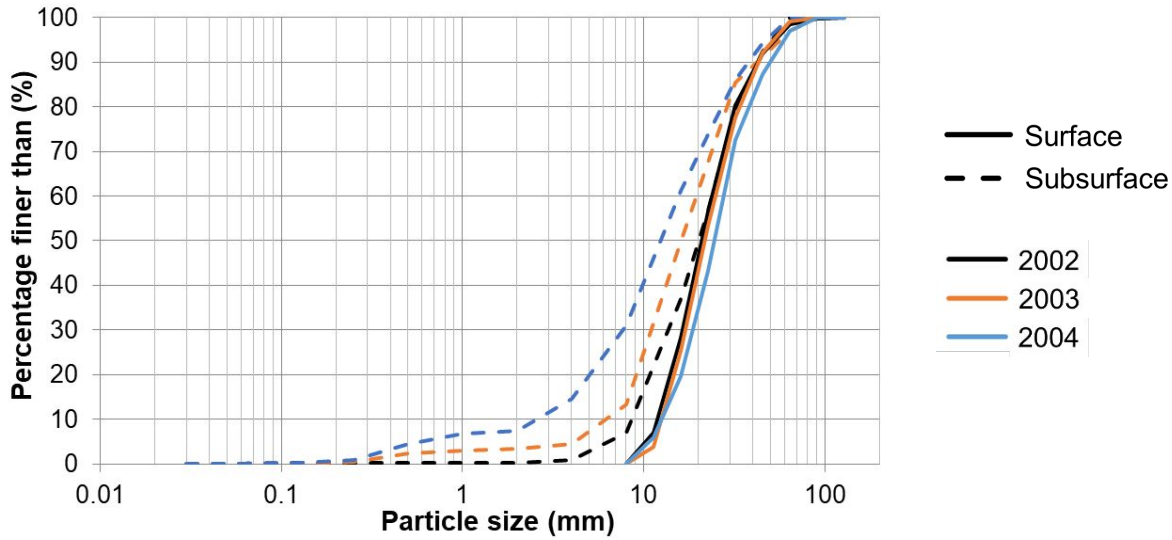

Pas de l'Ase

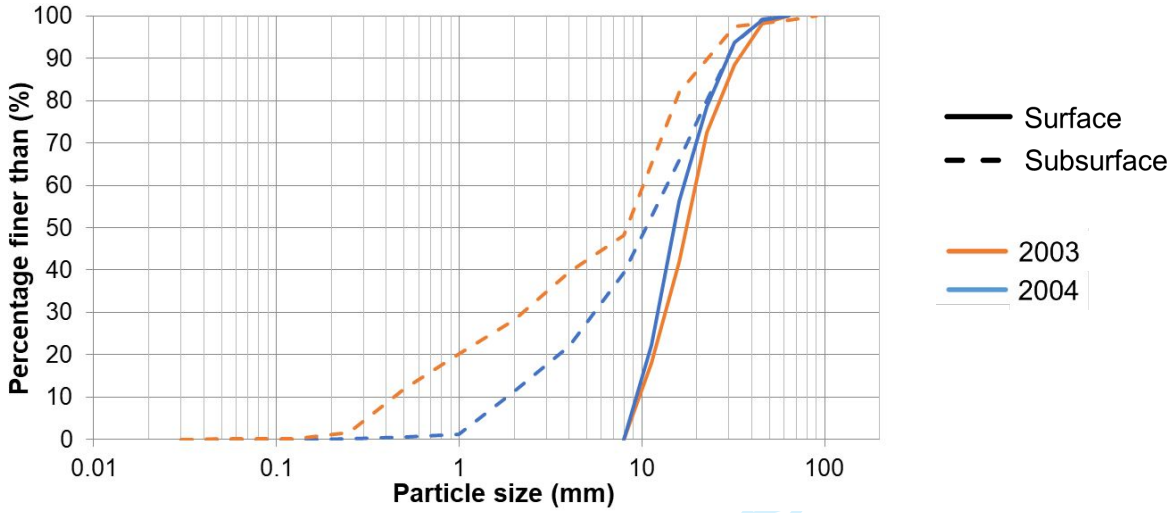

Móra 1.1

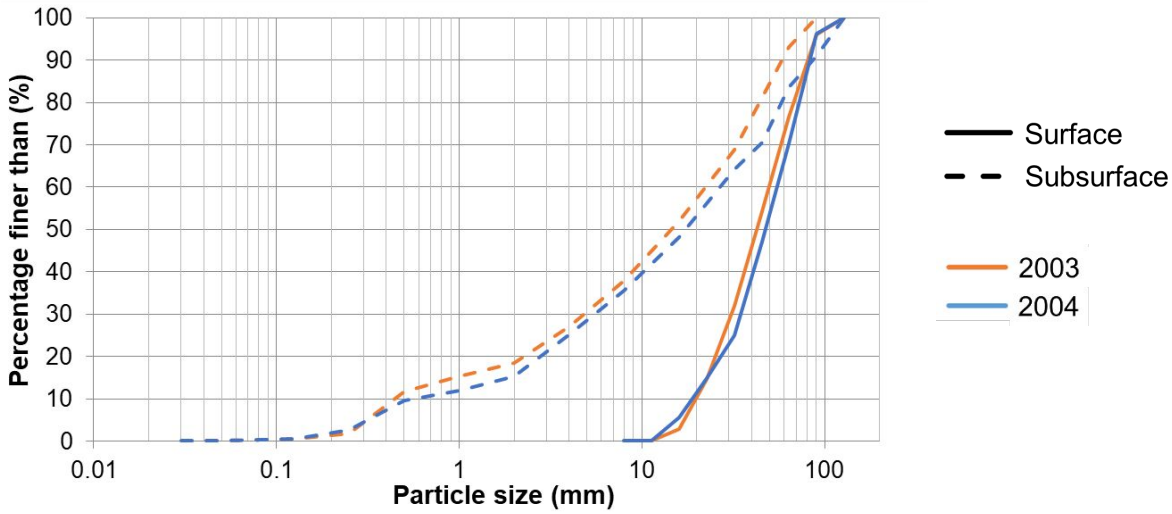

Móra 1.2

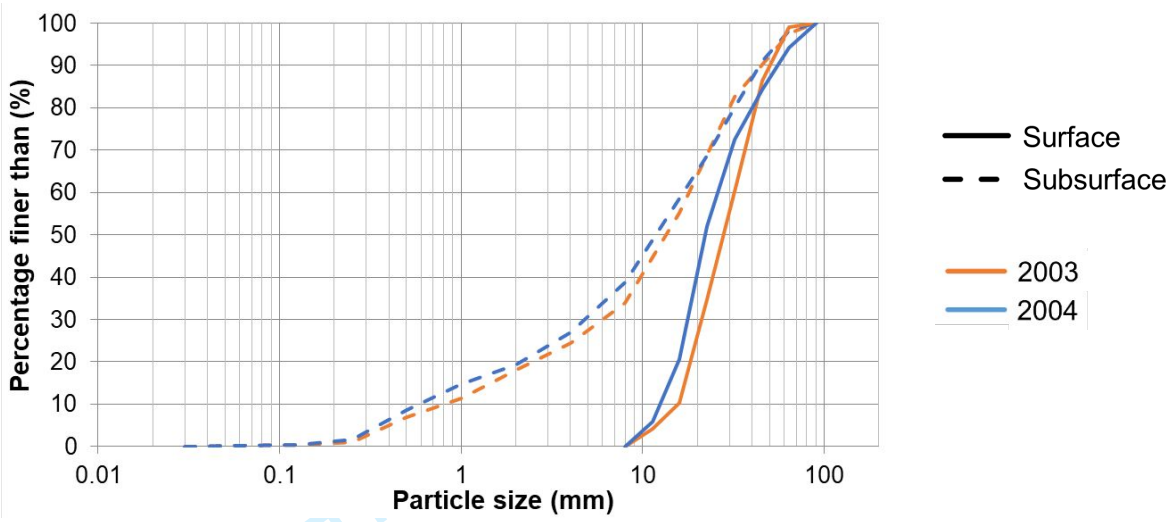

Móra 2

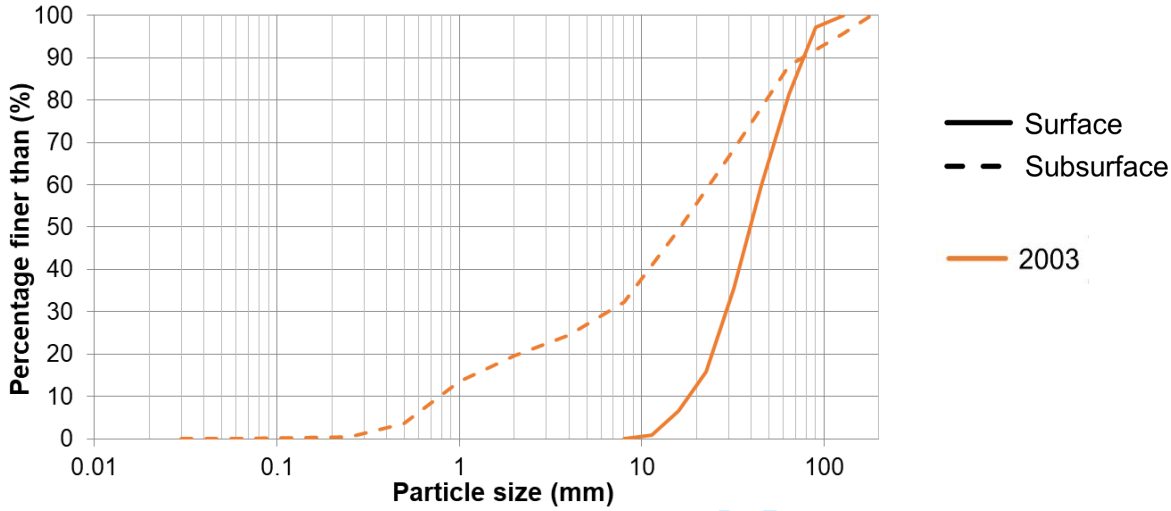

Móra 3

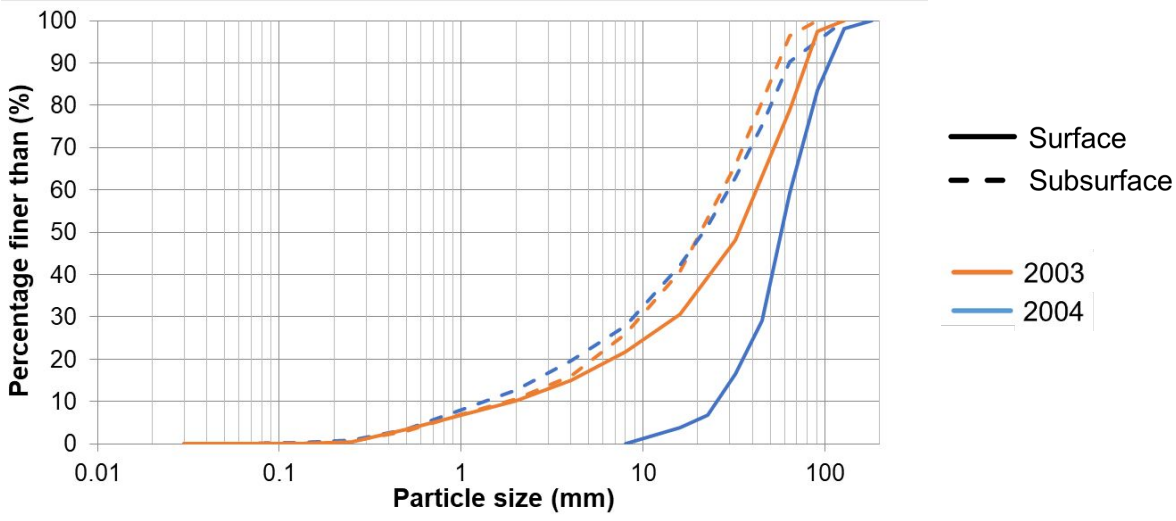

Tivenys – Combined surface and subsurface material

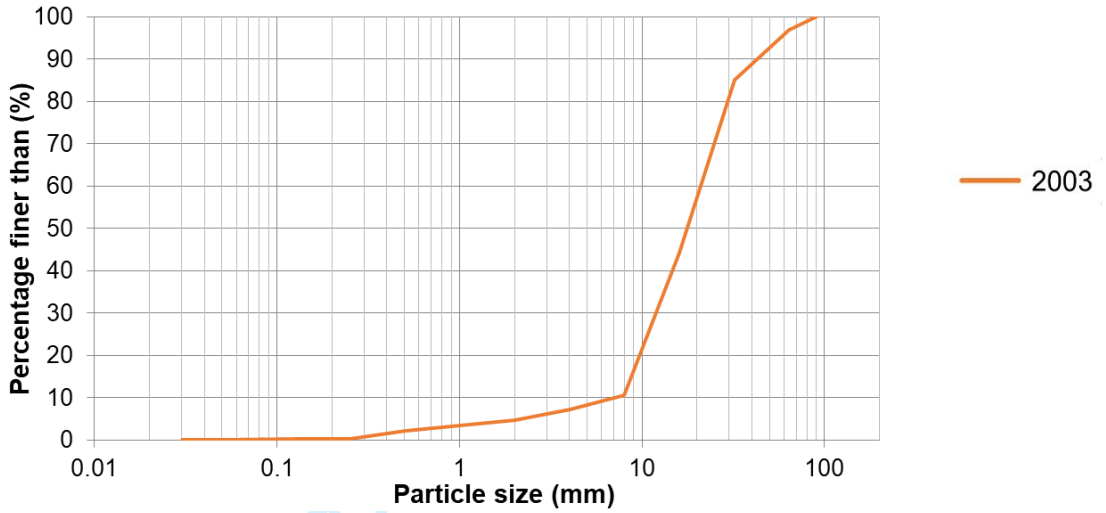

Tortosa – Combined surface and subsurface material

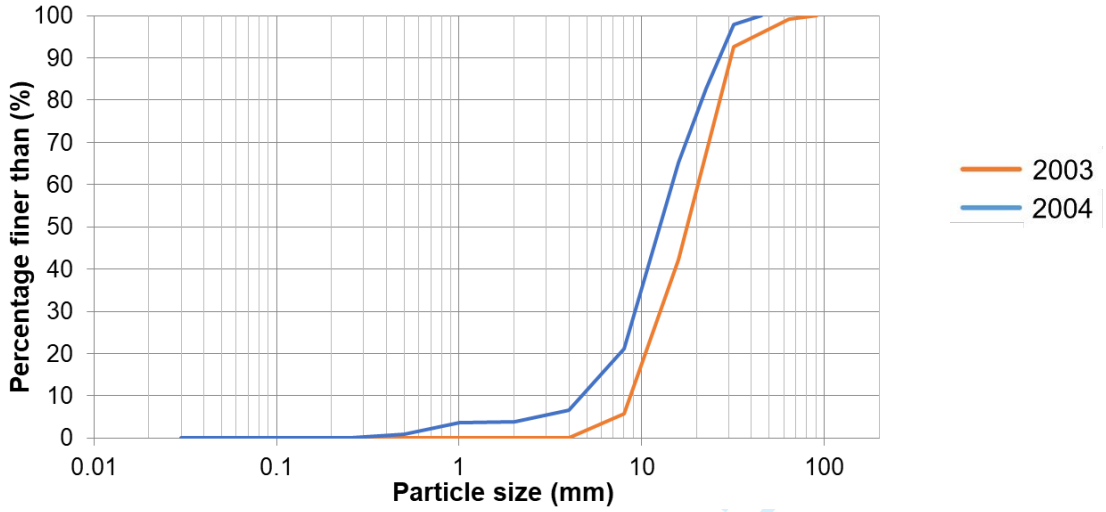

Table S1.1. Previous works published in the study river reaches and their main highlights. Only the articles related to bedload transport and riverbed material have been included.

Reference	Objectives / Methods	Highlights
Vericat et al. 2006	• To describe the breakup and reestablishment of the armour layer in a large regulated river. Methods: - GSD samplings (pebble count for surface material and volumetric method and area-by-weight for the subsurface material) - Bed load samplings (Helley Smith sampler 152 mm intake). Study period: 2002-2004	• Break-up of the armour layer and riverbed incision by large floods. • Reestablishment of the coarse surface layer by small floods. • Increment of the bedload transport after armour layer (partial or total) disruption. • Lower Ebro river channel was still active 40 years after dam construction.
Vericat and Batalla, 2006	• To analyse the sediment transport through the lower River Ebro during two consecutive hydrological years. Methods: - Flow (from official gauging stations and routed by the Muskingum method. - Suspended sediment transport (collection of depth integrated water and suspended sediment samples with a US DH74 during low flows and floods) - Bedload transport (Helley Smith samplers of 76 mm and 152 mm intake). Study period: 2002-2004	• Upstream the dam, most of the sediment was transported in suspension (99.5%), while downstream the dam the transport was 60% in suspension and 40% as bedload. • Specific sediment yield upstream the dams was three to four times higher than downstream the dams. • The sediment trapping by the dams was around 90% of suspended load and 100% of bedload. • Sediment load upstream the dam mainly provided by tributaries, and downstream the dam it came mainly from bank erosion.
Vericat and Batalla, 2007	• To analyse the behaviour of different bedload fractions. Methods: - Flow discharge (water stage and conversion to discharge). - Bedload transport (Helley Smith sampler 152 mm intake). - GSD samplings (pebble count for surface material and area-by-weight for the subsurface material). Study period: 2003-2004	• Under limited sediment supply conditions, partial transport controls the coarsening of the riverbed surface. • The reestablishment of the armour layer changes particle entrainment due to hiding and reduction of dimensionless critical shear stress. • The reestablishment of the armour layer causes a reduction in bedload transport rates due to the lower availability of fine fractions on the surface. • The reestablishment of the armour layer causes a progressive reduction of the sediment net export from the reach.

↓ *…continued in the next page*

↑ *…continued from previous next page*

Vericat et al., 2008	• To examine the bed material mobility in the River Ebro on the adjustment phase (to attain a post-dam quasi-equilibrium state) of the river. - To assess the effects of partly–competent flows on the GSD. - To assess the effects of partly-competent flows on the changes of the armour layer. Methods: - Bedload transport (painted areas and lines). - Active layer (scour chains). - GSD samplings (pebble count for surface material and volumetric method for the subsurface material). - Surface GSD changes (i.e. photography comparison). Study period: 2003-2004	• Existing disequilibrium between the rate of sediment supply from upstream and the ability of the flow to entrain and transport these particles. Most medium and coarse gravels were exported from the sections, but larger particles were not mobilised. • The riverbed surface coarsening responded to the limited sediment supply conditions combined with the frequent occurrence of competent flows. • Sedimentary dynamics in the lower Ebro are still evident at interannual scale 4 decades after dam closure.

Table S1.2. Previous works published in the study river reaches and their main highlights

Study site	Survey Date	Discharge (m^3/s)	Mean active layer depth (mm)	Mean painted tracers travel length (m)	Mean magnetized tracers travel length (m)	Mean painted tracers D_{50} travel length (m)
Presa Flix	*03/12/2002 (tracers and scour chains installation)*					
	05.12.2002	1408	0	30.14	-	50
	06.02.2003	2133	77.67	1.47	-	1.97
	08.12.2003	989	13.9	1.19	-	-
	29.01.2004	685	5.83	1.05	-	-
Flix meander	*29/11/2002 (tracers and scour chains installation)*					
	05.12.2002	1407	37	5.12	-	12.8
	06.02.2003	2130	242	-	-	-
	08.12.2003	987	108	-	-	-
	29.01.2004	685	8	-	-	-
Flix	*03/10/2002 (tracers and scour chains installation)*					
	05.12.2002	1787.5	-	3.36	-	6.1
	06.02.2003	2480	537	-	-	-
	08.12.2003	1383	11.67	1.59	-	1.85
	29.01.2004	1084.5	72.5	-	-	-
Pas de l'Ase	*03/10/2002 (tracers and scour chains installation)*					
	06.02.2003	2434	90	9.44	-	9.7
	08.12.2003	1367	68.33	1.31	-	-
	29.01.2004	1082	25	8.82	-	10.1
Móra 1.1 and 1.2	*02-03/10/2020 (tracers and scour chains installation)*					
	06.02.2003	2498	108.75	9.71	-	-
	06.02.2003	2498	59.75	31.24	-	37.95
	08.12.2003	1355	22.67	0.66	-	-
	08.12.2003	1355	17.4	0.89	-	-
	29.01.2004	1081	12.81	1.09	-	-
	29.01.2004	1081	13	1.34	-	1.4
Móra 2	06.02.2003	2498	-	-	-	-
Móra 3	*02/10/2002 (tracers and scour chains installation)*					
	06.02.2003	2498	135	8.87	-	-
	08.12.2003	1355	51.67	6.45	2.86	5.65
	29.01.2004	1081	13.75	3.31	3.85	1.93
Tivenys	*04/10/2002 (tracers and scour chains installation)*					
	06.02.2003	2451	521.67	-	-	-
Tortosa	*19/10/2002 (tracers and scour chains installation)*					
	06.02.2003	2422	138.75	9	-	9
	08.12.2003	1296.5	55	-	-	-

[a] Painted area 1 = 70% particles mobilised; Painted area 2 = 75 % particles mobilised
[b] Magnetized tracers (no RFID)

2. RIVER MUGA DATA

The Muga is a 758 km^2 catchment located in the NE of the Iberian Peninsula. It ranges from 1443 masl at the headwaters to the sea level at the Mediterranean Sea. The River Muga is regulated by a large dam (Darnius, 61 hm^3) since 1969, which has completely changed the hydrological regime of the river and generated a sediment deficit downstream the dam (Piqué et al., 2016; Piqué et al., 2017).

This study focuses on the Upper Muga (Figure S2.1), one sub-basin draining the reservoir, thus not regulated. This sub-basin drains an area of 84.1 km^2 of Paleogene and Cretaceous marls and conglomerates. The Upper Muga sub-basin is under the domain of the Mediterranean climate, with mean annual temperature around 11-14ºC, and a mean annual precipitation of 850-1150 mm. Main land use is forest (90% of the basin). Mean monthly flow at the sub-basin outlet for the study years was 1.3 m^3/s (SD ±9.4 m^3/s) in 2012-2013, 0.54 m^3/s (SD ±1.4 m^3/s) in 2013-2014, and 0.99 m^3/s (SD ±5.4 m^3/s) in 2014-2015. Annual maximum flow was 353 m^3/s, 24.7 m^3/s, and 164 m^3/s for the three study years, respectively (Piqué et al., 2017).

Study Sites and Methods

Riverbed dynamics were indirectly measured in one location close to the mouth of the Upper Muga sub-basin (Figures S2.2 and S2.3) from October 2013 to April 2015.

- Grain size distribution (Figure S2.4): Surface material was sampled by the pebble count procedure (Wolman, 1954), while subsurface material was sampled using the volumetric method (Church et al., 1987).

- Particle travel length: Measured from painted areas and RFID-tagged particles. Tables S2.1 and S2.2.

- Active layer depth: Measured by the scour chain method. Tables S2.1 and S2.2.

Figure S2.3 and S2.4 present the cross sections and grain-size distribution, respectively, of the study sites in the River Muga, while tables S2.1 and S2.2 summarise the papers where part of the data used in this manuscript has been published. It is worth to mention that most of the data on riverbed mobility (based on tracers) and active layer (based on scour-chains) were not published before.

Figure S2.1. a) Location map of the River Muga, and b) location of the study site in the Upper Muga sub-basin.

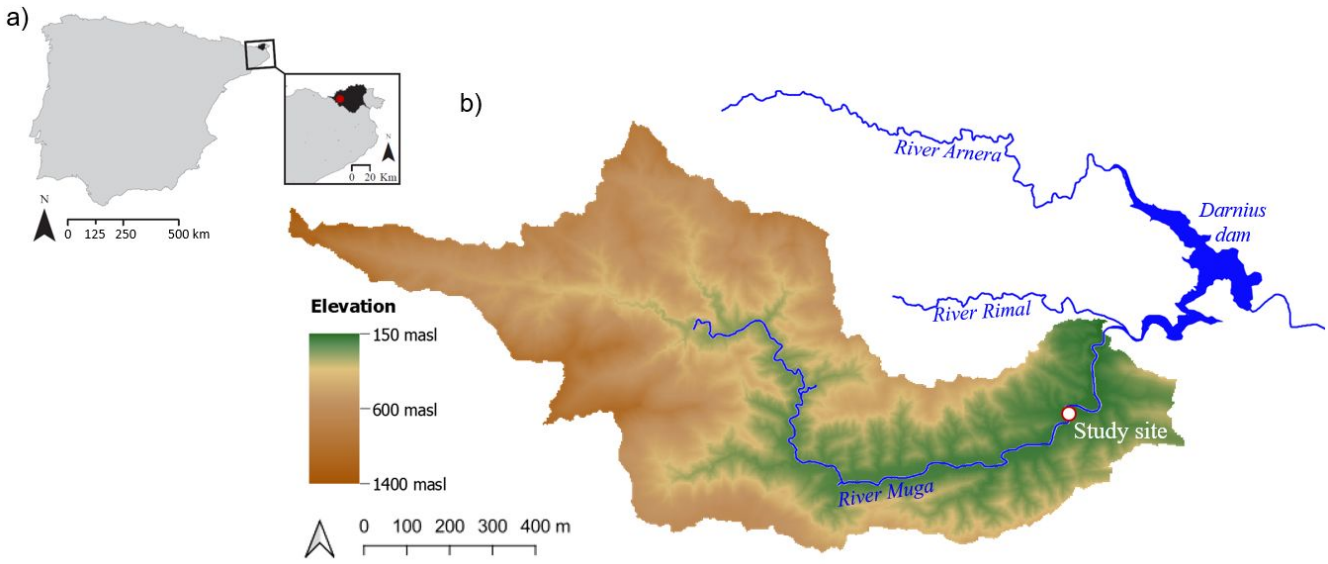

Figure S2.2. Photographs the study site for 25/07/2013. a) General view of the reach, and b) Detail of the bar and cross-section where measurements were carried out.

Figure S2.3. Cross-section of the study site and main channel characteristics.

Channel morphology: Riffle-pool / Slope: 0.008 m/m / Width: 19.2 m / Q_{bkf}: 8.9 m^3/s

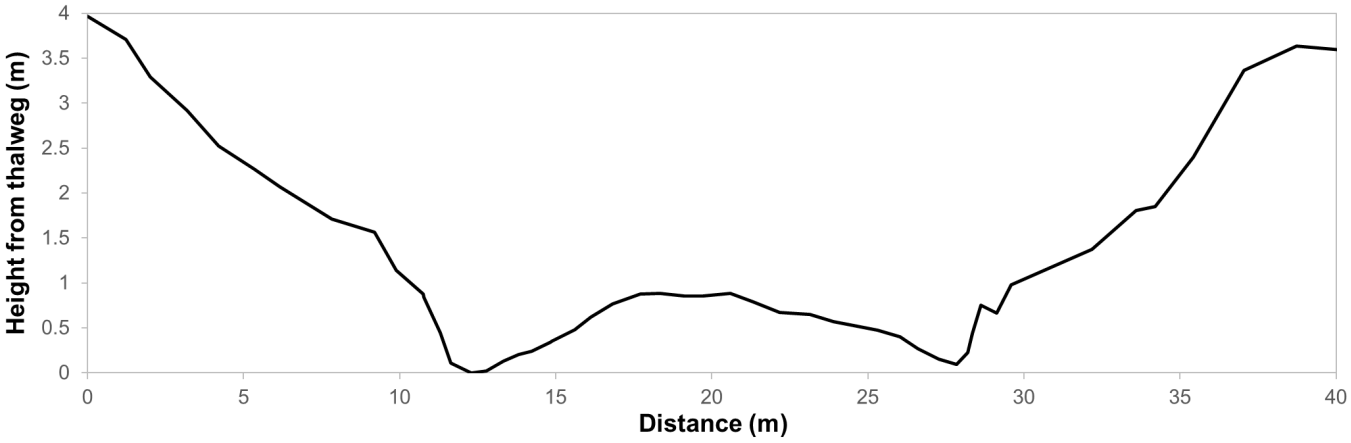

Figure S2.4. Grain size distribution of surface and subsurface material in the study site.

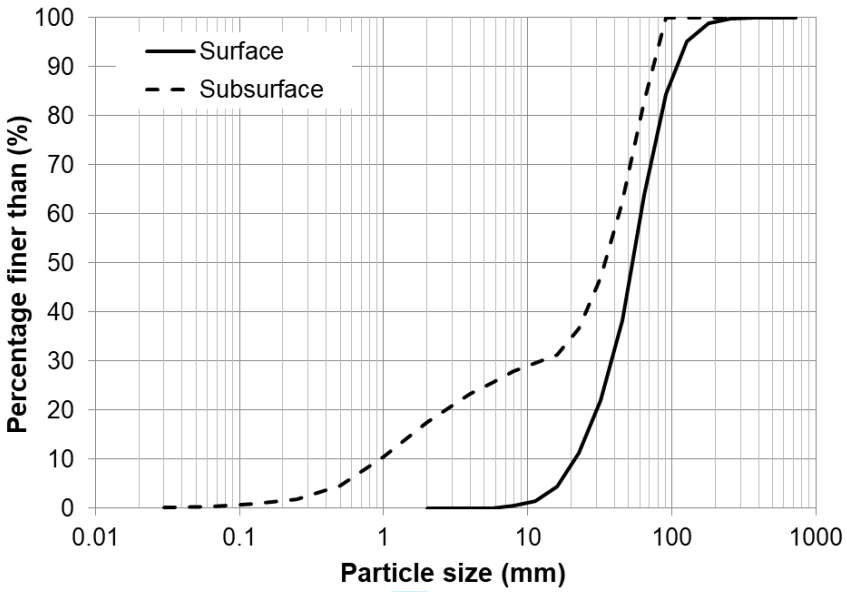

Table S2.1. Previous works published in the study river reaches and their main highlights. Only the articles related to bedload transport and riverbed material have been included.

Reference	Objectives/Methods	Highlights
Piqué et al. 2017	• To construct the sediment budget of a highly regulated Mediterranean river. • To determine the role of the reservoir on the upper basin water and sediment dynamics. • To quantify the sediment deficit downstream from the dam. Methods: - Dicharge (measurement of water stage and transformation into discharge). - Suspended sediment transport (turbidity probes installation and calibration to obtain suspended sediment concentration). - Bedload transport (indirect methods as painted areas, tagged tracers and scour chains). Study period: 2012-2015	• Flow patterns upstream and downstream the dam differ due to reservoir operation. • Upstream, sediment transport is restricted to floods and occurs in short periods of time. • Downstream, suspended sediment transport predominates; bedload is negligible. • Sediment trapping in the reservoir reaches up to 95% of the total load.

Table S2.2. Data used in the papers for the study sites.

Flood event number	Date flood peak	Discharge (m^3/s)	Duration competent flood (min)	Water volume competent flood (hm3)	Accumulated water volume since last flood (hm^3)	Mean active layer depth (mm)	Mean painted tracers travel length (m)	Mean RFID tracers travel length (m)	Mean painted tracers D_{50} travel length (m)	Mean RFID tracers D_{50} travel length (m)
01/10/2013 (tracers and scour chains installation)										
2[a]	19/11/ 2013	26.08	2930	2.58	3.90	146	1.27	0.94	0.98	2.9
3[b]	04/04/2014	16.97	1305	0.84	5.43	29	0.97	-	0.54	-
4[c]	29/09/2014	27.34	462	0.36	7.18	196.25	0.16	1.72	-	0.4
5[d]	29/11/2014	177.64	4392	10.04	12.14	-	-	125.32	-	378.18
6[e]	21/03/014	101.07	2715	4.49	10.43	60	8.79	0.56	6.78	0.13

[a] From installation to survey 2.
[b] RFID were not looked for.
[c] RFID data for floods 3 a- 4.
[d] RFID data for flood 5.
[e] RFID data for flood 6.

REFERENCES

Batalla, R.J., Kondolf, G.M., Gómez, C.M. (2004). Reservoir-induced hydrological changes in the Ebro River basin, NE Spain. *Journal of Hydrology*, 290: 117– 136.

Church, M.A., McLean, D.G., Wolcott, J.F. (1987) River Bed Gravels: Sampling and Analysis. In: Thorne, C. R., Bathurst, J. C. and Hey, R. D. (eds). *Sediments transport in Gravel Bed Rivers*, John Wiley and Sons, New York; pp. 43-88.

Kellerhals, R., Bray, D.I. (1971). Sampling procedures for coarse fluvial sediments. *Journal of the Hydraulics Division ASCE*, 97: 1165-1180.

Piqué, G., Batalla, R.J., Sabater, S. (2016). Hydrological characterization of dammed rivers in the NW Mediterranean region. *Hydrological Processes*, 30 (11): 1691-1707.

Piqué, G.; Batalla, R.J.; López, R. and Sabater, S. (2017). The fluvial sediment budget of a dammed river (upper Muga, southern Pyrenees). *Geomorphology*, 293 (A), 211-226.

Tena, A., Batalla, RJ. (2013). The sediment budget of a large river regulated by dams (The lower River Ebro, NE Spain). *Journal of Soils and Sediments*, 13: 966-980.

Vericat, D., Batalla, R.J. (2005). Sediment transport in a highly regulated fluvial system during two consecutive floods (Lower Ebro River, NE Spain). *Earth Surface Processes and Landforms*, 30: 385–402.

Vericat, D., Batalla, R.J. (2006). Sediment transport in a large impounded river: The lower Ebro,NE Iberian Peninsula. *Geomorphology*, 79: 72-92.

Vericat, D., Batalla, R.J., Garcia, C. (2006). Breakup and reestablishment of the armour layer in a large gravel-bed river below dams: The lower Ebro. *Geomorphology*, 76: 122– 136

Vericat, D., Batalla, R.J. (2007). Fractional bedload transport during small floods in a regulated gravel-bed river. *Zeitschrift für Geomorphologie*, 51 (2): 227-240.

Vericat, D., Batalla, R.J., Garcia, C. (2008). Bed-material mobility in a large river below dams. *Geodinamica Acta*, 21 (1-2): 3-10.

Wolman, M. (1954). A method for sampling coarse river-bed material. *American Geophysical Union Transactions*, 35: 951–956, 1954.

SUPPLEMENTARY MATERIAL TO "*THE ACTIVE LAYER IN GRAVEL-BED RIVERS: AN EMPIRICAL APPRAISAL*". DOCUMENT 2.

ACTIVE LAYER NORMALIZED BY THE SURFACE D_{84}

With the aim to grasp how the vertical dimension of the active layer scales to surface grain-size, we have normalized the active depth by the median size (D_{50}) of the surface grain-size distribution (GSD) for several analysis in the present paper. However, the active layer has been often related to the diameter of the coarse particles of the streambed surface, particularly to the 90-th percentile (D_{90}). Unfortunately, this information was not available for some of the case studies compiled for the present research.

Thus, in order to evaluate how the active layer thickness scales to the coarser grain-size fractions in the streambed, in the enclosed pages we are going to repeat some of the analysis and graphs shown in the main body of the manuscript, but this time normalizing the active depth by the 84-the percentile (D_{84}) of the surface GSD.

Nevertheless, for this analysis, we took the D_{90} instead of the D_{84} for some of the datasets. This was the case of Belgium rivers, extracted from Houbrechts et al., 2012, who provided information for the D_{90} but not the D_{84}. In case of data from Carling (1987) and Gottesfeld et al. (2004), information on the D_{84} was not provided. Then, we approached the D84 as 2 times the D_{50}, following Rickenmann and Recking (2011) and Recking (2013), who observed that the D_{84} is on average ~2 times the D_{50} in a large database of gravel-bed rivers.

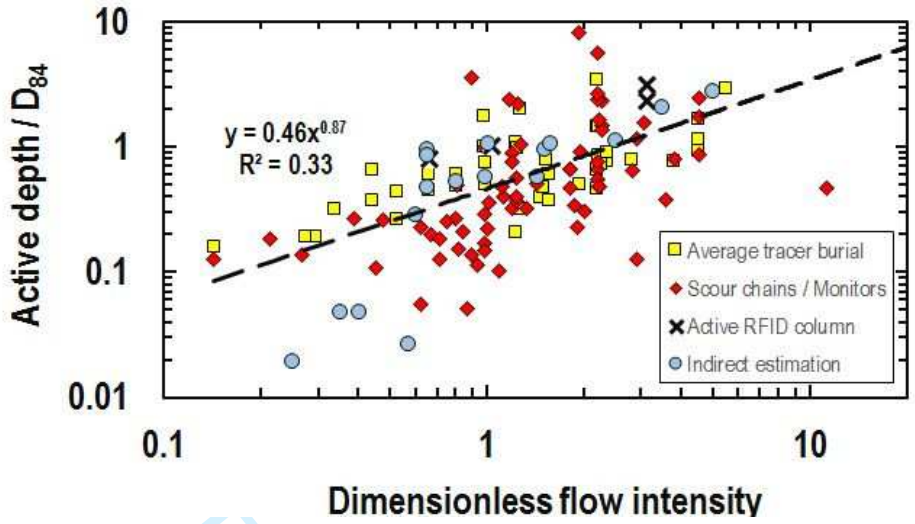

Figure S2.1. Active depth (normalized by the surface D_{50}) plotted versus dimensionless flow intensity. In this figure, data have been grouped according to field methodology.

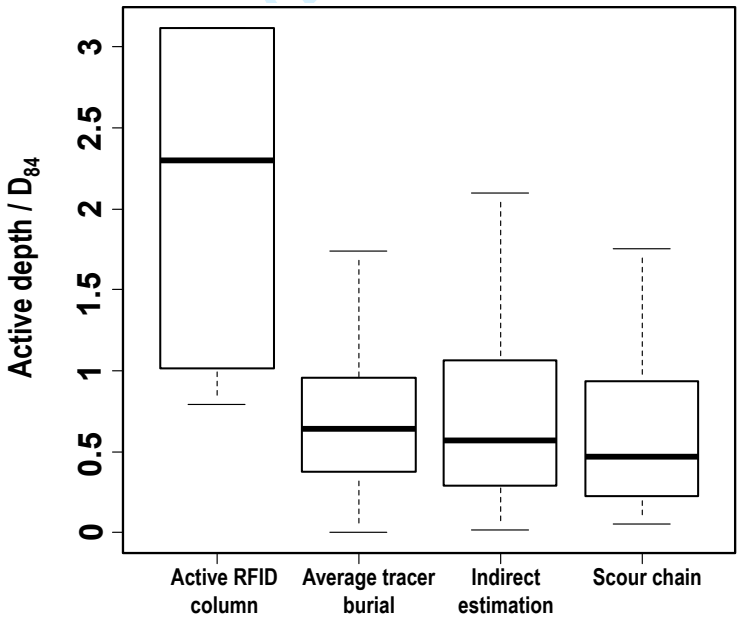

Figure S2.2. Differences in the active depth / D_{84} ratio. The boxes represent the range between the 25th and 75th percentiles, the dark lines the 50th percentile and the whiskers the upper and lower values corresponding to 1.5 times the interquartile range. Number of data: i) Average tracer burial: 69; ii) Scour chains/monitors: 71; iii) Indirect estimation: 17; iv) Active RFID: 5.

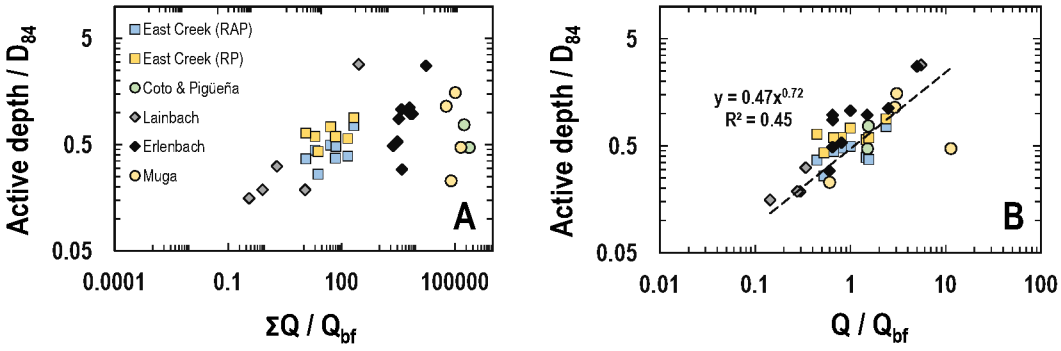

Figure S2.3. A: Active depth (normalized by the median size of bed surface) plotted versus the time-integrated dimensionless flow intensity, i.e. the cumulated flow discharge divided by the bankfull flow discharge. B: Active depth (normalized by the median size of bed surface) plotted versus the peak dimensionless flow intensity.

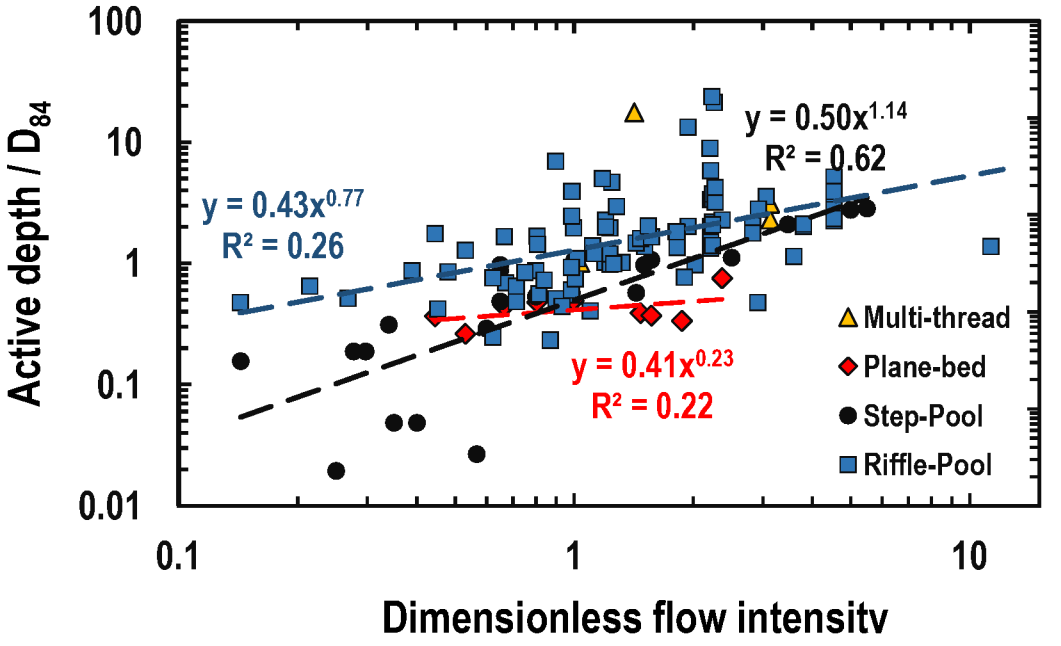

Figure S2.4. Active depth Active depth (normalized by the surface D_{84}) plotted versus dimensionless flow intensity. Data have been grouped according to channel style.

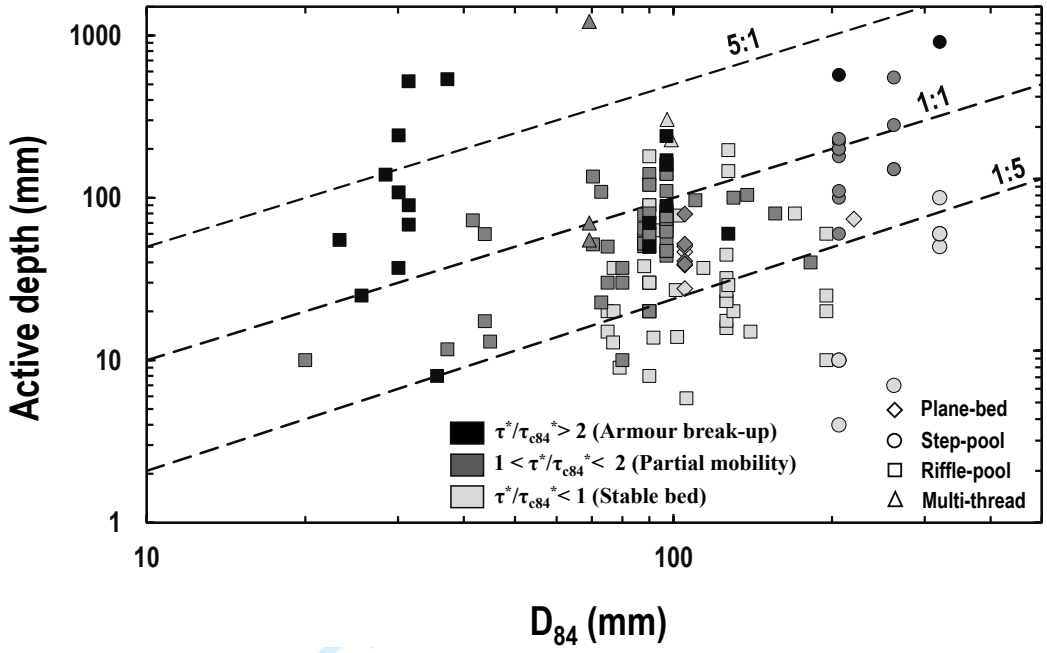

Figure S2.5. Active depth plotted versus the 84-th percentile of the surface sediment (D_{84}). Data were grouped according to streambed mobility conditions, quantified using the transport stage ratio (τ^* / τ_{c84}^*). τ^* is the peak Shields stress estimated based on the 84-th percentile of the surface sediment (D_{84}). τ_{c84}^* is the critical Shields stress for the surface D_{84}, computed based on Recking (2009).

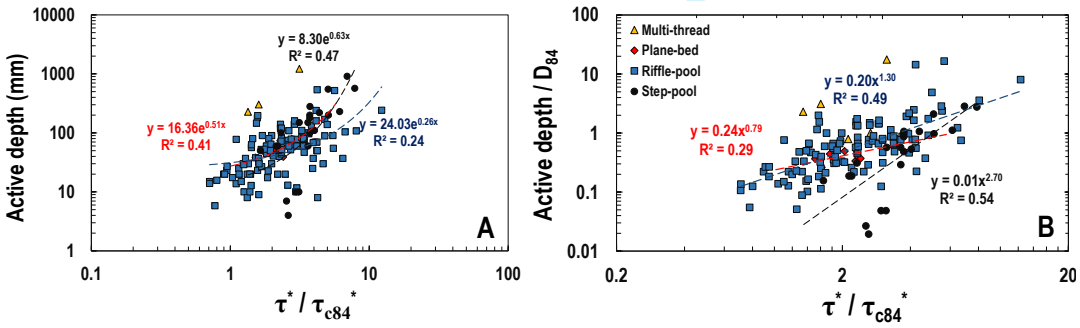

Figure S2.6. A: Transport stage estimated using a slope dependent critical Shields for the D_{84} of surface sediment (τ_{c84}^*), computed following Recking (2009). τ^* is the peak Shields stress estimated based on the D_{84} of the surface sediment. B: Active depth, normalized by the D_{84}, plotted versus the transport stage ratio.

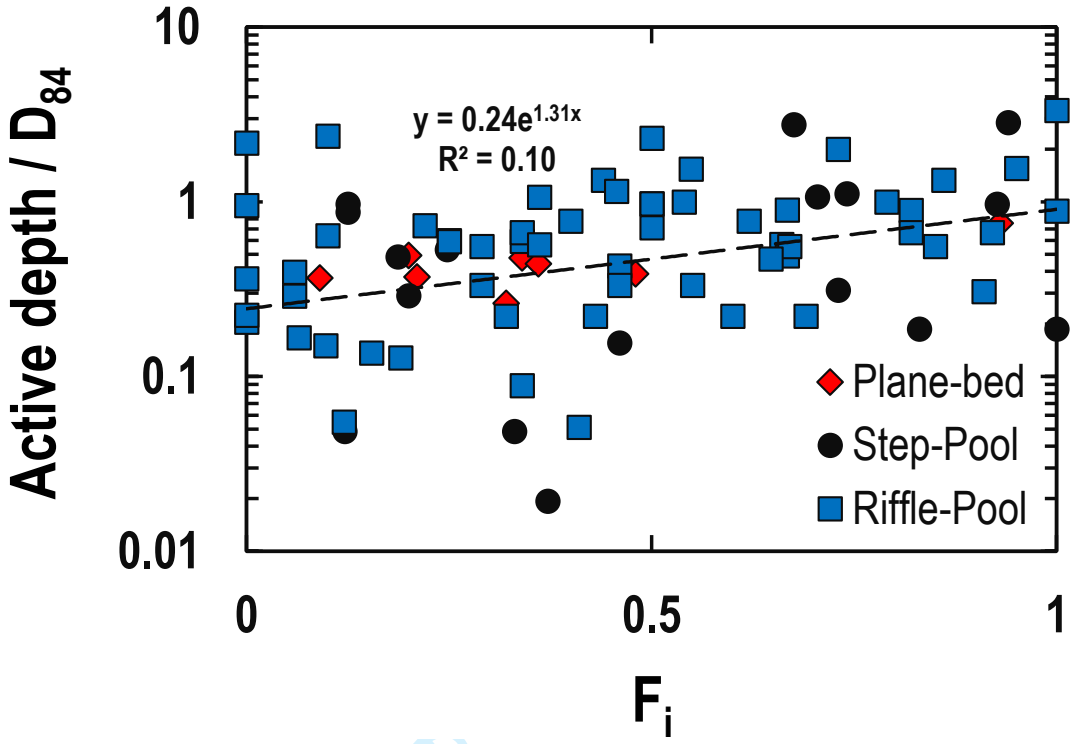

Figure S2.7. Active depth (normalized by the median size of bed surface), plotted versus the fraction of mobile tracers (Fi). Number of data: i) PB: 8; ii) SP: 17; iii) RP: 64.

Variable	Coefficient	Standard error	t	*p-value*	VIF[1]	LMG[2]
Intercept	-1.407	0.261	-5.396	0.000[++]	-	-
log D_{84}	0.847	0.113	7.493	0.000[++]	1.432	0.182
log τ^*/τ_c^*	1.405	0.170	8.282	0.000[++]	1.943	0.432
dBR	1.564	0.320	4.894	0.000[++]	1.026	0.114
dTr	0.198	0.128	1.551	0.123	1.027	0.015
log Q/Q_{bf}	0.245	0.078	3.166	0.002[++]	1.437	0.257

Residual standard error: 0.693 on 132 degrees of freedom. Multiple R^2: 0.573. Adjusted R^2: 0.557. F-statistic: 35.42 on 5 and 132 degrees of freedom. *p-value* = 2.2 x 10-6.

Table S2.1. Summary results of the stepwise multiple regression analysis using D_{84} as grain-size metrics. [1] Variance Inflation Factor. [2] Relative fraction of R^2 explained by each variable. [++] Variable statistically significant at a 95% confidence level.

REFERENCES

Carling PA. (1987) Bed stability in gravel streams, with reference to stream regulation and ecology. In: Richards, K. S. (ed). River Channels: Environment and ProcessK, Instit. of Br. Geogr. Oxford, England; pp. 321-347.

Gottesfeld AS, Hassan MA, Tunnicliffe JF and Poirier RW. (2004) Sediment dispersion in salmon spawning streams: The influence of floods and salmon redd construction. Journal of the American Water Resources Association 40: 1071–1086.

Houbrechts G, Van Campenhout J, Levecq Y, Hallot E, Peeters A and Petit F. (2012) Comparison of methods for quantifying active layer dynamics and bedload discharge in armoured gravel-bed rivers. Earth Surface Processes and Landforms 37: 1501-1517.

Recking A. (2013) An analysis of nonlineary effects on bedload transport prediction. Journal of Geophysical Research: Earth Surface 118 (3): 1264-1281.

Rickenmann D and Recking A. (2011). Evaluation of flow resistance in gravel-bed rivers through a large field data set. Water Resources Research, 47, W07538.

SUPPLEMENTARY MATERIAL TO "*THE ACTIVE LAYER IN GRAVEL-BED RIVERS: AN EMPIRICAL APPRAISAL*". DOCUMENT 1.

1. RIVER EBRO DATA

The River Ebro is located in the NE of the Iberian Peninsula, and drains an area of 85,530 km^2. It is regulated by almost 190 dams that impound >60% of the annual runoff of the basin (Batalla et al., 2004). Mean annual precipitation in the basin is around 600 mm, with high temporal and spatial variability. Rainfall ranges from 900-2000 mm at the headwaters, to 300 mm and 500 mm at the central depression and Mediterranean zone, respectively.

This study focuses on the lowermost reach of the River Ebro, from the Flix dam to the mouth in the Mediterranean Sea (Figure S1.1). This reach is located immediately downstream the dam chain composed by Mequinenza (1534 hm^3, built in 1966), Riba-roja (207 hm^3, 1969), and Flix (11 hm^3, 1948), which impound the 97% of the catchment. These dams have altered the magnitude and frequency of floods downstream, being reduced in 25% (Batalla et al., 2004). Sediment transport processes have been also altered due to the high trapping efficiency of the reservoir (90% for fine sediments and 100% for bedload), which translates in a reduced sediment supply to the study reach (Vericat and Batalla, 2005). Mean annual discharge at the lowermost gauging station (Tortosa) is 438 m^3/s, and the annual water yield is 13,810 hm^3 with a SD ±5474 hm^3 (Tena and Batalla, 2013).

Study Sites and Methods

Riverbed dynamics were studied in ten study sites (Figures S1.2 and S1.3) downstream the mentioned dam chain from October 2002 to September 2004.

- Grain size distribution (Figure S1.4): When an armour layer was present, surface and subsurface sediments were sampled separately. Surface grain size distribution was measured by the pebble count method (Wolman, 1954) and the area-by-weight method (Kellerhals and Bray, 1971). Subsurface material was sampled by the volumetric method (Church et al., 1987). Where there was no armour layer, surface and subsurface sediments were sampled together with the volumetric method.

- Particle travel length: Measured by painted areas and painted lines in the ten study sites, and by magnetic tracers in two of the sites (Tables S1.1 and S1.2).

- Active layer depth: Measured by the scour chain method, by the exposure of metallic rods, and by the burial of tracers (Tables S1.1 and S1.2).

Figure S1.3 and S1.4 present the cross sections and grain-size distribution, respectively, of the study sites in the lower River Ebro, while tables S1.1 and S1.2 summarise the papers where part of the data used in this manuscript has been published. It is worth to mention that most of the data on riverbed mobility (based on tracers) and active layer (based on scour-chains) were not published before.

Figure S1.1. a) Location map of the River Ebro and b) location of the study sites in the lower Ebro.

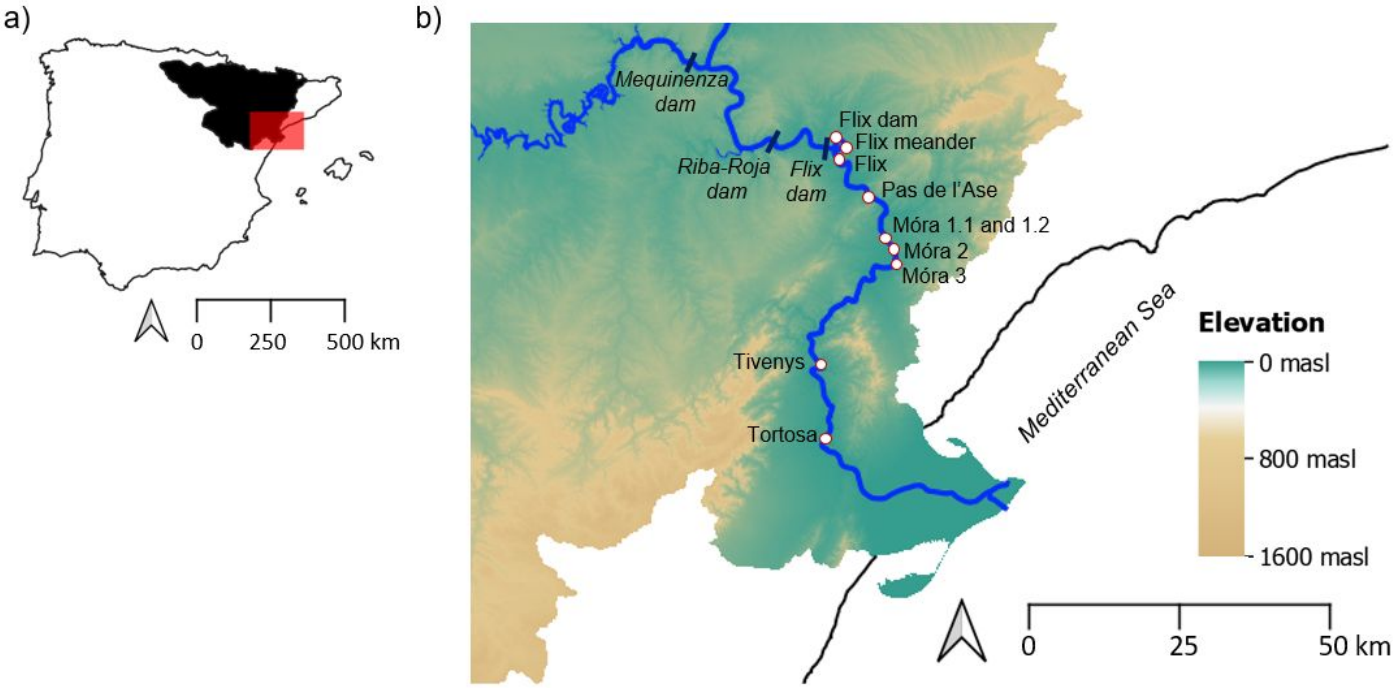

Figure S1.2. Photographs the study sites.

Flix dam – 27/07/2004

Flix meander – 27/07/2004

Flix – 18/07/2003

Pas de l'Ase – 18/07/2003

Móra 1.1 – 24/07/2003

Móra 1.2 – 24/07/2003

Móra 2 – 23/12/2002

Móra 3 – 25/07/2003

Tivenys – 28/07/2003

Tortosa – 28/07/2003

Figure S1.3. Cross-sections of the study sites.

Flix dam

Channel morphology: Riffle-pool / Slope: 0.00085 m/m / Width: 250 m / $Q_{bankfull}$: 1100 m^3/s

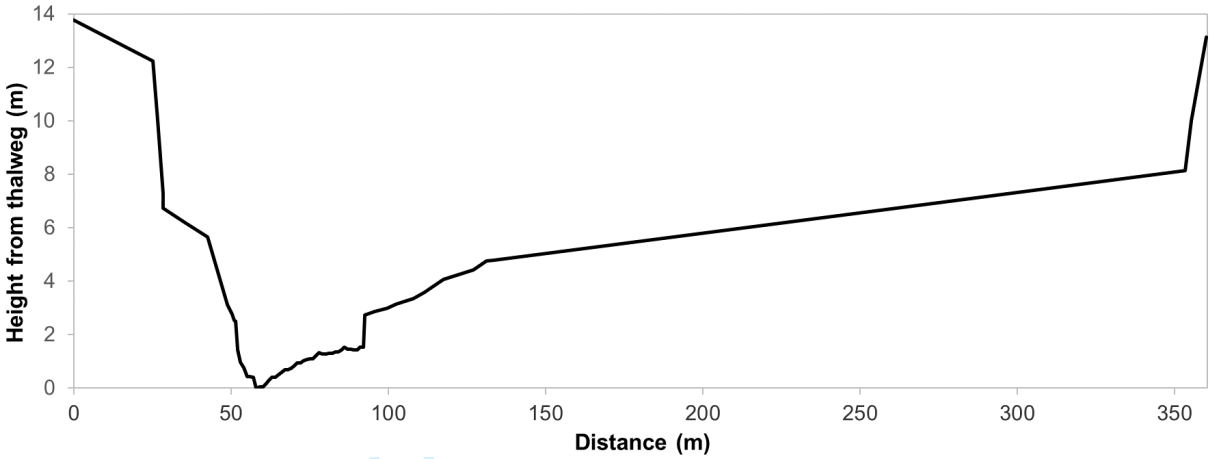

Flix meander

Channel morphology: Riffle-pool / Slope: 0.00085 m/m / Width: 108.5 m / $Q_{bankfull}$: 1100 m^3/s

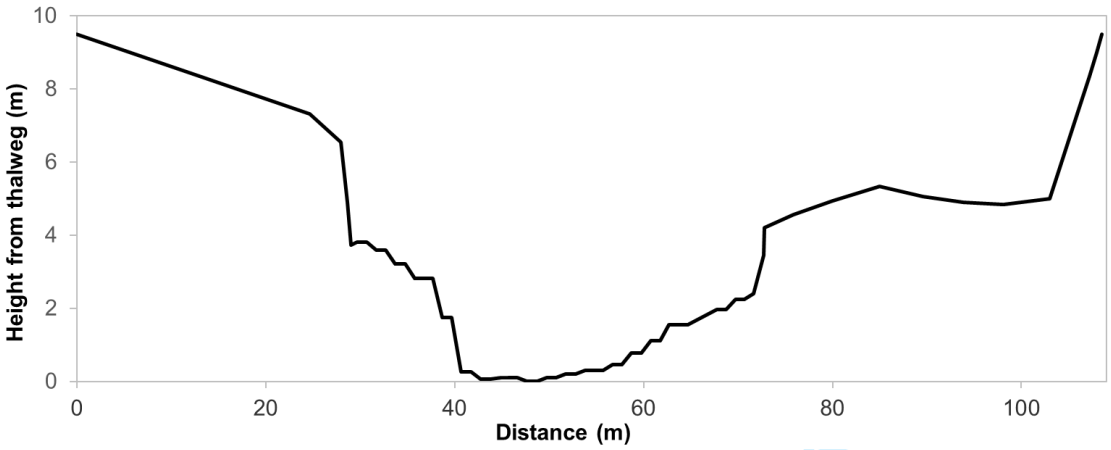

Flix

Channel morphology: Riffle-pool / Slope: 0.00085 m/m / Width: 205.5 m / $Q_{bankfull}$: 1100 m^3/s

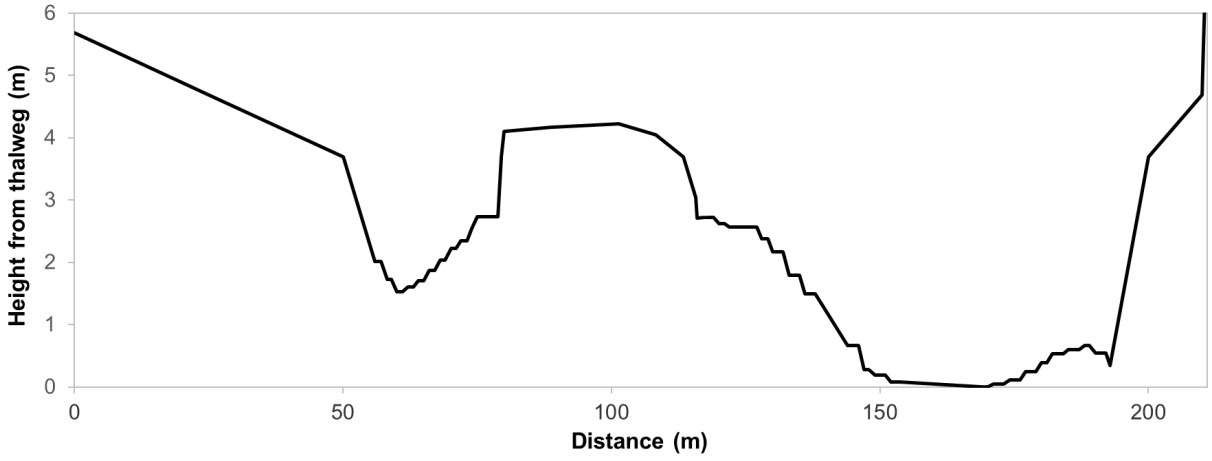

Móra 1.1

Channel morphology: Riffle-pool / Slope: 0.00085 m/m / Width: 161.6 m / $Q_{bankfull}$: 1100 m^3/s

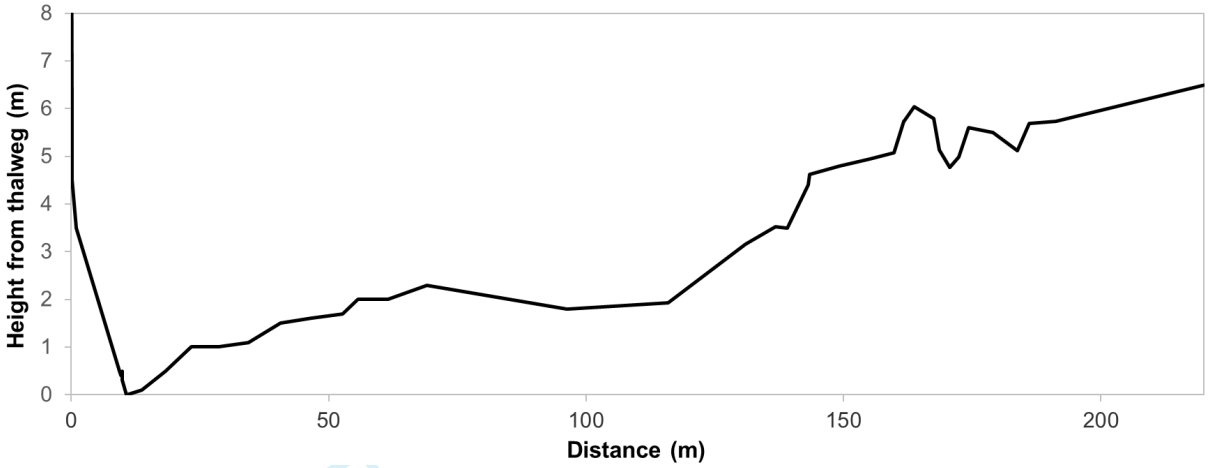

Móra 1.2

Channel morphology: Riffle-pool / Slope: 0.00085 m/m / Width: 275.4 m / $Q_{bankfull}$: 1100 m^3/s

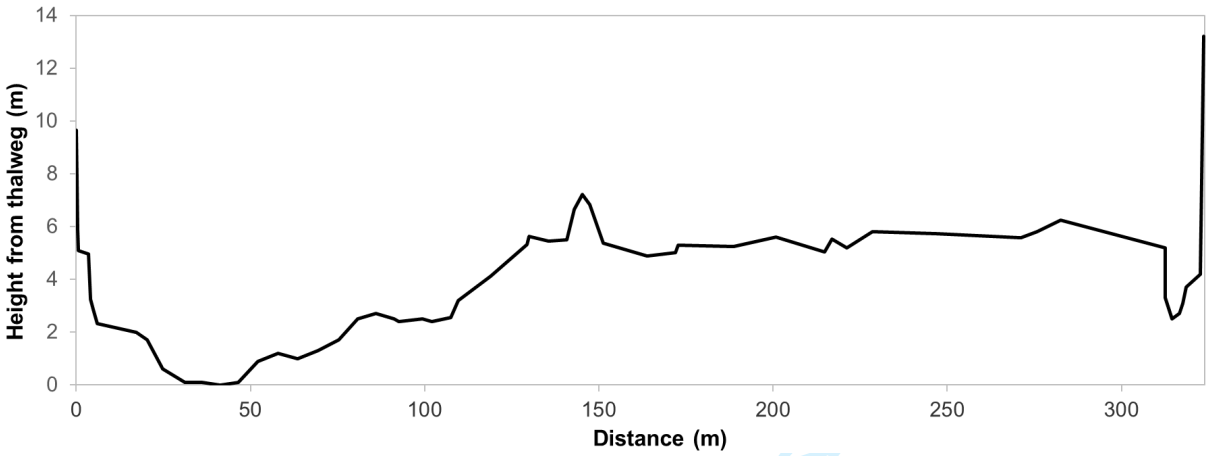

Móra 3

Channel morphology: Riffle-pool / Slope: 0.00085 m/m / Width: 177 m / $Q_{bankfull}$: 1100 m^3/s

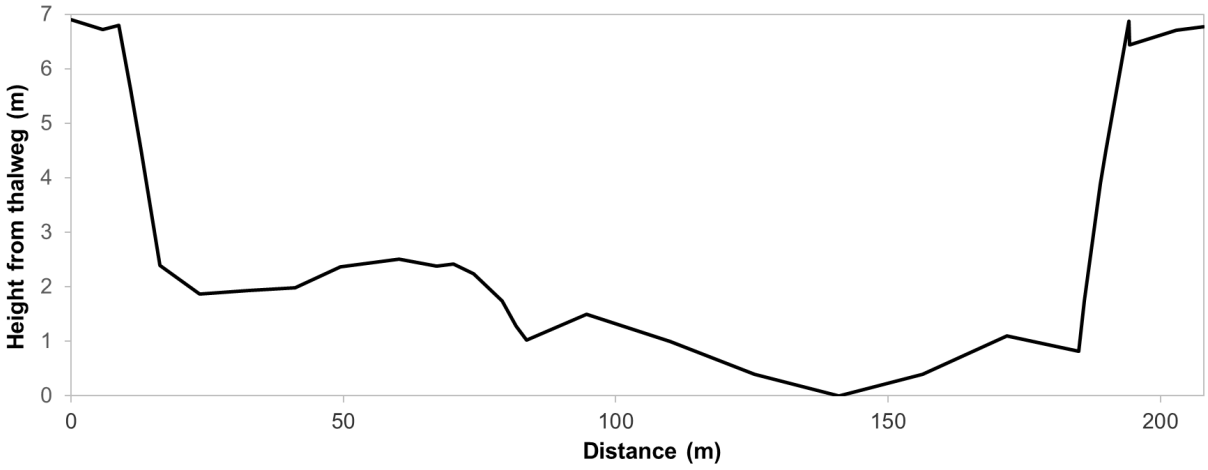

Figure S1.4. GSD of river bed material in the study sites. Measurements were done in July 2002, July 2003, and July 2004 (except for Tortosa in 2004, which were carried out in August).

Flix dam

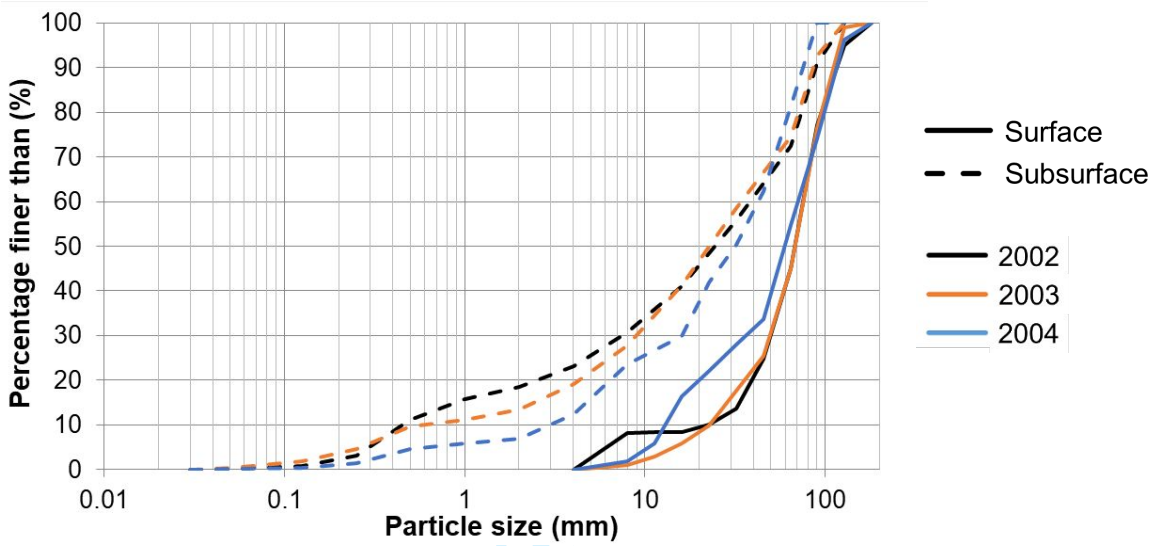

Flix meander – Combined surface and subsurface material

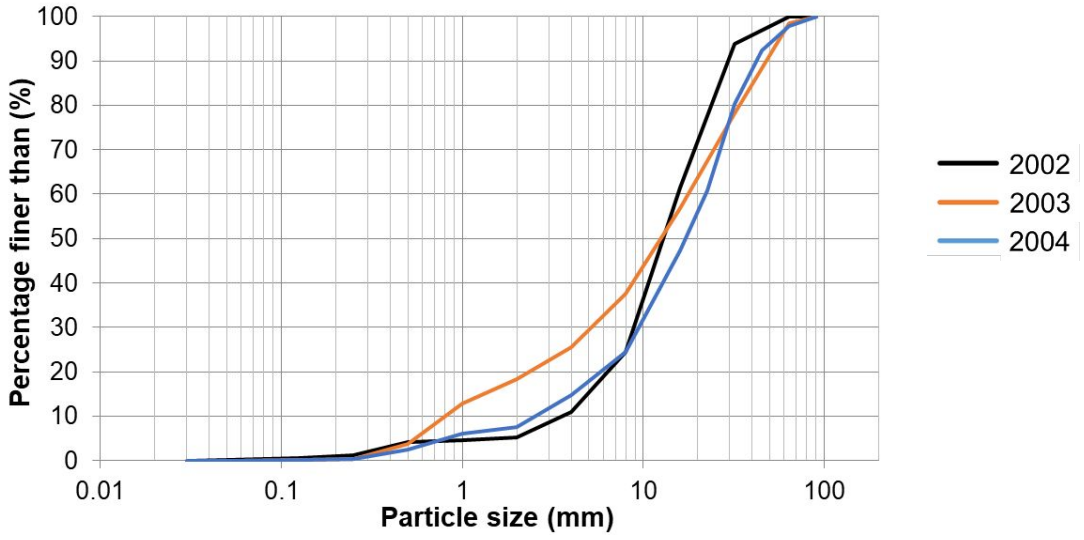

Flix

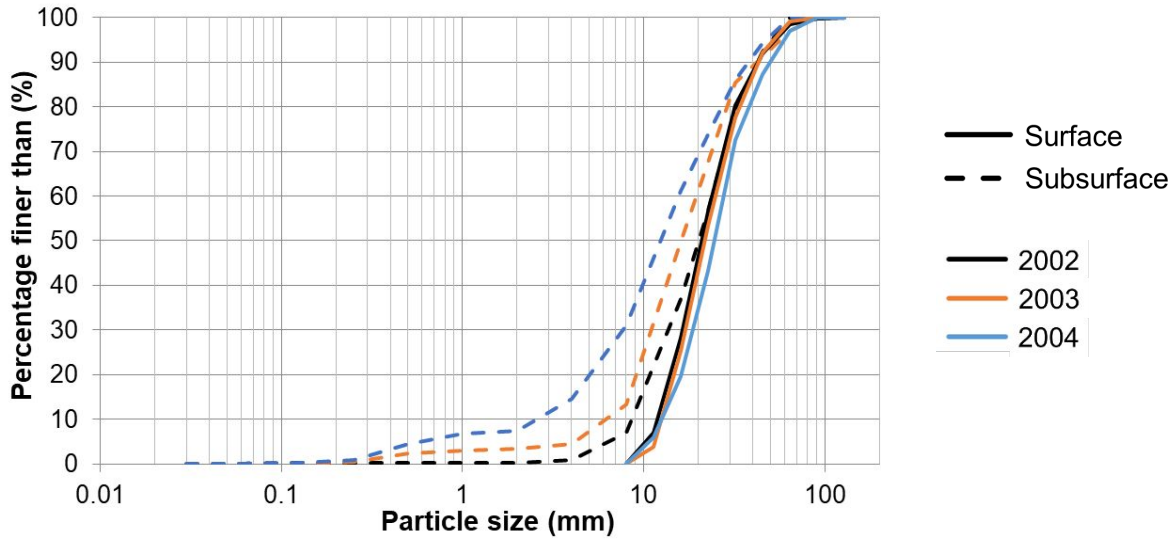

Pas de l'Ase

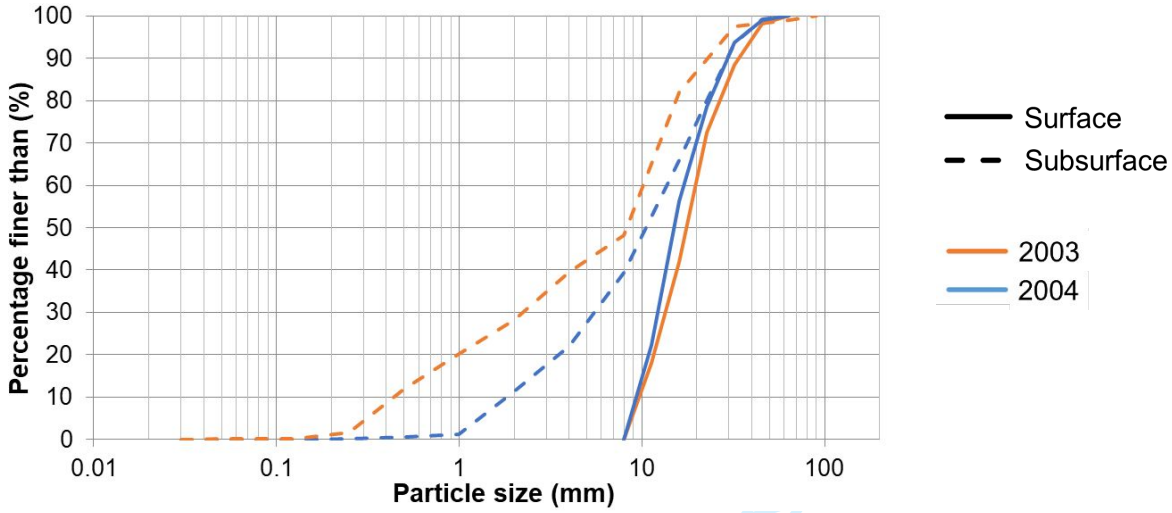

Móra 1.1

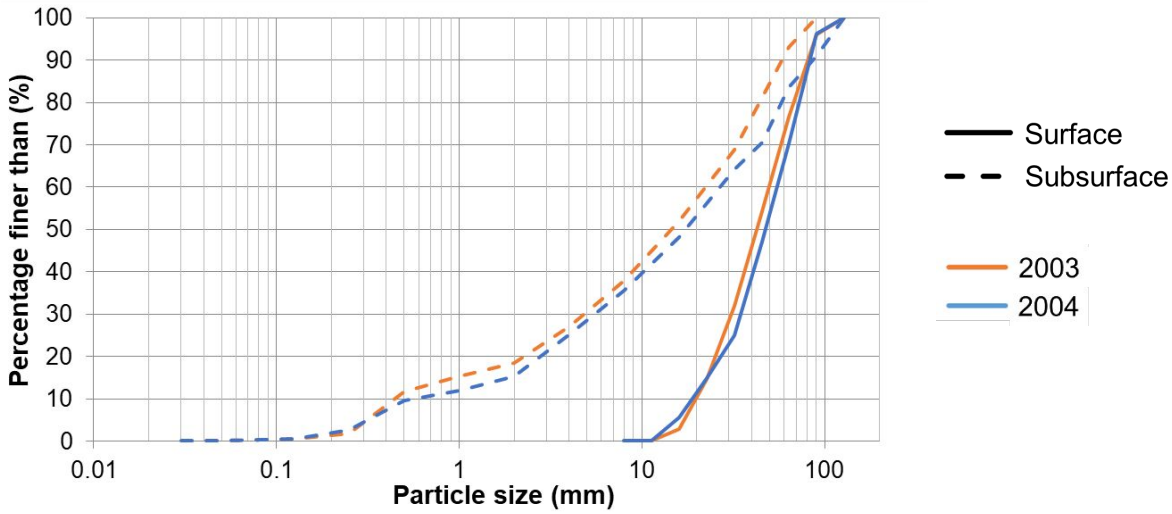

Móra 1.2

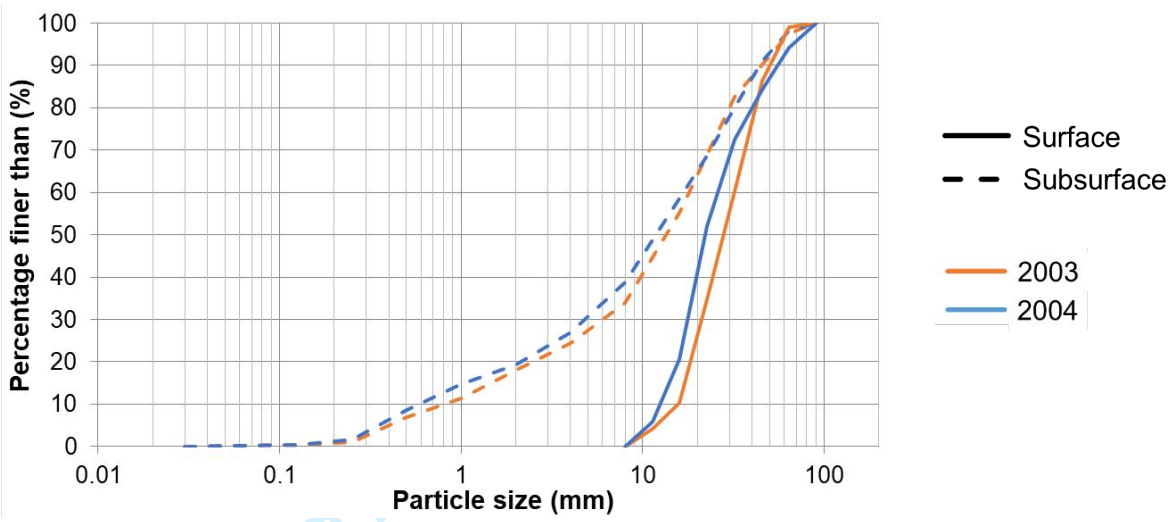

Móra 2

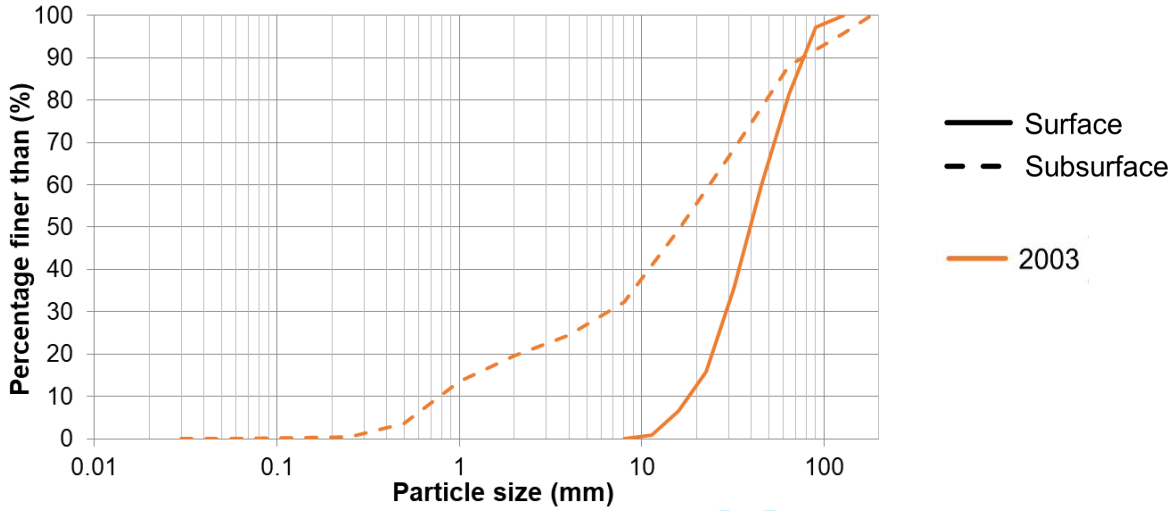

Móra 3

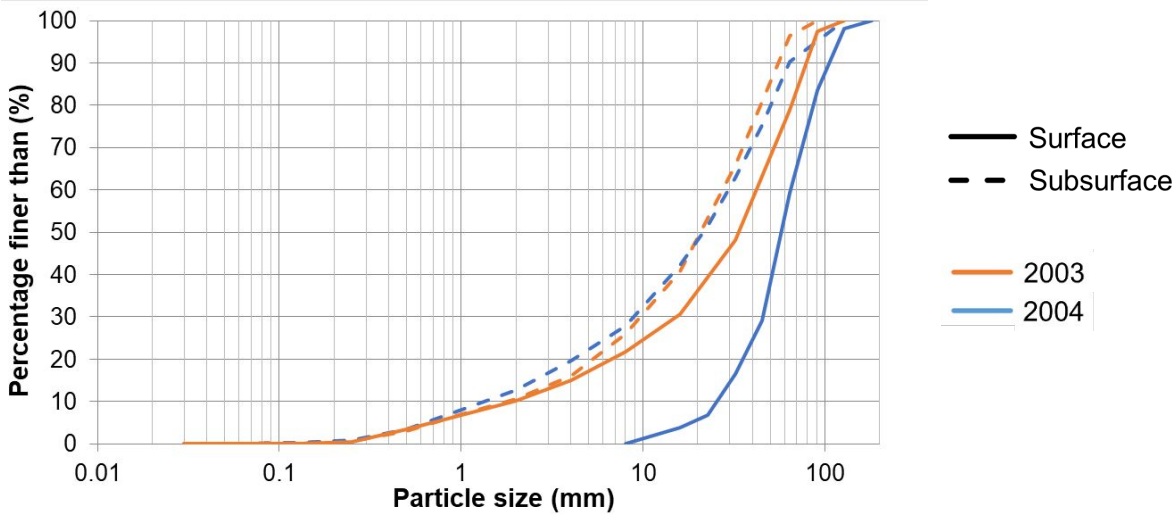

Tivenys – Combined surface and subsurface material

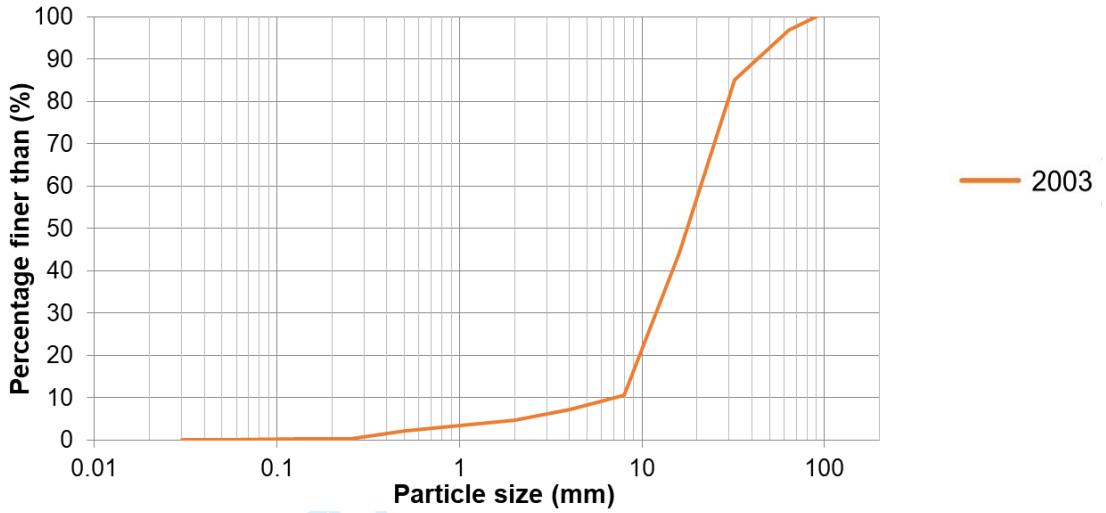

Tortosa – Combined surface and subsurface material

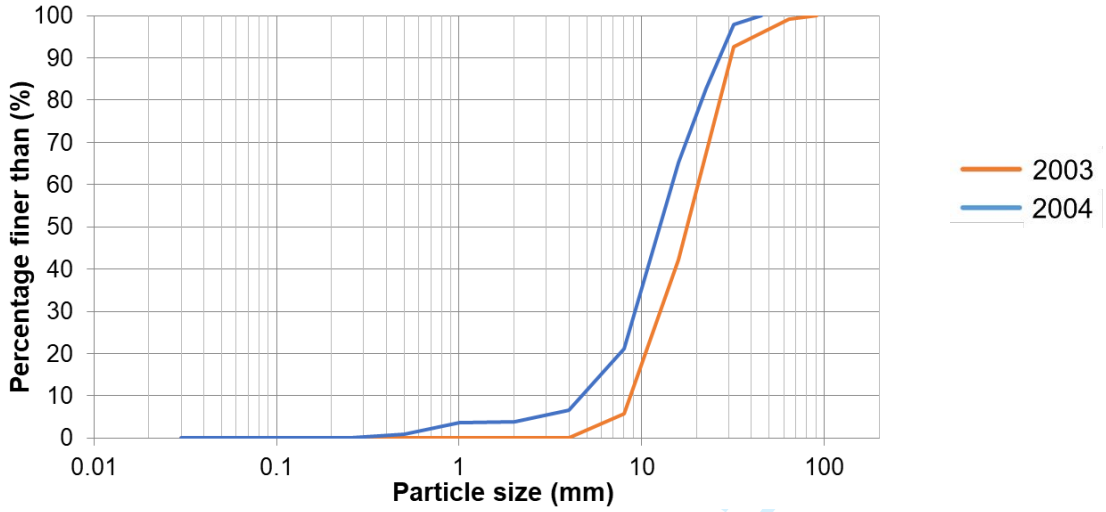

Table S1.1. Previous works published in the study river reaches and their main highlights. Only the articles related to bedload transport and riverbed material have been included.

Reference	Objectives / Methods	Highlights
Vericat et al. 2006	• To describe the breakup and reestablishment of the armour layer in a large regulated river. Methods: - GSD samplings (pebble count for surface material and volumetric method and area-by-weight for the subsurface material) - Bed load samplings (Helley Smith sampler 152 mm intake). Study period: 2002-2004	• Break-up of the armour layer and riverbed incision by large floods. • Reestablishment of the coarse surface layer by small floods. • Increment of the bedload transport after armour layer (partial or total) disruption. • Lower Ebro river channel was still active 40 years after dam construction.
Vericat and Batalla, 2006	• To analyse the sediment transport through the lower River Ebro during two consecutive hydrological years. Methods: - Flow (from official gauging stations and routed by the Muskingum method. - Suspended sediment transport (collection of depth integrated water and suspended sediment samples with a US DH74 during low flows and floods) - Bedload transport (Helley Smith samplers of 76 mm and 152 mm intake). Study period: 2002-2004	• Upstream the dam, most of the sediment was transported in suspension (99.5%), while downstream the dam the transport was 60% in suspension and 40% as bedload. • Specific sediment yield upstream the dams was three to four times higher than downstream the dams. • The sediment trapping by the dams was around 90% of suspended load and 100% of bedload. • Sediment load upstream the dam mainly provided by tributaries, and downstream the dam it came mainly from bank erosion.
Vericat and Batalla, 2007	• To analyse the behaviour of different bedload fractions. Methods: - Flow discharge (water stage and conversion to discharge). - Bedload transport (Helley Smith sampler 152 mm intake). - GSD samplings (pebble count for surface material and area-by-weight for the subsurface material). Study period: 2003-2004	• Under limited sediment supply conditions, partial transport controls the coarsening of the riverbed surface. • The reestablishment of the armour layer changes particle entrainment due to hiding and reduction of dimensionless critical shear stress. • The reestablishment of the armour layer causes a reduction in bedload transport rates due to the lower availability of fine fractions on the surface. • The reestablishment of the armour layer causes a progressive reduction of the sediment net export from the reach.

↓ *…continued in the next page*

↑ *…continued from previous next page*

Vericat et al., 2008	• To examine the bed material mobility in the River Ebro on the adjustment phase (to attain a post-dam quasi-equilibrium state) of the river. - To assess the effects of partly–competent flows on the GSD. - To assess the effects of partly-competent flows on the changes of the armour layer. Methods: - Bedload transport (painted areas and lines). - Active layer (scour chains). - GSD samplings (pebble count for surface material and volumetric method for the subsurface material). - Surface GSD changes (i.e. photography comparison). Study period: 2003-2004	• Existing disequilibrium between the rate of sediment supply from upstream and the ability of the flow to entrain and transport these particles. Most medium and coarse gravels were exported from the sections, but larger particles were not mobilised. • The riverbed surface coarsening responded to the limited sediment supply conditions combined with the frequent occurrence of competent flows. • Sedimentary dynamics in the lower Ebro are still evident at interannual scale 4 decades after dam closure.

Table S1.2. Previous works published in the study river reaches and their main highlights

Study site	Survey Date	Discharge (m^3/s)	Mean active layer depth (mm)	Mean painted tracers travel length (m)	Mean magnetized tracers travel length (m)	Mean painted tracers D_{50} travel length (m)
Presa Flix	*03/12/2002 (tracers and scour chains installation)*					
	05.12.2002	1408	0	30.14	-	50
	06.02.2003	2133	77.67	1.47	-	1.97
	08.12.2003	989	13.9	1.19	-	-
	29.01.2004	685	5.83	1.05	-	-
Flix meander	*29/11/2002 (tracers and scour chains installation)*					
	05.12.2002	1407	37	5.12	-	12.8
	06.02.2003	2130	242	-	-	-
	08.12.2003	987	108	-	-	-
	29.01.2004	685	8	-	-	-
Flix	*03/10/2002 (tracers and scour chains installation)*					
	05.12.2002	1787.5	-	3.36	-	6.1
	06.02.2003	2480	537	-	-	-
	08.12.2003	1383	11.67	1.59	-	1.85
	29.01.2004	1084.5	72.5	-	-	-
Pas de l'Ase	*03/10/2002 (tracers and scour chains installation)*					
	06.02.2003	2434	90	9.44	-	9.7
	08.12.2003	1367	68.33	1.31	-	-
	29.01.2004	1082	25	8.82	-	10.1
Móra 1.1 and 1.2	*02-03/10/2020 (tracers and scour chains installation)*					
	06.02.2003	2498	108.75	9.71	-	-
	06.02.2003	2498	59.75	31.24	-	37.95
	08.12.2003	1355	22.67	0.66	-	-
	08.12.2003	1355	17.4	0.89	-	-
	29.01.2004	1081	12.81	1.09	-	-
	29.01.2004	1081	13	1.34	-	1.4
Móra 2	06.02.2003	2498	-	-	-	-
Móra 3	*02/10/2002 (tracers and scour chains installation)*					
	06.02.2003	2498	135	8.87	-	-
	08.12.2003	1355	51.67	6.45	2.86	5.65
	29.01.2004	1081	13.75	3.31	3.85	1.93
Tivenys	*04/10/2002 (tracers and scour chains installation)*					
	06.02.2003	2451	521.67	-	-	-
Tortosa	*19/10/2002 (tracers and scour chains installation)*					
	06.02.2003	2422	138.75	9	-	9
	08.12.2003	1296.5	55	-	-	-

[a] Painted area 1 = 70% particles mobilised; Painted area 2 = 75 % particles mobilised
[b] Magnetized tracers (no RFID)

2. RIVER MUGA DATA

The Muga is a 758 km^2 catchment located in the NE of the Iberian Peninsula. It ranges from 1443 masl at the headwaters to the sea level at the Mediterranean Sea. The River Muga is regulated by a large dam (Darnius, 61 hm^3) since 1969, which has completely changed the hydrological regime of the river and generated a sediment deficit downstream the dam (Piqué et al., 2016; Piqué et al., 2017).

This study focuses on the Upper Muga (Figure S2.1), one sub-basin draining the reservoir, thus not regulated. This sub-basin drains an area of 84.1 km^2 of Paleogene and Cretaceous marls and conglomerates. The Upper Muga sub-basin is under the domain of the Mediterranean climate, with mean annual temperature around 11-14ºC, and a mean annual precipitation of 850-1150 mm. Main land use is forest (90% of the basin). Mean monthly flow at the sub-basin outlet for the study years was 1.3 m^3/s (SD ±9.4 m^3/s) in 2012-2013, 0.54 m^3/s (SD ±1.4 m^3/s) in 2013-2014, and 0.99 m^3/s (SD ±5.4 m^3/s) in 2014-2015. Annual maximum flow was 353 m^3/s, 24.7 m^3/s, and 164 m^3/s for the three study years, respectively (Piqué et al., 2017).

Study Sites and Methods

Riverbed dynamics were indirectly measured in one location close to the mouth of the Upper Muga sub-basin (Figures S2.2 and S2.3) from October 2013 to April 2015.

- Grain size distribution (Figure S2.4): Surface material was sampled by the pebble count procedure (Wolman, 1954), while subsurface material was sampled using the volumetric method (Church et al., 1987).

- Particle travel length: Measured from painted areas and RFID-tagged particles. Tables S2.1 and S2.2.

- Active layer depth: Measured by the scour chain method. Tables S2.1 and S2.2.

Figure S2.3 and S2.4 present the cross sections and grain-size distribution, respectively, of the study sites in the River Muga, while tables S2.1 and S2.2 summarise the papers where part of the data used in this manuscript has been published. It is worth to mention that most of the data on riverbed mobility (based on tracers) and active layer (based on scour-chains) were not published before.

Figure S2.1. a) Location map of the River Muga, and b) location of the study site in the Upper Muga sub-basin.

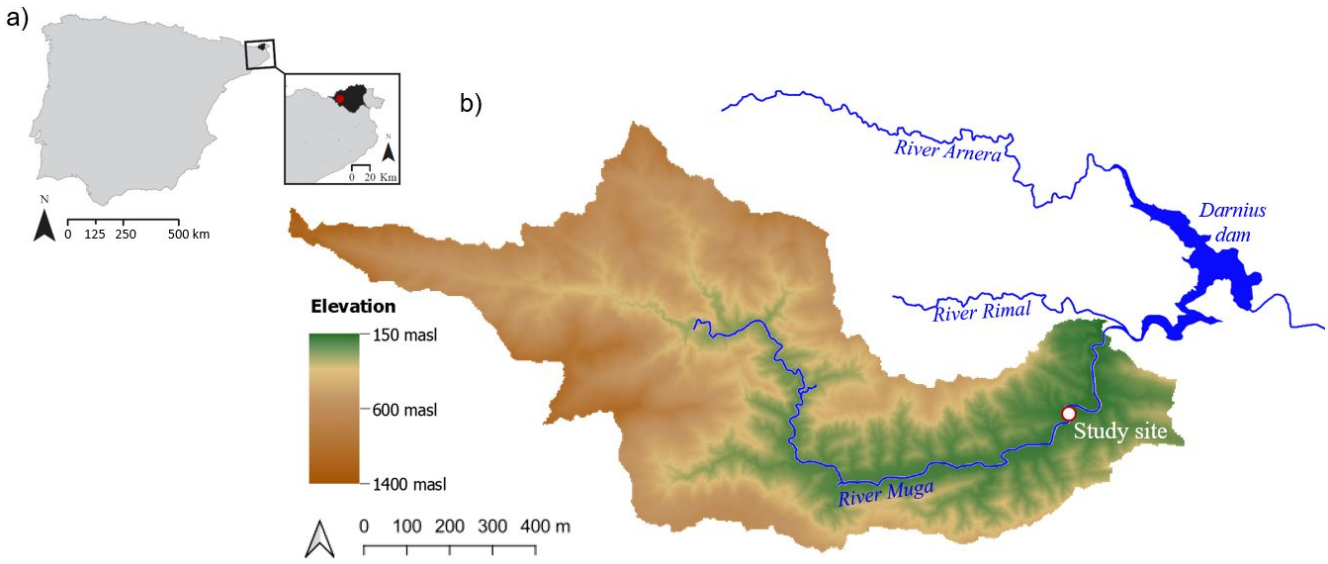

Figure S2.2. Photographs the study site for 25/07/2013. a) General view of the reach, and b) Detail of the bar and cross-section where measurements were carried out.

Figure S2.3. Cross-section of the study site and main channel characteristics.

Channel morphology: Riffle-pool / Slope: 0.008 m/m / Width: 19.2 m / Q_{bkf}: 8.9~~14.6~~ m^3/s

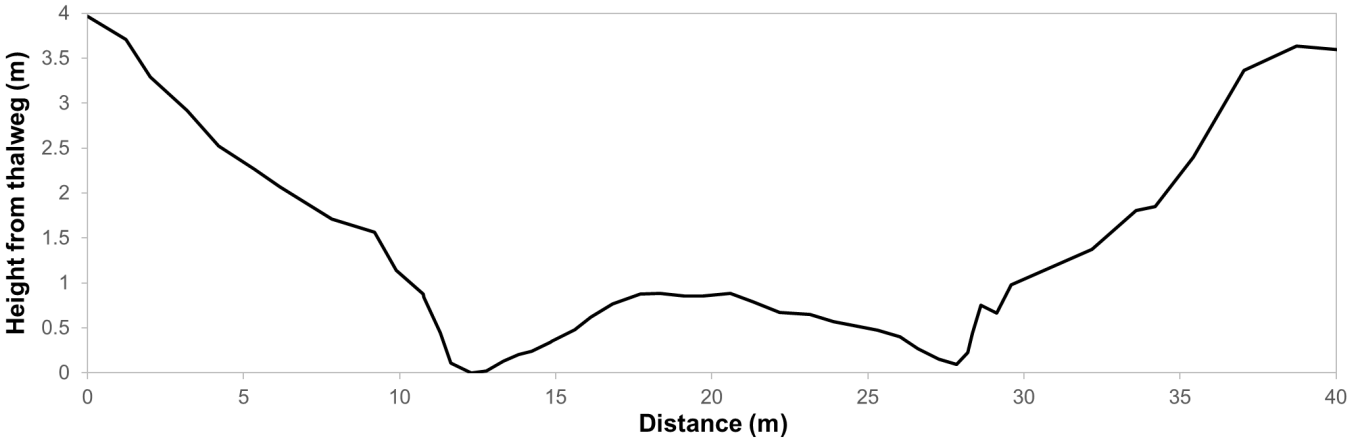

Figure S2.4. Grain size distribution of surface and subsurface material in the study site.

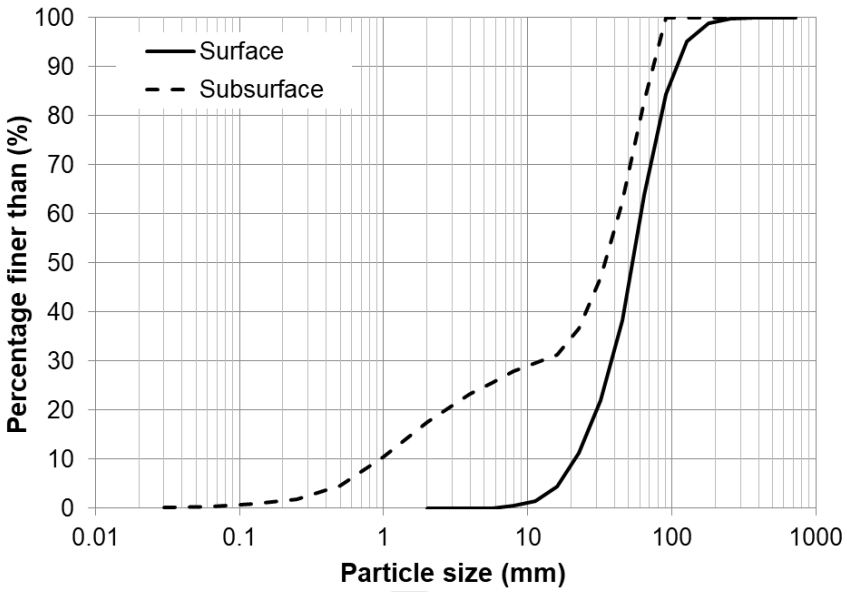

Table S2.1. Previous works published in the study river reaches and their main highlights. Only the articles related to bedload transport and riverbed material have been included.

Reference	Objectives/Methods	Highlights
Piqué et al. 2017	• To construct the sediment budget of a highly regulated Mediterranean river. • To determine the role of the reservoir on the upper basin water and sediment dynamics. • To quantify the sediment deficit downstream from the dam. Methods: - Dicharge (measurement of water stage and transformation into discharge). - Suspended sediment transport (turbidity probes installation and calibration to obtain suspended sediment concentration). - Bedload transport (indirect methods as painted areas, tagged tracers and scour chains). Study period: 2012-2015	• Flow patterns upstream and downstream the dam differ due to reservoir operation. • Upstream, sediment transport is restricted to floods and occurs in short periods of time. • Downstream, suspended sediment transport predominates; bedload is negligible. • Sediment trapping in the reservoir reaches up to 95% of the total load.

Table S2.2. Data used in the papers for the study sites.

Flood event number	Date flood peak	Discharge (m^3/s)	Duration competent flood (min)	Water volume competent flood (hm3)	Accumulated water volume since last flood (hm^3)	Mean active layer depth (mm)	Mean painted tracers travel length (m)	Mean RFID tracers travel length (m)	Mean painted tracers D_{50} travel length (m)	Mean RFID tracers D_{50} travel length (m)
01/10/2013 (tracers and scour chains installation)										
2[a]	~~18~~19/11/2013	~~39.125~~26.08	2930	~~4.17~~2.58	~~5.33~~3.90	146	1.27	0.94	0.98	2.9
3[b]	04/04/2014	~~29.95~~16.97	1305	~~1.43~~0.84	5.43~~6.94~~	29	0.97	-	0.54	-
4[c]	29/09/2014	~~35.2~~27.34	462	~~0.513~~0.36	7.18~~8.86~~	196.25	0.16	1.72	-	0.4
5[d]	29/11/2014	~~103.79~~177.64	43962	~~14.94~~10.04	12.14~~17.96~~	-	-	125.32	-	378.18
6[e]	21/03/014	~~59.44~~101.07	2715~~625~~	~~6.08~~4.49	10.43~~24.81~~	60	8.79	0.56	6.78	0.13

[a] From installation to survey 2.
[b] RFID were not looked for.
[c] RFID data for floods 3 a- 4.
[d] RFID data for flood 5.
[e] RFID data for flood 6.

REFERENCES

Batalla, R.J., Kondolf, G.M., Gómez, C.M. (2004). Reservoir-induced hydrological changes in the Ebro River basin, NE Spain. *Journal of Hydrology*, 290: 117– 136.

Church, M.A., McLean, D.G., Wolcott, J.F. (1987) River Bed Gravels: Sampling and Analysis. In: Thorne, C. R., Bathurst, J. C. and Hey, R. D. (eds). *Sediments transport in Gravel Bed Rivers*, John Wiley and Sons, New York; pp. 43-88.

Kellerhals, R., Bray, D.I. (1971). Sampling procedures for coarse fluvial sediments. *Journal of the Hydraulics Division ASCE*, 97: 1165-1180.

Piqué, G., Batalla, R.J., Sabater, S. (2016). Hydrological characterization of dammed rivers in the NW Mediterranean region. *Hydrological Processes*, 30 (11): 1691-1707.

Piqué, G.; Batalla, R.J.; López, R. and Sabater, S. (2017). The fluvial sediment budget of a dammed river (upper Muga, southern Pyrenees). *Geomorphology*, 293 (A), 211-226.

Tena, A., Batalla, RJ. (2013). The sediment budget of a large river regulated by dams (The lower River Ebro, NE Spain). *Journal of Soils and Sediments*, 13: 966-980.

Vericat, D., Batalla, R.J. (2005). Sediment transport in a highly regulated fluvial system during two consecutive floods (Lower Ebro River, NE Spain). *Earth Surface Processes and Landforms*, 30: 385–402.

Vericat, D., Batalla, R.J. (2006). Sediment transport in a large impounded river: The lower Ebro,NE Iberian Peninsula. *Geomorphology*, 79: 72-92.

Vericat, D., Batalla, R.J., Garcia, C. (2006). Breakup and reestablishment of the armour layer in a large gravel-bed river below dams: The lower Ebro. *Geomorphology*, 76: 122– 136

Vericat, D., Batalla, R.J. (2007). Fractional bedload transport during small floods in a regulated gravel-bed river. *Zeitschrift für Geomorphologie*, 51 (2): 227-240.

Vericat, D., Batalla, R.J., Garcia, C. (2008). Bed-material mobility in a large river below dams. *Geodinamica Acta*, 21 (1-2): 3-10.

Wolman, M. (1954). A method for sampling coarse river-bed material. *American Geophysical Union Transactions*, 35: 951–956, 1954.